Strangeness Production at COSY-ANKE: pp → ppϕ

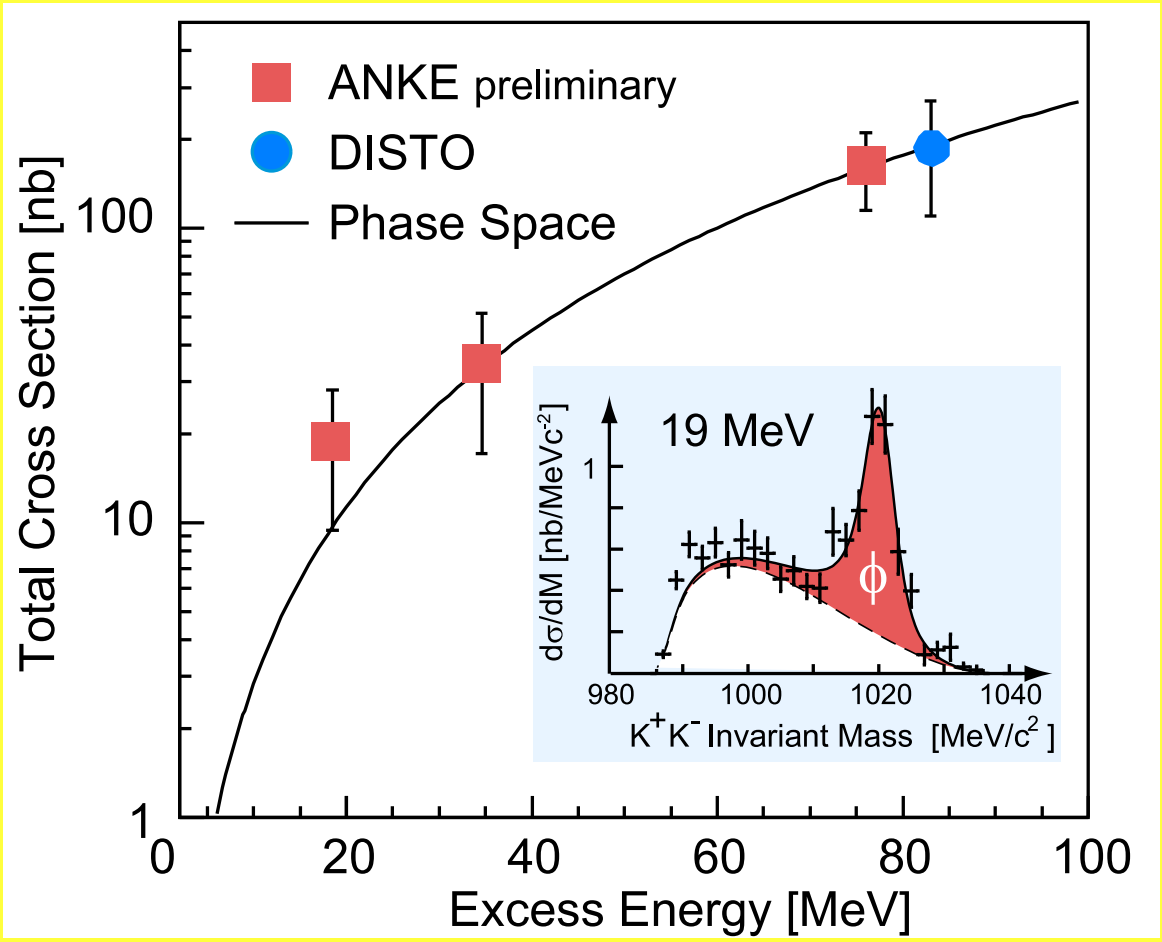

Annual Report 2004

Institut für Kernphysik / COSY

draft March 3, 2005

Cover picture:
The reaction $pp \to pp\phi$ has been studied with the ANKE spectrometer at excess energies Q = 19, 35, and 76 MeV by detecting the K^+K^- decay mode of the ϕ-meson. At each of these excess energies about 200-400 ϕ mesons have been identified. The total ϕ cross sections from ANKE are shown together with a data point from DISTO. The insert shows the invariant K^+K^- mass distribution for the lowest measured energy. The ϕ peak is on top of a broad distribution from non-resonant kaon production, while the background from misidentified particles is less than 4%.

Preface

The year 2004 had been marked by events and activities that will be of strategic relevance for our institute. In February our institute was reviewed together with the GSI within the framework of the "Program Oriented Funding", which represents a new paradigm for science funding of the Helmholtz centres. This evaluation took place at the GSI, scrutinizing the Research Program "Physics of Hadrons and Nuclei", which is part of the Research Field "Structure of Matter".

As the major recommendations of this council, an "on-site" and "in-depth" review of the future activities of the institute, especially with respect to our close collaboration with GSI within the FAIR-project was proposed as well as to present a full proposal for the transfer of WASA from Uppsala to COSY to a dedicated review committee. The HGF-Senate has decided to postpone/defer any decision on budgets for the years 2006 to 2009 until the findings of the on-site review, which will take place in April 2005, are available.

The WASA proposal has been critically examined in October 2004 by an extended program advisory committee. It concluded unanimously that this detector in connection with COSY would constitute an outstanding physics opportunity and that the proposed physics program has unquestionably strategic relevance.

The institute has significantly intensified its engagement in the FAIR-project, which will set the stage for the mid- and long-term perspective in hadron physics. In collaboration with other partners our institute has taken on a leading role in the consortium that is planning, designing (and later building) the "High Energy Storage Ring" (HESR) of FAIR. In 2004 the IKP has played a prominent role in the timely completion of the Technical Reports for HESR, PANDA, PAX and FLAIR.

As outlined in our PoF-application, the institute has the following strategy for its future position within the scientific portfolio of the Helmholtz organisation (HGF):

- Scientific exploitation of COSY and its experimental facilities:
  - Hadron physics with hadronic probes
  - Preparatory investigations for the FAIR project of GSI (Darmstadt)
- Involvement in FAIR:
  - Planning, designing and building of HESR, the "High Energy Storage Ring" for anti-protons
  - Contributions to antiproton experiments and corresponding detector systems (PANDA, PAX, FLAIR)

It is evident that the timescale for the transition from COSY to HESR needs to be intertwined with the actual realization of the FAIR-project. As a result of an intense discussion within CANU (COSY Association of Networking Universities), it was agreed that COSY will be an indispensable experimental facility for the intervening period in order to sustain a viable hadron physics community. An efficient migration of the CANU-user community to the HESR is only conceivable if experimental activities can continue nearly seamlessly.

As mentioned above, we intend to transfer WASA (currently installed at CELSIUS of TSL, Uppsala, Sweden) to COSY — a corresponding Memorandum-of-Understanding between Uppsala University and FZJ was signed in December. As significant resources will be allocated to the HESR, PANDA, and other activities related to the FAIR-project, WASA — together with ANKE and TOF — will be the only detector systems operated at COSY in the near future. We already phased out nuclear spectroscopy and JESSICA during the past year.

As in the years before we had meetings of our international advisory committees, the IKP-Beirat and PAC for the COSY experimental program. I would like to take the opportunity to thank all of its members for their valuable advice and constructive discussions.

We also have had retirements of colleagues in 2004; I would like to mention: Prof. Detlev Filges and Prof. Kurt Kilian, long-term director of IKP I. I want to express our deep thanks to all retirees for their work and contributions as well as our best wishes for their future. We are very pleased to have successors for two retired directors (J. Speth, K. Kilian):

- Prof. Ulf-G. Meißner, holding a chair at the "Helmholtz Institut für Strahlen- und Kernphysik" at the "Rheinische Friedrich-Wilhelms Universität Bonn", who had acted as provisional director of the IKP-theory since 2003, took over as director in October.
- Prof. James Ritman from the "Justus-Liebig Universität Gießen", holding now a chair at the "Ruhr-Universität Bochum", is the new head of IKP I since September.

A hearty welcome and all the best to the new leadership and to all other new staff members of IKP. In closing, I would like to thank all colleagues, collaborators, friends from within the institute, the Research Center (FZJ) — in particular ZAM, ZAT and ZEL — and national and international universities and institutions for their support and dedication that was key to make COSY a world class facility and the IKP a center for hadron physics with hadronic probes.

Jülich, February 2005 Hans Ströher

Contents

1 Detectors at COSY

Currently, COSY harbors four experiments at internal target stations — **ANKE**, **COSY-11**, **EDDA** and **PISA** — as well as three external facilities — **BIG KARL** (with ENSTAR, GEM and HIRES), **COSY-TOF** and **JESSICA**.
ANKE and **COSY-11** are magnetic spectrometers with a wide momentum acceptance for charged particles. They are both well suited to study meson-production processes close to thresholds with particle emission into forward direction. At the non-magnetic **EDDA** detector $\vec{p}\vec{p}$ elastic scattering has been studied and the device is now being used as a beam polarimeter. Both **PISA** and **JESSICA** are detectors which have been used for the investigation of spallation processes induced by GeV protons. **BIG KARL** is a high resolution magnetic spectrometer which is supplemented by the GEM and ENSTAR detectors at larger emission angles. The non-magnetic spectrometer **COSY-TOF** measures the velocity and direction of charged particles with large angular acceptance thus allowing for the kinematically complete reconstruction of events with up to one neutral particle.
So far all detectors at COSY are "photon-blind". This will change with the **WASA** detector which is planned to be transfered from CELSIUS (Uppsala, Sweden) to COSY in 2005. **WASA** can detect both neutral and charged particles with a large angular-momentum acceptance. **WASA**, **ANKE** and **COSY-TOF** will be the only detector systems at COSY in the near future.

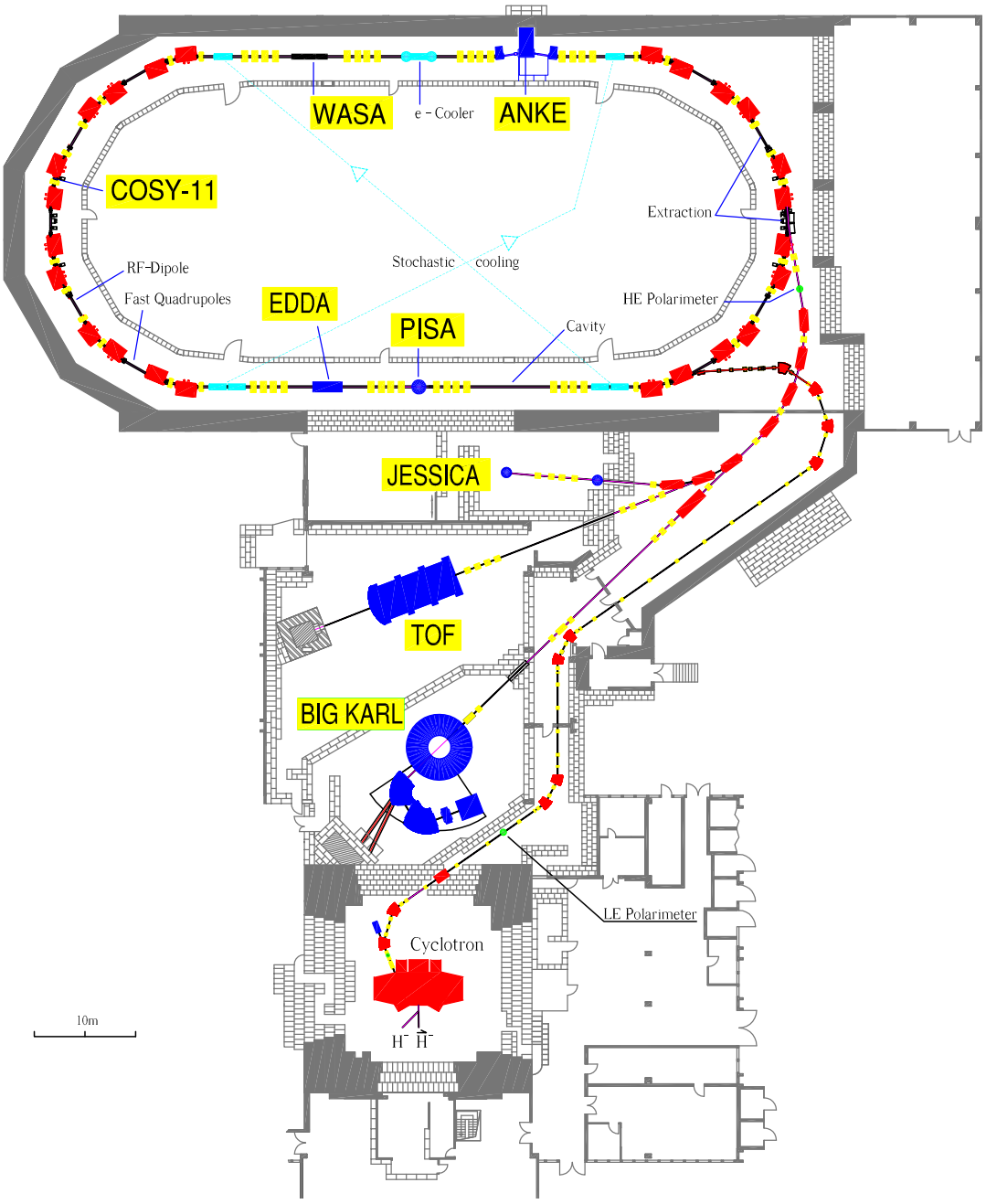

1.1 Internal Detectors

1.1.1 ANKE

ANKE is a magnetic spectrometer at an internal target position of COSY. Together with its dedicated detection systems it allows to separate from the circulating COSY beam and momentum analyze ejectiles, which result from beam-target interactions and are emitted into forward angles around 0°. The spectrometer consists of 3 dipole magnets (D1–D3) which impose a closed orbit bump on the circulating COSY beam. Since D2 (see photograph in Fig. 1) is movable perpendicular to the beam direction, the momentum range covered can be varied independently of the beam energy. The huge D2-gap height of ∼20 cm provides a large geometrical acceptance, which is particularly advantageous for correlation measurements with threshold kinematics.

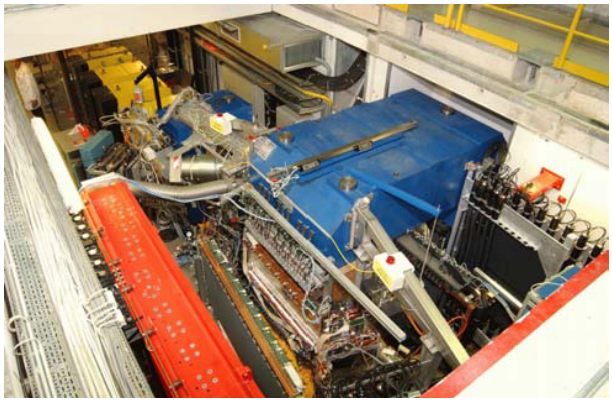

Fig. 1: Photo of ANKE and the detection systems which are located around the spectrometer dipole D2 (blue).

The detection systems of ANKE comprise *(i)* tracking detectors and *(ii)* scintillator hodoscopes in forward direction, both to the right and the left side of the beam, *i.e.* for positive and negative reaction products. In addition, dedicated detectors like range telescopes and Čerenkov counters are installed for the identification of rare events, *e.g.* $K^{+,-}$, within a huge background (see section 2.4). Around the target position, silicon detector telescopes can optionally be installed to detect particles like slow "spectator" protons.

The targets, which have been utilized at ANKE up to now, are thin solid material foils (carbon, copper, silver, gold) and hydrogen or deuterium cluster-jets. Luminosities of a few times 10^{32} cm^{-2}s^{-1} (10^{31} cm^{-2}s^{-1}) have been achieved with unpolarized beams. During 2005 the polarized internal target (PIT, see section 7.1.1), which has been developed at IKP II during the past years, will be installed. In combination with a storage cell, this will allow for double polarization experiments at ANKE.

In the beginning of 2005 ANKE will be used for the first time for measurements during COSY energy ramping in order to study the reactions $dp \to {}^3\mathrm{He}\eta$ and $dd \to {}^3AN\pi$ around thresholds.

1.1.2 COSY-11

The research program of the COSY-11 collaboration concentrates on physics of the near threshold meson production in different flavor and spin channels. For this reason the high resolution COSY-11 zero-degree magnetic spectrometer has been upgraded during the last years as shown in Fig. 2 and was additionally equipped with *i)* de-

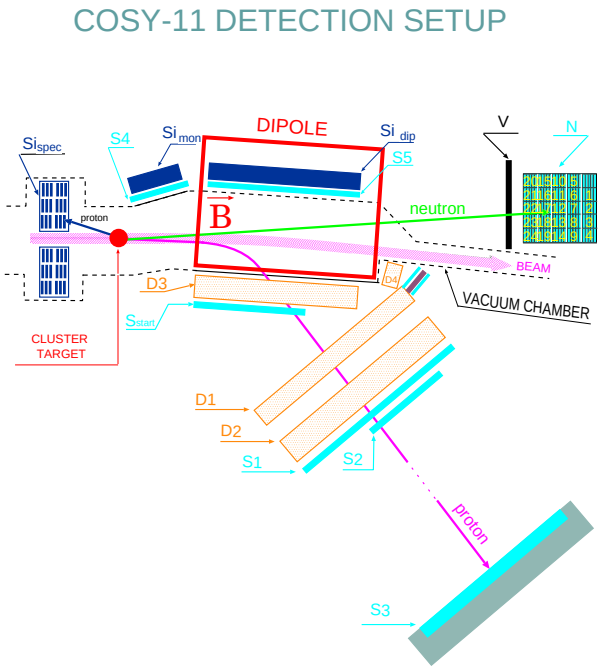

Fig. 2: Schematic view of the COSY-11 setup.

tectors for registering neutrons, deuterons, spectator protons, *ii)* a c-shaped hexagonal chamber (D3) extending the acceptance for kaons and low momentum particles and *iii)* a system for the determination of the beam polarization. These extensions allow for studies of the production mechanism and meson-nucleon interaction as a function of spin and isospin degrees of freedom. For example the measurements of the quasi-free $pn \to pn\eta$ and $pn \to pn\eta'$ reactions are being performed by detecting all outgoing nucleons from the $pd \to p_{\mathrm{sp}}pnX$ reaction and using the missing mass technique for identifying the events under investigation.

1.1.3 EDDA

The EDDA detector, schematically shown in Fig. 3, consists of two cylindrical detector shells. The solid angle coverage is 30° to 150° in $\Theta_{\mathrm{c.m.}}$ for elastic proton-proton scattering and about 85% of 4π. The outer detector shell consists of overlapping scintillator bars (B), semirings (R) and semirings made of scintillating fibers (FR). The inner detector shell (HELIX) is a cylindrical hodoscope consisting of four layers of 2.5 mm diameter plastic scintillating fibers which are helically wound in opposing di-

rections so that coincidence of hits in the lefthanded and righthanded helices gives the point at which the ejectile traversed the hodoscope. The 640 scintillating fibers are connected to 16-channel multianode photomultipliers and read out individually using the LeCroy proportional chamber operation system PCOS III. Combined with the spatial resolution of the outer detector shell, the helix fiber detector provides for vertex reconstruction with a FWHM resolution of 1.3 mm in x- and y-direction and 0.9 mm in z-direction. The resulting polar and azimuthal angular resolutions are about 0.3° and 1.3° FWHM for pp scattering events.

The detector was used by the EDDA collaboration to measure differential cross sections, analyzing powers A_N and spin correlation parameters A_{NN}, A_{SS} and A_{SL} of the elastic proton-proton scattering over a wide energy range. It is now used as very efficient polarimeter for the TRIC and SPIN@COSY experiments and for the preparation of highly polarized proton and deuteron beams for the experiments ANKE, COSY11, TOF and GEM.

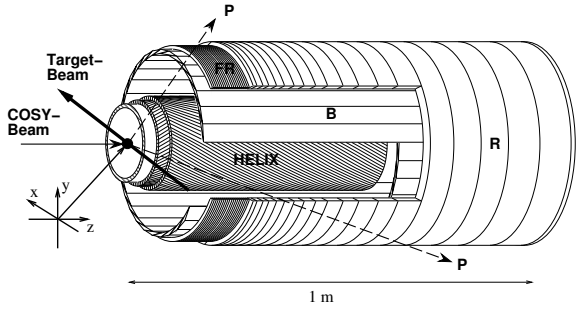

Fig. 3: Scheme of the EDDA detector. The outer hodoscope consists of scintillator bars B, scintillator semi-rings R and semi-rings made of scintillating fibers FR. The inner hodoscope HELIX consists of four layers of scintillating fibers helically wound in opposing directions.

The polarized atomic hydrogen beam target is shown in Fig. 4. Hydrogen atoms with nuclear polarization are prepared in an atomic-beam source with dissociator, cooled nozzle, permanent sixpole magnets, and RF-transition unit. In the dissociator, hydrogen is dissociated in an inductively coupled 350 W RF-discharge and passes through an aluminum nozzle cooled to about 30 K and a skimmer. About $5 \cdot 10^{16}$ hydrogen atoms per second are produced. The comparable low temperature of the nozzle leads to a decreased velocity (most probable velocity 1.3 km/s) of the atomic beam and thus an increased target thickness. The atomic beam source selects hydrogen atoms in a pure hyperfine state (m_j=+1/2, m_I=+1/2), in order to achieve a high polarization in a weak magnetic holding field. Here, m_j and m_I are the magnetic quantum numbers of the electron and proton spins, respectively. The effective target thickness of the atomic beam is about $2 \cdot 10^{11}$ atoms/cm^2, the polarization is more than 90 %. For the TRIC experiment a storage cell has been installed which allows target thicknesses of about $2 \cdot 10^{13}$ atoms/cm^2.

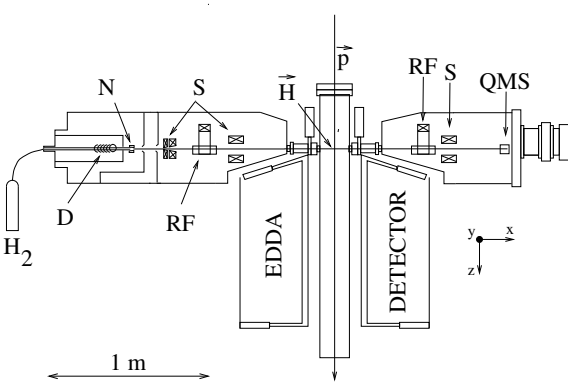

Fig. 4: Polarized COSY beam $\vec{p}$ and polarized atomic beam target $\vec{H}$ with dissociator D, cooled nozzle N, permanent sextupole magnets S, RF transitions and Breit-Rabi polarimeter in the atomic beam dump consisting of RF transition, sextupole magnet S and quadrupole mass spectrometer QMS.

1.1.4 PISA

The PISA experiment aims at systematic investigations on the complex mechanisms raised by pN spallation, multifragmentation, fission and vaporization reactions. At the internal beam of COSY, PISA studies proton induced reactions up to 2500 MeV on a wide range of target nuclei. For the measurement of total and double differential production cross sections Bragg Curve Detectors, silicon telescopes and phoswich detectors are being employed. These detectors are mounted at various angles with respect to the direction of the incident internal proton beam as shown in Fig. 5.

The correlation of time-of-flight from multi-channel plates and the energy E deposited in the BCD-volume allows for the separation of following isotopes: ^{6}Li, ^{7}Li, ^{8}Li, ^{7}Be, ^{9}Be, ^{10}Be, ^{10}B, ^{11}B, ^{11}C, ^{12}C, ^{13}C, ^{14}C and ^{13}N, ^{14}N. The design of the BCD as well as a typical output signal from the BCD is shown in Fig.5.

The maximum of the curve corresponds to the so called Bragg peak proportional to the charge of particle. The integral over the whole length of a signal describes the kinetic energy E of the particle. The rather low energy threshold of the BCD ($\leq$ 1 MeV/nucleon) allows one to explore the kinetic energy spectra of ejectiles well below the respective Coulomb barriers and the measurement of elemental distributions of fragments ranging from He up to Si. Such a small energy threshold was feasible due to the use of rather thin targets of the order of 50–200 μg/cm^2. A distinguished element resolution of ΔZ between 10% and 12% per amu has been found.

In addition, in order to detect also very energetic light ejectiles (H, He, Li,...) the setup is equipped with cooled ($-25°$) Si-telescopes (50–6000 μm) and phoswich detectors.

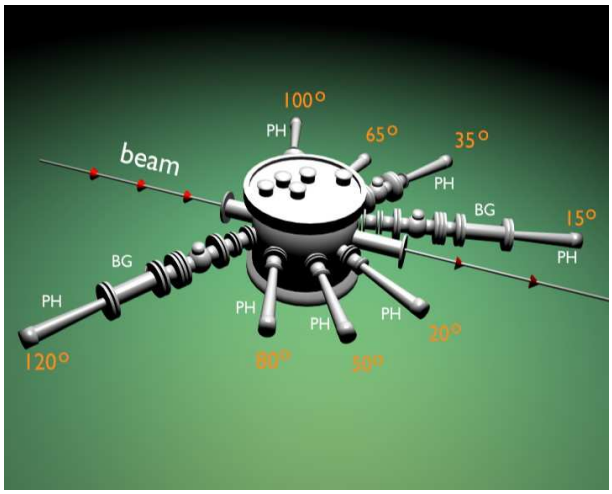

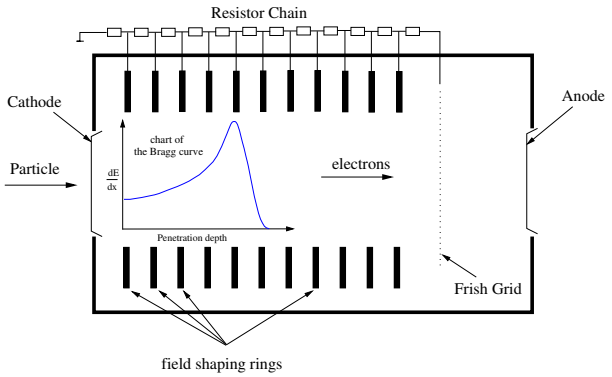

Fig. 5: Upper: Scattering chamber of PISA with the two full detector arms mounted at 15° and 120° equipped with Bragg curve-detectors (BCD), channelplate- (inside chamber) and phoswich detectors. Lower: Schematic layout of the Bragg Curve Detector.

1.2 External Detectors

1.2.1 BIG KARL, GEM, ENSTAR

The setup of the magnetic spectrograph Big Karl is shown in Fig. 6. It has a high resolution focal plane (3Q2DQ) with a momentum resolution of $\Delta p/p < 5 \cdot 10^{-5}$ and a momentum acceptance of $\pm 4.5\%$. The maximal proton momentum that can be bent is 1080 MeV/c. The dipole exit (3QD) has an acceptance of $\pm 50\%$ and maximal proton momentum of 3240 MeV/c. The ejectile momenta as well as two angles can be measured with the help of multiwire drift chambers (MWDC). Additional time-of-flight measurements allow for particle identification and thus for the derivation of a four-momentum vector.

The magnetic spectrograph has additional detector components for different purposes. Cherenkov detectors in the time-of-flight path allow one to veto pions and thus enrich kaons in a data sample. A system with spaghetti-shaped scintillators allow for the vertex measurement of charges particles. This was used, for example, in the measurement of ϕ-meson production in a $pd \rightarrow {}^3\mathrm{He}K^+K^-$ reaction.

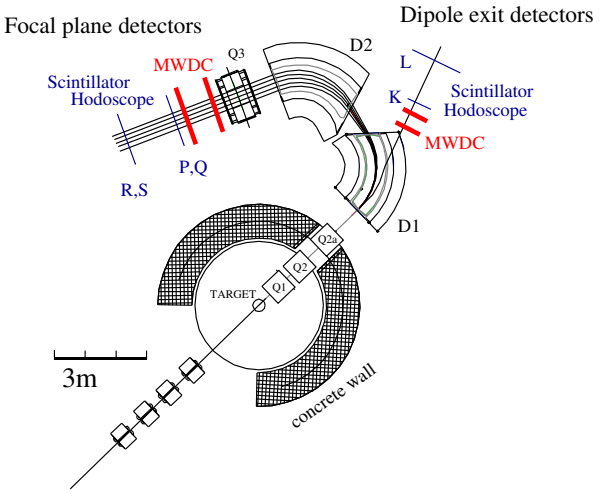

Fig. 6: External target station with magnetic spectrograph Big Karl. The quadrupole magnets are labeled by Q1, Q2, Q2a, and Q3, the dipole magnets by D1 and D2. An exit port at the first dipole side yoke allows one to dump the beam in a block of concrete shielded iron (not shown). Behind the quadrupole magnet Q3 is the focal-plane area with detectors discussed in the text.

The angular acceptance of the spectrometer is extended by the germanium wall which consists of four annular detectors made from high purity germanium. The first detector (Quirl) has Archimedes' spirals with opposite orientation on the front and the rear side. It yields a ΔE signal as well as the position. The following detectors have wedge structures and serve as calorimeters.

Another detector at Big Karl is ENSTAR. It has a cylindrical arrangement of scintillators — read out by optical fibers — in three layers around the target. A proposed GEM experiment foresees the coincidence measurement of ^{3}He with BIG KARL and decay products of η-mesic nuclei in the new ENSTAR detector. The whole detector mounted around the target is shown in Fig. 7.

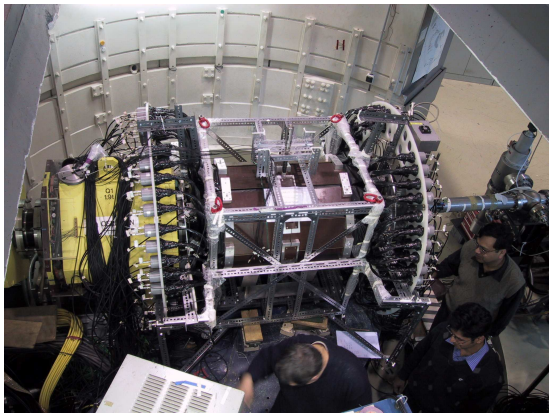

Fig. 7: Upper: Front side of the ENSTAR detector. The thick pieces with triangular shape belong to the outer layer. The ring supports the phototubes. Lower: The ENSTAR detector installed at the target position. The beam enters from the right.

In a test run the ENSTAR detector was exposed to reaction products from $pp \rightarrow pp$, $pp \rightarrow d\pi^+$ and $p^{12}C \rightarrow pX$ at a beam momentum of 870 MeV/c. The second reaction was employed to set up the coincidences between BIG KARL focal plane detectors and ENSTAR. The third was used to study the particle identification properties of ENSTAR: a delayed start as well as the stop signal were generated by ENSTAR. In addition to a peak, mainly from protons, the decay curve of positively charged pions has been found. A fit of an exponential yielded a life time of 26 ns which is the particle data book value. The detector is now ready to take data.

1.2.2 COSY-TOF

The physics goal of the COSY-TOF Collaboration is the examination of particle production in proton-proton and proton-deuteron collisions from threshold up to some 100 MeV excess energy. Due to the kinematical completeness of the measurements the full set of variables can be determined, including total and differential cross sections, angular distributions, and Dalitz plots.
The time-of-flight spectrometer TOF is a detector at an external beam line of the Cooler Synchrotron COSY. *pp* and *pd* reactions are examined by determining the velocities and directions of charged particles in the final state. The target contains liquid hydrogen or liquid deuterium. The implementation of a polarized target is under way, as described in section 7.1.3. The detector is realized as a cylindrical vacuum vessel. Particle velocities are determined from the time difference between start and stop scintillators and the length of the flight path. The time-of-flight can be measured with an accuracy of 250 ps. The stop scintillators cover the inner surface of the vessel within the cylindrical form (barrel detector) as well as on the end cap (central hodoscope and ring hodoscope). The target is located in the vacuum vessel. Particles emerging in forward direction will penetrate the start detectors. Two start counter systems can be installed alternatively. One system is optimized for minimum radiation length: a ring of 0.5 mm thick scintillators is read out via hollow light guides (start system 1). A second system is used, when particles are to be measured which decay into charged particles shortly behind the target. Using a highly segmented annular silicon microstrip detector and two fiber hodoscopes with crossed layers of scintillating fiber, the tracks of the secondary particles can be determined precisely enough to calculate the decay vertex (start system 2). Behind the vacuum tank, a wall of thick scintillation counters can be used for neutron detection. The end caps can be attached either concave or convex, so that distances between the target and the central hodoscope ranging from 0.5 m to 10 m can be realized .
In order to probe the existence of the pentaquark state Θ^+, for which evidence was seen in an earlier COSY-TOF experiment (see section 2.3), the collaboration concentrated on the completion of a high-statistics experiment. Improved tracking was accomplished by an additional layer of fibers in one of the hodoscopes (Fig. 8).

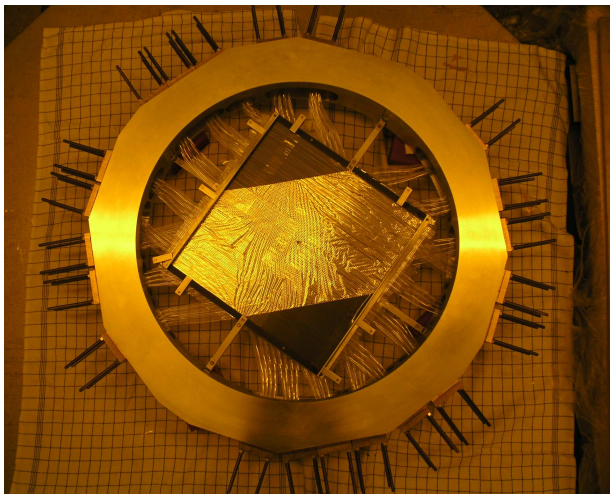

Fig. 8: At the University of Erlangen, a new layer was added to this fiber hodoscope.

1.2.3 JESSICA

The JESSICA experiment is a full scale mock-up of the ESS (European Spallation Source) target-moderator-reflector assembly. Because of the low proton beam intensity COSY is particularly suitable for studying the neutronic performance of advanced moderators, because radiolysis and activation levels are negligible. Furthermore the neutronic performance can be studied and the gathered data can be linearly scaled to higher beam intensities as they will be available in high power spallation neutron sources. The experiment uses a proton beam with a kinetic energy of 1.3 GeV, a pulse length of about 0.5 μs, a repetition rate of 0.05 Hz and an intensity up to 10^9 protons per pulse. To extract such a short pulsed beam, which was beyond the initial design of COSY, a fast kicker extraction has been developed. The proton beam hits the liquid-metal target containing 35 l mercury and thereby causes a hadronic cascade which leads to the emission of neutrons. The reflector consists of lead rods filling 80 % of the volume. Inside the reflector four moderators are positioned, two above and two below the target. One moderator is used for experiments and can be filled with different moderator materials and can be operated at any temperature between 10 K and 300 K. The arrangement of the experiment with its devices is shown in Fig. 9.
The characteristic of a moderator material can be investigated by determining the energy spectrum of as well as the thermalization time of the neutrons leaving the moderator surface. By moving a graphite crystal into the neutron beam neutrons with a specific energy can be separated from the neutron beam by Bragg reflection. The time-of-flight spectrum of the these neutrons can be used to determine the pulse width and decay constants in order to characterize the pulse structure which is important for the design of neutron scattering instruments at pulsed spallation neutron sources. JESSICA is a unique experiment for moderator research because it is able to measure

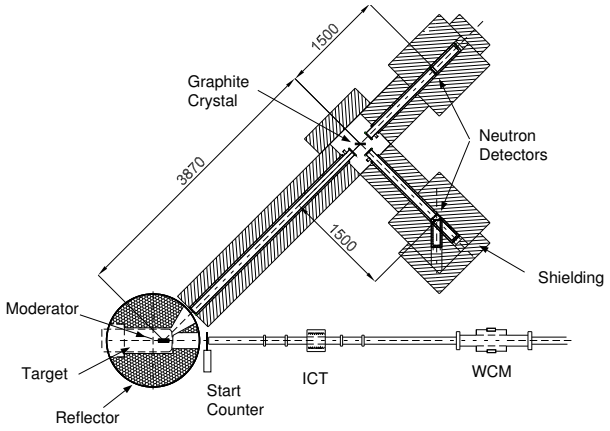

Fig. 9: Schematic drawing of the experimental setup of the JESSICA experiment with proton beam monitors (ICT, WCM), start counter, neutron detectors, analyser crystal, and target-moderator-reflector assembly.

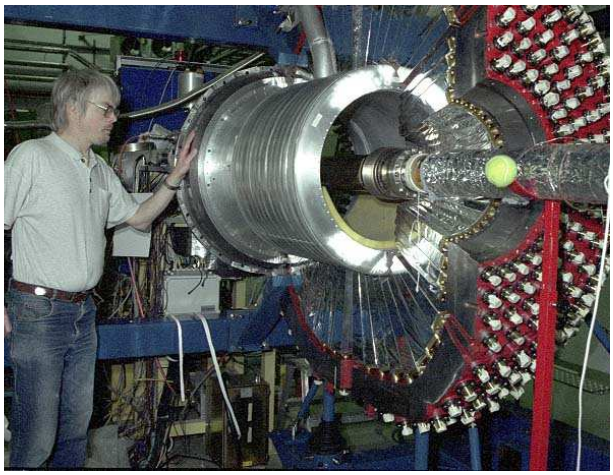

Fig. 10: The open WASA detector during installation at CELSIUS. The superconducting solenoid is surrounded by two half-spheres with CsI crystals inside the magnetic field return yoke (red).

the number of incident protons per pulse. This opens the possibility to normalize the experimental data on an absolute scale and allowing the validation of radiation transport codes and new developed neutron scattering law data S(α,β,T). α denotes the impulse transfer of the neutron and β the energy transfer of the neutron to the molecule at a given temperature T.

1.3 WASA at COSY

The WASA detector ("Wide Angle Shower Apparatus", see Fig. 10) is currently installed at the CELSIUS facility in The Svedberg Laboratory (TSL), Uppsala Sweden. This 4π detector was built in the 1990s by a Swedish-Polish-German-Russian-Japanese collaboration with the aim of studying rare reactions and decays. After the end of the experimental program at CELSIUS in summer 2005, the device will be relocated to COSY.

Early measurements with a subset of the WASA detector have produced a lot of new data close to threshold energies in pp and pd collisions for single and double pion, as well as η production. These data have given new information on the importance of different nucleon resonances and their excitation modes. The current experiments with the full 4π WASA detector include further meson production channels as well as a search for the Θ^+ resonance. In addition medium rare decay channels of the η are investigated in terms of Dalitz distributions.

While CELSIUS delivers maximum beam momenta of 2.1 GeV/c, COSY offers significantly higher momenta up to 3.7 GeV/c with polarized and phase-space cooled proton and deuteron beams, thus well above the threshold for η′ production in pp interactions. WASA is a large acceptance detector for neutral and charged ejectiles from hadron-induced interactions. Almost any final state of pN, pd and dd reactions can be detected with large efficiency, resulting in a major expansion of the experimental potential both of WASA and COSY, where a photon detector has been missing up to now. The WASA target consists of a beam of frozen hydrogen or deuterium pellets of about 25 μm diameter, allowing luminosities of up to 10^{32} cm^{-2}s^{-1} in interactions with the circulating beam in COSY.

The primary physics objectives for WASA at COSY will be tests of fundamental symmetries (C, P, T and their combinations) via η and η′ decays and the investigation of low-energy QCD which is governed by the broken chiral and isospin symmetries. The latter is related to the mass difference of the up and down quarks. Further topics for WASA will be searches for and investigation of (crypto-) exotic hadrons, such as the light scalar mesons $a_0/f_0(980)$, Pentaquarks like the Θ^+ and hyperon resonances.

The decays of η and η′ mesons are a testing ground for symmetry breaking. Issues like C-, P-, T-, isospin- and SU(3)-symmetry breaking, the pseudoscalar mixing angle, and the structure of the η′ can be addressed. At COSY more than 10^6 η′ mesons can be produced per day and their subsequent hadronic, radiative, leptonic, and forbidden decays can be detected with WASA. The expected event rates will substantially improve the quality of the world data set.

Meson production in isospin-selective reactions, like $dd \rightarrow \alpha X$, is well suited to search for isospin-violating processes. If a system X with isospin I=1 is observed in this reaction isospin symmetry must be violated. Pioneering measurements have been performed at the Indiana Cooler on the reaction $dd \rightarrow \alpha\pi^0$. At COSY such studies can be extended to higher energies and, in particular, to the reaction $dd \rightarrow \alpha\pi^0\eta$, which should be driven by the isospin-violating a_0-f_0 mixing.

The WASA-at-COSY project is a cooperative effort of many institutions, in particular TSL and FZJ. The collaboration currently comprises 137 members from 24 insti-

Fig. 11: The COSY accelerator hall. The arrow indicates the future position of WASA in one of the straight sections of COSY.

tutes in 7 countries. WASA will be shipped to Jülich in autumn 2005 and the experimental program is expected to start in the beginning of 2007. Further details about the project and the planned physics programme can be found in the proposal for “WASA at COSY” (nucl-ex/0411038) or on the web page of the collaboration http://www.fz-juelich.de/ikp/wasa.

2 Major Physics Results at COSY

COSY has been operated for 31 weeks in 2004 for experiments, exploiting both polarized and unpolarized proton and deuteron beams (see Appendix D). Investigations, ranging from spallation reactions in proton-nucleus reactions, over meson production in both pp and pA interactions, to searches for the asserted pentaquark state have been conducted. Since there is a long lead time between data taking and analysis, almost no final results from these measurements are available but (mostly) from earlier years. Many of the results which are presented here are preliminary since they have not been published yet.

Unlike the years before we have arranged the following sections according to the physics, and not the detection system they have been obtained at. Naturally, each of the described physics issues can be addressed by measuring different processes. Thus in most cases different detectors have been employed, depending on the particles involved and the reaction kinematics.

η and η' physics: ANKE and COSY-11 have been used for the measurement of η/η'-production processes following pp, pd and dd collisions. These investigations will be continued at WASA (with focus on rare η and η' decays) and BIG KARL (η-mesic nuclei).

Investigation of light scalar mesons: ANKE is being used for measuring the $K\bar{K}$ decay channels of the $a_0/f_0(980)$. Later the $\pi\eta$ decays will be measured at WASA in order to investigate the isospin-violating a_0/f_0 mixing.

$K\bar{K}$ and ϕ-meson production: Measurements of the $pp \to ppK^+K^-$ reaction have been carried out at COSY-11 (below the ϕ threshold) and ANKE (above) .

Pentaquark searches: In 2004 the search for the Pentaquark Θ^+ continued at COSY-TOF. Double polarization measurements are being prepared here (see section 7.1.3) aiming at the parity determination of the Θ^+. WASA will allow for systematic studies of neutral decay channels of possible Pentaquark states.

Kaons in the nuclear medium: The K^+ in-medium production has been measured at ANKE. It is planned to extend these studies to K^+K^-- and ϕ-meson production.

Few-body physics: The measurements have been carried out at ANKE and BIG KARL. After installation of the polarized internal target (see section 7.1.1) these studies will be continued at ANKE in double-polarization experiments.

2.1 η and η' Physics

Experimental studies of η- and η'-production both in photon- and hadron-induced reactions has successfully increased the data base in the last few years. Near threshold, η-production differs considerably from pion production due to the strong coupling of the $S_{11}(1535)$ resonance to the η-nucleon decay channel. This leads to threshold enhancements of the η-production cross sections which are compatible with a rather large η-nucleon scattering length of 0.4 fm. Threshold enhancements persist in few-nucleon systems and have been the basis of speculations concerning the existence of bound η-nucleus systems. The η'-proton interaction near threshold appears to be much weaker than the η-proton interaction.

The main obstacle for experimental studies involving *neutral* ground state mesons is their too short life-time which prohibits their utilization as secondary beams. However, the study of their interaction with hadrons is accessible via the influence on the cross sections and excitation functions of production reactions (*e.g.* $NN \to NN\,meson$). The influence of the relatively weak nucleon-meson interaction may be magnified when producing the meson in the vicinity of two (or more) nucleons.

2.1.1 η and η' Production in pp Collisions

Precision data on the $pp \to pp\eta$ (η') reaction obtained with a stochastically cooled proton beam and the COSY-11 spectrometer allow for the comparison with predictions based on a homogenously populated reaction phase space. The energy dependences of the total cross sections are presented in Fig. 12. Comparing the data to the arbitrarily normalized phase space integrals (dashed lines) reveals that for both reactions the final-state interactions enhance the total cross section by more than an order of magnitude at low excess energies.

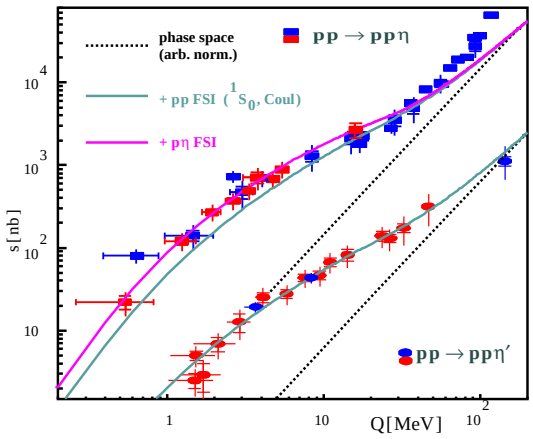

Fig. 12: Excitation functions of the reactions $pp \to pp\eta'$ and $pp \to pp\eta$. Red data points denote COSY-11 results.

While the η' production data are well described (light blue solid line) by the modulation of the phase space with the pp-FSI, in case of the η-meson the interaction

between the nucleons is evidently not sufficient to reproduce the increase of the total cross section for very low excess energies and above ≈ 60 MeV, as can be concluded from the comparison of the data and the upper blue line in Fig. 12. This line was normalized to the data in the excess-energy range between 15 and 40 MeV. The enhancement of the total cross section for higher energies can be assigned to the onset of higher partial waves. The discrepancy closer to threshold can be explained by the influence of the attractive η-proton interaction. A similar effect close to threshold has also been observed in photo-production data, $\gamma\, d \to p\, n\, \eta$, indicating that the phenomenon is independent of the production process but rather related to the η-nucleon interaction.
The violet line in Fig. 12 corresponds to a simple phenomenological model based on the factorization of the transition amplitude into the constant primary production and the on-shell incoherent pairwise interaction among the outgoing particles.

2.1.2 η Mesons in Few-body Systems

The COSY-11 facility also permits to study meson production in the three nucleon system for investigation of the reaction mechanisms and the meson-^{3}He interaction. As an example Fig. 13 shows the production amplitude for the $pd \to {}^3\mathrm{He}\eta$ reaction. The COSY-11 data (red points) strongly supports the fit using a Watson factor for the ^{3}Heη-FSI with the scattering length $a(\eta{}^3\mathrm{He}) = (3.3 + i1.5)$ fm (solid line in Fig. 13) and only weak contributions from a production according to the resonance model (dashed line).

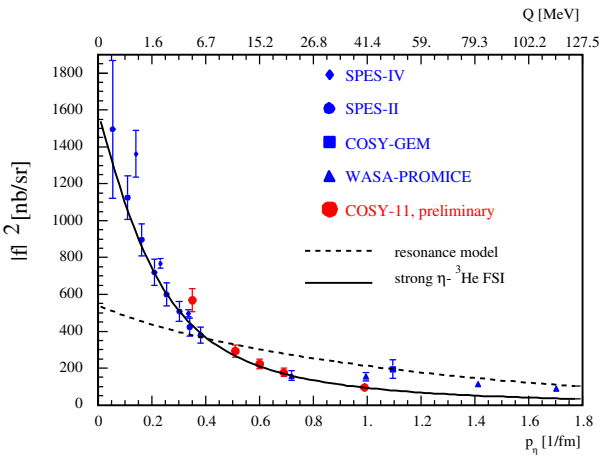

Fig. 13: Average squared production amplitude as a function of the η cm-momentum for the $pd \to {}^3\mathrm{He}\eta$ reaction.

Since He-η bound states can exist in S-wave only, one important quantity is the η-nucleus S-wave scattering length. In order to determine its value the contribution of the S-wave amplitude to the total cross section must be known. This requires the precise measurement of angular distributions.
For the ^{4}Heη system angular distributions have not been successfully measured yet and the existing data on the total cross section cover only energies up to $Q = 8$ MeV. Consequently, for the analysis of these data (left spectrum of Fig. 14) and the extraction of the scattering length a dominant S-wave contribution had to be assumed.

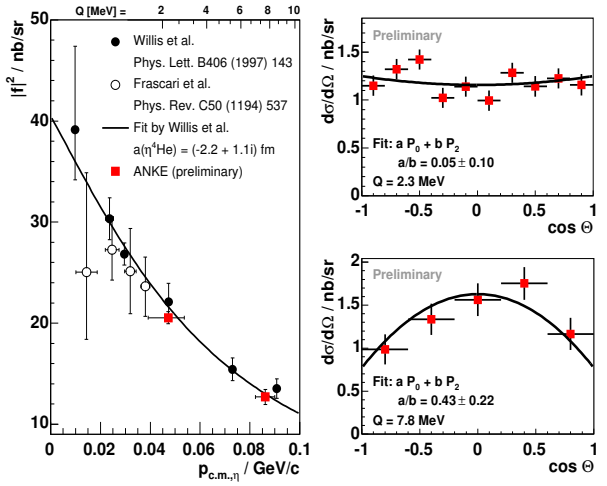

Fig. 14: Preliminary results of the $dd \to {}^4\mathrm{He}\eta$ measurement at ANKE. Left: Production amplitude squared versus η momentum in c.m.. Right: Angular distributions. The solid lines show a fit with a combination of the Legendre polynomials P_0 and P_2. Only statistical errors are plotted.

In order to improve the experimental situation, the reaction $dd \to {}^4\mathrm{He}\eta$ has been measured with ANKE at $Q = 2.3$ and 7.8 MeV and, more recently, at $Q = 22$ and 43 MeV. For the first two Q values preliminary results are shown in Fig. 14. The total cross sections are in good agreement with the existing data and the angular distribution at lower energy is consistent with S-wave production. However, already at $Q = 7.8$ MeV the data show a significant contribution from higher partial waves.

2.2 Scalar and Vector Mesons

2.2.1 Light Scalar Mesons

An experimental program is under way at COSY aiming at the investigation of the light scalar mesons $a_0/f_0(980)$ with ANKE — and later with WASA. The final goal of the measurements is to determine the isospin-violating (IV) a_0-f_0 mixing amplitude from a measurement of the IV reaction $dd \to \alpha(\pi^0\eta)$. This quantity is expected to be a measure of the $K\bar{K}$ content of these states which is largely unknown.
At COSY, the a_0 and f_0 resonances can selectively be produced since the isospin in the initial system can be chosen: a $pp \to dX$ reaction must lead to a_0^+ $(I = 1)$ production whereas a $dd \to \alpha X$ process — neglecting small IV contributions which are the final goal of this program — is a filter for the f_0 $(I = 0)$ resonance.
Both, the a_0 and the f_0 can decay into $K\bar{K}$, whereas in the non-strange sector the decays are into different final states according to their isospin, $a_0^{0,\pm} \to (\pi^{0,\pm}\eta)_{I=1}$ and $f_0 \to (\pi\pi)_{I=0}$. Thus, only by measuring the non-strange

decay channels IV effects can be investigated. Such measurements are planned for WASA at COSY. Measurements of the $K\bar{K}$ final state with at least one charged kaon have already been performed at COSY with magnetic spectrometers.

Three experimental runs on the reactions $pp \to dK^+K^0/d\pi^+\eta$ (at an excess energy of $Q = 48$ MeV) $pp \to dK^+K^0$ (105 MeV) and $pn \to dK^+K^-$ have been performed at ANKE during the years 2001–2004. The data from the first experiment have been analyzed and reveal a dominance of K^+K^0 production in the a_0 channel with a cross section of about 30 nb, thus demonstrating the feasibility of scalar-meson studies at COSY.

The analysis for the $\pi^+\eta$ final state is affected by the small (forward) acceptance of ANKE for this reaction and by the fact that the η meson can only be identified by a $d\pi^+$ missing-mass criterion. Nevertheless, employing a dynamical model for the a_0^+ production allows one to deduce a total cross section of $\sigma(pp \to da_0^+ \to d\pi^+\eta) = (1.1 \pm 0.3_{\mathrm{stat}} \pm 0.7_{\mathrm{sys}})$ μb for the production of $\pi^+\eta$ via the scalar $a_0^+(980)$ resonance and $\sigma(pp \to d\pi^+\eta) = (3.5 \pm 0.3_{\mathrm{stat}} \pm 1.0_{\mathrm{sys}})$ μb for the non-resonant production. Data of significantly higher quality can be obtained with the WASA detector which will offer a larger angular acceptance and η identification by detecting decay photons.

The ANKE data on the $dK^+\bar{K}^0$ final state not only allow one to study the K^+K^0 system but have also been analyzed in terms of the dK^0 interaction. This FSI reflects itself in a modification of the invariant dK^0 mass distribution which has been fitted within the Watson-Migdal approach. This fit — when jointly analyzed with K^-p and K^-d scattering data — favors a small dK^0 scattering length, $\mathrm{Im}a_{\bar{K}d} \leq 1.3$ fm and $|\mathrm{Re}a_{\bar{K}d}| \leq 1.3$ fm, see Fig. 15.

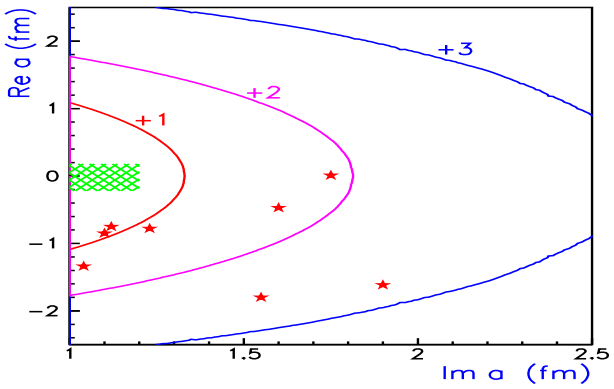

Fig. 15: Real *vs.* imaginary part of the $d\bar{K}^0$ scattering length. The contour lines ($\chi^2 + 1, +2, +3$) show a fit to $pp \to dK^+K^0$ data from ANKE for $Q = 46$ MeV. The best fit is indicated by the green area. Red stars denote results from model calculations found elsewhere in literature.

As the next step the reaction $dd \to \alpha K^+K^-$ will be measured at ANKE. These data are a necessary prerequisite for the $dd \to \alpha(\pi^0\eta)$ measurements with WASA since they provide the cross section for the isospin-allowed f_0 production. Furthermore, information about the $K^-\alpha$ scattering length can be expected and the data might be sensitive to the (non-) existence of narrow $K^-\alpha$ bound states which have been claimed in literature.

2.2.2 $K\bar{K}$ and ϕ Mesons

The analysis of the COSY-11 data on the $pp \to ppK^+K^-$ reaction, as shown in Fig. 16, revealed that for the ppK^+K^- system the influence of the mutual interaction among final state particles seems to be much stronger than observed for the $pp\eta$ and $pp\eta'$ systems, see section 2.1.1.

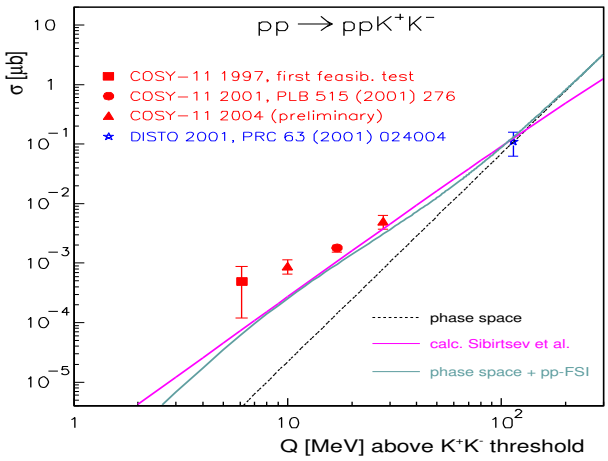

Fig. 16: Excitation function for the $pp \to ppK^+K^-$ reaction.

At $Q = 10$ MeV, the data differ from the phase-space predictions by about one order of magnitude in case of the η'. This can be fully related to the pp-FSI but almost two orders of magnitude in the case of the K^+K^- production cannot be explained by the pp-FSI alone (solid red line in Fig. 16). Yet the univocal explanation for the strong rise of the cross section at threshold awaits further theoretical analysis. The observed discrepancy may shed new light on the long standing question concerning the study of the interaction between K^+ and K^- mesons, related to the investigations of the nature of the scalar mesons a_0/f_0. Furthermore, within this channel, the pK^- interaction can be studied which is strongly related to the $\Lambda(1405)$.

The reaction $pp \to pp\phi$ has been studied with ANKE at excess energies Q = 19, 35, and 76 MeV by detecting the K^+K^- decay mode of the ϕ-meson. At each of these excess energies about 200–300 ϕ mesons have been identified. Figure 17 shows the efficiency corrected K^+K^- invariant mass distributions Q = 19 and 35 MeV as well as the total ϕ cross sections for all three energies. The ANKE data point at $Q = 76$ MeV is close to the one from DISTO measured at $Q = 83$ MeV.

In addition to the information on the energy dependence of ϕ production, the ANKE data will also provide — in combination with SPES-III and COSY-TOF (section 2.2.3) results on ω production — the ϕ/ω cross-section ratio below the existing DISTO measurements.

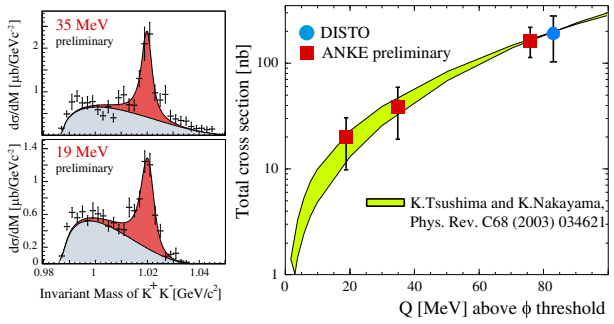

Fig. 17: (a) and (b) efficiency corrected K^+K^- invariant mass distributions at excess energies of 19 and 35 MeV. The blue-shaded areas indicate the non-resonant contributions based on four-body phase space. The total distribution is the sum of non-resonant and φ meson production (red area) including the detector resolution. In (c) the total φ cross sections from ANKE are shown together with the DISTO point. The error bars include the systematic uncertainties.

The Okubo-Zweig-Iizuka (OZI) rule states that processes with disconnected quark lines in the initial or final state are suppressed. Accordingly, the production of φ mesons from initial non-strange states is expected to be substantially suppressed relative to ω meson production. The cross-section ratio for φ and ω meson production under similar kinematical conditions should then be in the order of $R_{\mathrm{OZI}} = \sigma_\phi/\sigma_\omega = tan^2\alpha_V = 4.2 \times 10^{-3}$ where $\alpha_V = 3.7^\circ$ is the deviation from the ideal φ-ω mixing angle. However, specific channels in $p\bar{p}$ annihilation have observed values of $R_{\phi/\omega}$ that exceed the limit given by the OZI rule by up to two orders of magnitude. Almost all of the existing data from pp and πN interactions as well as in mesonic and radiative decays indicate a φ-to-ω ratio of $3 \times R_{\mathrm{OZI}}$. Only the ratio derived from φ meson production measured at DISTO at $Q = 83$ MeV shows a 7 times larger value than R_{OZI}. The new ANKE results on φ meson production confirm the enhanced ϕ/ω ratio at $Q \sim 80$ MeV. The ANKE φ-to-ω ratio at $Q = 19$ MeV is $3 \times R_{\mathrm{OZI}}$ and thus significantly smaller than at the DISTO excess energy.

2.2.3 ω Production

The COSY-TOF studies on meson producing reactions have recently been focussed on the $pp \to pp\omega$ channel. Detecting the two protons and the charged pions of the $\omega \to \pi^+\pi^-\pi^0$ decay, the events of interest could be separated from the dominating physical background of ρ-production by means of the missing mass technique. As a result total cross sections as well as angular distributions could be obtained for excess energies of $Q = 93$ and 173 MeV. An important aspect of these studies stems from the still not quite solved question of the validity of the OZI-rule. A likely explanation for the large violation of the OZI-rule at $Q \sim$90 MeV is that different partial waves contribute to the reaction. However, this assumption has to be ruled out based on the analysis of the angular distributions from COSY-TOF and DISTO. The angular distributions for both mesons shown in Fig. 18 are essentially isotropic.

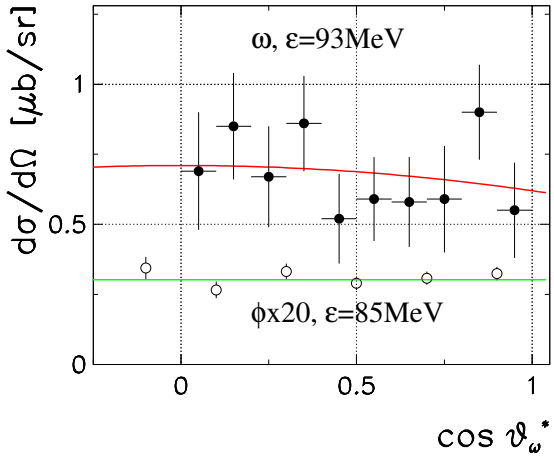

Fig. 18: Comparison of ω and φ angular distributions in their respective CM-systems. The DISTO data have been scaled by a factor of 20.

2.3 Pentaquark Search

In 2004, the COSY-TOF collaboration published evidence for a narrow resonance in the K^0p system of the reaction $pp \to \Sigma^+K^0p$, which could be the hypothetical pentaquark state Θ^+. In order to get precise information about the existence or non-existence of this state the collaboration concentrated on the preparation and accomplishment of a new measurement of this reaction with an improved detector and better statistics. For more accurate tracking, a further layer of a fiber hodoscope was installed, see section 1.2.2.

During seven weeks of beam time at COSY, more than 10^9 events with a trigger condition for two charged tracks in the start counters and four charged tracks in the stop counters were recorded. Online control of the data was performed by reconstructing $pp \to \Lambda K^+p$ events, which are triggered by the same conditions as the Σ^+K^0p events. In Fig. 19, the missing mass spectrum of K^+p, obtained within 4 hours, is shown. A clear Λ peak is visible.

At least a factor 5 better statistics compared to the 2004 published COSY-TOF data can be expected by an extrapolation of the number of measured Λ reactions to the total beam time.

Forthcoming activities are trying to pin down the quantum numbers of the Θ^+. In particular, the parity has not yet been determined experimentally and theoretical predictions allow for both possibilities. It is of utmost importance to determine $\pi(\Theta^+)$ to further constrain the internal dynamics and structure of this exotic state. The measurement requires transverse polarized protons in the initial state provided by a polarized beam and a polarized target,

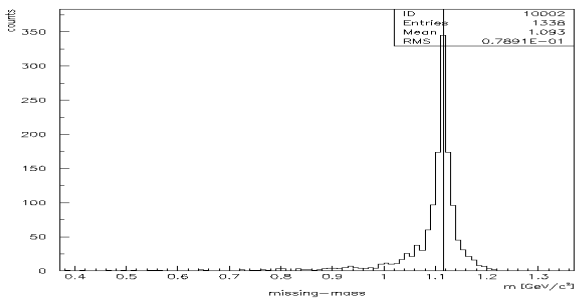

Fig. 19: Online missing mass distribution of K^+p from the reaction $pp \to K^+pX$ showing a clean Λ signal.

respectively. The implementation of a polarized target is under way, as described in section 7.1.3.

2.4 Kaons in the Nuclear Medium

The measurement of proton-induced K^+-meson production in nuclei was one of the primary goals for building the ANKE spectrometer. In particular, ANKE allows for the measurement of low momentum kaons down to ∼150 MeV/c. The inclusive measurements have been finalized and double differential cross sections at forward angles ($\theta_{lab} < 12°$) are now available for beam energies T_p ranging from 1.0 to 2.3 GeV and C, Cu, Ag and Au as target nuclei. These data yield information about the K^+ production processes and about the in-medium properties of the K-mesons at normal nuclear density $\rho = \rho_0$.

A direct comparison of the cross sections from ANKE data with those from the literature is not possible since the different data sets have been obtained for non-overlapping kinematic parameters (*i.e.* beam energies, kaon emission angles and momenta). Thus a parameterization has been invented, describing the invariant cross sections in terms of few Lorentz-invariant variables Δm (excitation energy of the target nucleus plus m_Λ), s (total energy), t (4-momentum transfer):

$$E\frac{d^3\sigma}{d^3p} \propto \Delta m^{N_0} \cdot \left(\frac{s}{s_0}\right)^{b_0 t}.$$

The parameters N_0, s_0, and b_0 have been obtained from a fit to the available data which is shown in Figure 20.

The Figure shows that the ANKE data taken at $T_p = 1.0$ GeV reach down very closely to the kinematic limit at $\Delta m = m_\Lambda$. Here only a Λ-Hyperon is produced and no energy can be transferred to excite the target nucleus. The initial target nucleus must take part in the reaction as a whole such that the effective target mass is $12 \cdot m_N$. An analysis of the 1.0 GeV momentum spectrum within a simple phase-space approach, in fact, revealed strong collective phenomena in the target nucleus: up to 6 nucleons must take part in the reaction or, alternatively, high intrinsic nucleon momenta (∼550 MeV/c) must be involved.

The different slopes below and above the free NN threshold ($T_p = 1.58$ GeV corresponding to $\Delta m \sim 2.0$ GeV/c^2)

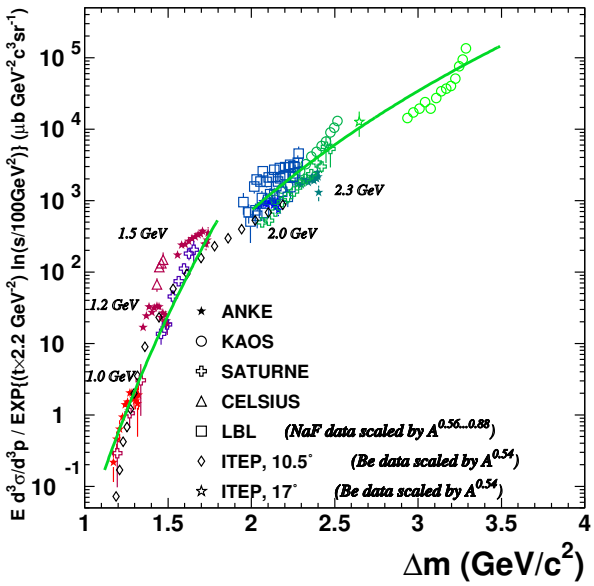

Fig. 20: World data set on inclusive kaon production in $pC \to K^+X$ reactions. The invariant cross sections - normalized by $(s/s_0)^{b_0 t}$ - are plotted as a function of the excitation energy Δm. The results of the fit – which allows to describe all data within a factor $\sim 2-3$ – using the above mentioned formula is shown by the solid green lines. The beam energies for the ANKE data are indicated.

indicate a change of the dominant K^+-production mechanism. This interpretation is in line with results of microscopical model calculations and recent K^+d coincidence measurements with ANKE. These show that below threshold the kaons are dominantly produced in two-step reactions with intermediate-pion formation, whereas at higher energies direct K^+ production on a single nucleon prevails.

Another important result from ANKE is that the low momentum part of the kaon spectra allows one to deduce the in-medium potential of K^+ mesons at $\rho = \rho_0$ with high accuracy. A value of $V_K = (22 \pm 3)$ MeV has been deduced. Corresponding measurements for K^--mesons are in preparation.

2.5 Few-Body Physics

2.5.1 d Breakup at High Momentum Transfer

The structure of the lightest nuclei at short distances ($r_{NN} < 0.5$ fm) or high relative momenta ($q > 1/r_{NN} \sim 0.4$ GeV/c) constitutes a fundamental problem in nuclear physics.

Recently, the unpolarized cross section of the $pd \to (pp)n$ reaction was measured at proton beam energies $T_p = 0.6 - 1.9$ GeV under kinematic conditions similar to backward pd elastic scattering with formation of a fast diproton in a $^1S_0$ state at low excitation energy ($E_{pp} < 3$ MeV). The analysis of the $pd \to (pp)_{^1S_0}n$ cross section,

based on a model for the $pd \to dp$ process, includes the one-nucleon exchange (ONE), single scattering (SS), and double pN scattering with excitation of a $\Delta(1232)$ isobar. The analysis employs modern NN potentials, *e.g.* CD-Bonn. A reasonable agreement with our data is achieved. In contrast, the widely used NN potentials like the Paris and especially the Reid Soft Core (RSC) potential lead to a strong disagreement with the data. This discrepancy can be traced back to a different high momentum behavior of the NN wave function.

New information about this reaction can be obtained from measurements of polarization observables. As a first step, the vector analyzing power A_y at T_p = 0.5 and 0.8 GeV of the reaction $\vec{p}d \to (pp)_{^1S_0}n$ has been determined. The experiment was performed at the ANKE spectrometer with about $3 \cdot 10^9$ stored protons vertically polarized. The beam polarization at T_p = 0.8 GeV was determined from precise pd-elastic analyzing power data. Since data at 0.5 GeV are not available, we resorted to the polarization export technique to obtain a calibrated polarization for 0.5 GeV.

Protons from the breakup reaction with $E_{pp} < 3$ MeV are detected from $\theta_{lab} = 0^\circ$ to 6.5° at both energies, the polar angles of the proton pairs range from $\theta_{cm} = 0^\circ$ to 14°. At both energies, the missing mass peak is observed at the neutron mass with (rms) peak widths of 16 MeV/c^2 (T_p = 0.5 GeV) and 20 MeV/c^2 (T_p = 0.8 GeV). The values of A_y in $\vec{p}d \to (pp)n$ at 0.5 and 0.8 GeV are shown in Fig. 21 as function of $\theta_n^{\text{c.m.}}$.

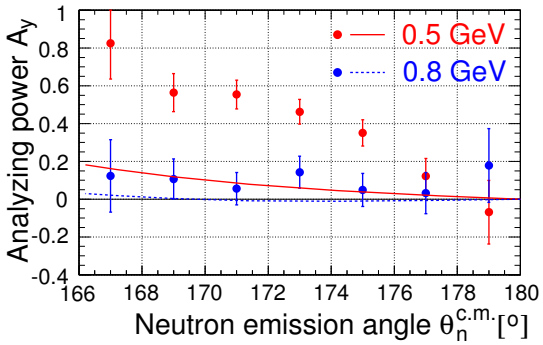

Fig. 21: Vector analyzing power A_y as function of the neutron polar angle $\theta_n^{\text{c.m.}}$ for T_p = 0.5 and 0.8 GeV. The lines show predictions for A_y from the ONE+SS+Δ model, with the CD-Bonn potential.

The measured A_y is almost zero at 0.8 GeV, in agreement with the predictions of the ONE+SS+Δ model. The increase of A_y with decreasing energy from 0.8 to 0.5 GeV is expected from the ONE+SS+Δ model. However, the magnitude is grossly underestimated. Different NN-interaction potentials (RSC, Paris) do not improve the description. Further insight into the deuteron breakup process at high momentum transfer can be expected from a measurement of the tensor analyzing power T_{20} in $p\vec{d} \to (pp)_{^1S_0}n$, in preparation at ANKE.

2.5.2 The Charge-Exchange Reaction $\vec{d}p \to (pp)n$

Using the polarized deuteron Charge-Exchange (CE) break-up reaction $p(\vec{d},2p)n$, where the final protons are in the $^1S_0$ state, one can access the spin-dependent amplitudes of the elementary np elastic scattering. For collinear kinematics one can directly reconstruct the two spin amplitudes by measuring the cross section and the analyzing power T_{20}.

The first test measurement was carried out at ANKE using a polarized deuteron beam at $p_d = 2400$ MeV/c.

Using the $\vec{d}p \to dp$, $\vec{d}p \to (2p)n$, $\vec{n}p \to d\pi^0$, and $\vec{p}d \to {}^3\text{He}\pi^0$ reactions, which all have large and well determined analyzing powers, a simultaneous calibration of the vector and tensor components of the polarized deuteron beam at COSY becomes possible for the first time. The average of the two ANKE measurements is $\alpha_z^{\text{ANKE}} = 0.72 \pm 0.02$, which is compatible with EDDA. However, the ANKE mean tensor parameter, $\alpha_{zz}^{\text{ANKE}} = 0.52 \pm 0.03$, is about one standard deviation lower than EDDA.

The $(\vec{d},2p)$ CE process was identified from the missing mass with respect to the proton pairs and time difference information. The spectra for all spin modes reveal a well defined neutron peak with a mean value of $M_X = 940.4 \pm 0.2$ MeV/c^2. The background was less than 2% and stable, so that the charge-exchange process could be reliably identified.

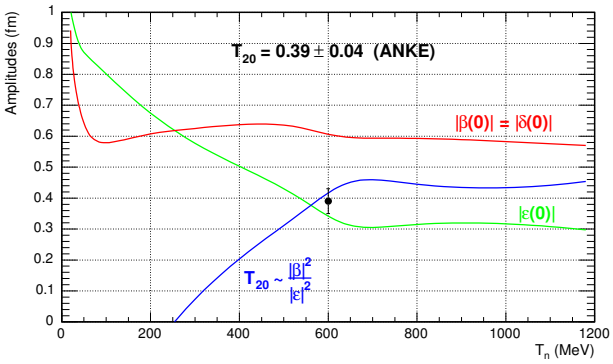

Fig. 22: Predictions for the moduli of the two independent $np \to pn$ scattering amplitudes at $t = 0$, taken from the SAID database, along with the associated prediction of T_{20} for $\vec{d}p \to (pp)(pp)_{^1S_0}n$ in impulse approximation. The latter is compared to our preliminary value of $T_{20} = 0.39 \pm 0.04$ at $\frac{1}{2}T_d = 600$ MeV.

Figure 22 shows predictions for the values of the moduli of the two forward spin-flip amplitudes, as functions of energy. In impulse approximation the forward differential cross section is proportional to $2|\beta(0)|^2 + |\varepsilon(0)|^2$ times form factors. In the region $E_{pp} \leq 2$ MeV, the final pp system is essentially pure S-wave and acceptance corrections largely cancel out for the analyzing powers. Thus, in the forward direction,

$$T_{20} = \sqrt{s}\left(\frac{|\beta(0)|^2 - |\varepsilon(0)|^2}{2|\beta(0)|^2 + |\varepsilon(0)|^2}\right)$$

so that the ratio of the two forward spin-dependent $np \to pn$ amplitudes can already be deduced from our preliminary results.
The energy dependence of the predicted T_{20} using the SAID input is also shown in Fig. 22, along with our value of $T_{20} = 0.39 \pm 0.04$. Alternatively, using this value, we obtain $|\beta(0)|/|\varepsilon(0)| = 1.86 \pm 0.15$, to be compared to SAID 1.79 ± 0.27. Thus, our statistical error is already superior.

2.5.3 *p-n* Final State Interactions

The question to which extend the spin-singlet, isospin-triplet state contributes to the *p-n* interaction in final state interactions (FSI) is a long standing problem. From low energy neutron scattering on protons it is known that the deuteron (isospin-singlet, $J = 1$, $l = 0$ and $l = 2$) is the only bound *p-n* state. The spin-singlet, isospin-triplet state is unbound with a resonance around 68 keV. A useful way of trying to extract the spin-singlet contribution is through the comparison of the overall strengths of the cross sections for *pn* and deuteron final states. Using final-state-interaction theory, Fäldt and Wilkin derived the extrapolation theorem which relates the normalization of the wave functions for *S*-wave bound and scattering states. This has been exploited to predict the double-differential cm cross section for the *S*-wave spin-triplet component in $pp \to \pi^+ pn$ in terms of the cross section for $pp \to \pi^+ d$:

$$\frac{d^2\sigma}{d\Omega dx}(pp \to \pi^+ \{pn\}_t) = \frac{p(x)}{p(-1)} \frac{\sqrt{x}}{2\pi(x+1)} \frac{d\sigma}{d\Omega}(pp \to \pi^+ d)\,.$$

Here x denotes the excitation energy ε in the np system in units of B_t, $x = \varepsilon/B_t$, and $p(x)$ and $p(-1)$ are the pion cm momenta for the *pn* continuum or deuteron respectively. The resulting cross section from the GEM experiment for the unbound *p-n* system is shown in Fig. 23.

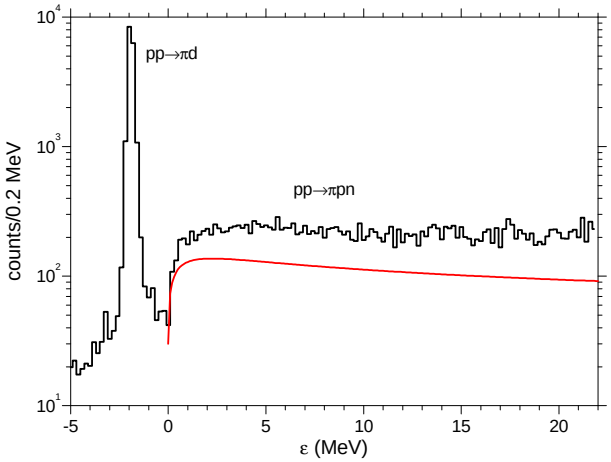

Fig. 23: The results from the GEM experiment (histogram) compared with the prediction (curve) of the *S*-wave FSI theory (see text).

There is a large difference between this cross section and the experimental one. This was not seen that clearly in previous experiments because limited resolution led to a leaking of cross section from the deuteron peak into the unbound region. Missing yield was usually attributed to the spin-singlet, isospin-triplet state. The corresponding spectrum calculated again within FSI theory was then smeared with the experimental resolution, yielding the fraction of the spin-singlet, isospin-triplet state. However, our present excellent resolution of only 100 keV yielded only a fraction of $< 10^{-4}$ for the ratio of the corresponding matrix elements squared. We can, therefore, exclude that this state contributes to the observed cross section. The only state left over, is the *D*-state, which can be thought to contribute to the *p-n* continuum, especially a *S-D* interference. This state was never found to be important in pion production nor in the *p-n* continuum. First calculations for the $pp \to \pi^+ d$ reaction, however, show its importance. Calculations for the three body final state are missing at present.

2.6 Spallation

2.6.1 PISA: Evaporation of Composite Particles from the Spallation of Au Nuclei

The measurement of total and double differential production cross sections following proton-induced reactions on a wide range of target nuclei and energies up to 2500 MeV is the essential goal of the PISA project. The intention is not only to systematically summarize and identify the essential high- and intermediate energy nuclear data, required in the framework of accelerator driven systems, but also to gain insights into the complex reaction mechanisms raised by spallation physics, multifragmentation, fission and vaporization being a quite active field of research.
The widely accepted mechanism of collisions of high energy protons with nuclei consists in the following two stage picture of the reaction: (i) the projectile induces an intranuclear cascade of nucleon-nucleon collisions which leads to the excitation of the nucleus, and (ii) the excited nucleus emits nucleons and various composite particles. Different theoretical approaches can be used in order to describe the reaction mechanism responsible for the excitation of the nucleus and for the emission of spallation products following the excitation of nuclear matter. We have used the INCL4.2 model for the description of the first stage of the reaction, and the Generalized Evaporation Model GEM for the second stage.
As can be seen in Fig. 24 the low energy component of the emitted ^{4}He can be well reproduced by the evaporation process, however, a significant contribution corresponding to the non-evaporative mechanism being present in the high energy part of the experimental spectra cannot be accounted for in the model.
The same effect is observed for heavier ejectiles like Li, Be or B. The evaporation of ejectiles from the equilibrium phase should be almost isotropic in the laboratory system since only a small velocity of the compound nucleus (of the order of $\beta \approx 0.0036$ along the beam direction) is predicted by calculation within INCL4.2. Thus, the high en-

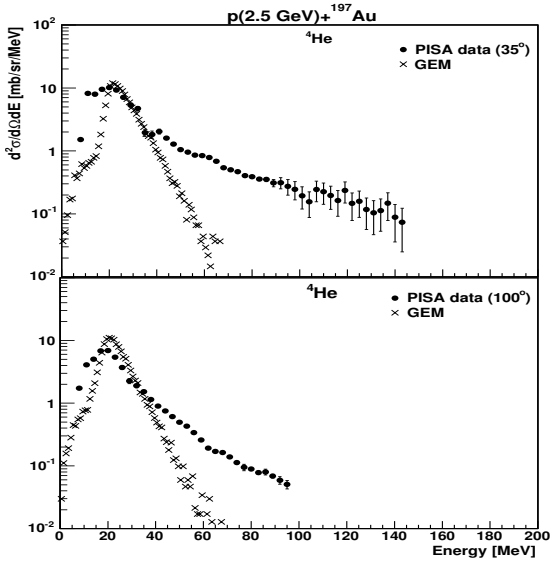

Fig. 24: Comparison between energy spectra of ^{4}He measured at 35° and 100° by PISA (•) and INCL4.2+GEM model calculations (x).

ergy tail of the spectra, which is evidently anisotropic in the laboratory system (see Fig.24), corresponds to some preequilibrium process.

In order to describe this preequilibrium contribution to the spectra, a phenomenological "moving source" model has been applied. A very good description of the spectra in particular for ^{4}He but also for heavier ejectiles was obtained. The Maxwell-Boltzmann distributions assume isotropic emission of the particles in the frame corresponding to the emitting source. The slower source represents the equilibrium process, *i.e.* it should reproduce results of INCL4.2+GEM calculations whereas the fast source corresponds to pre-equilibrium emission. Thus the velocity of the slower source was fixed at the value predicted by the INCL4.2 model for the resulting compound nucleus (β=0.0036). Other parameters of the slow source, *i.e.* the temperature parameter and the total (angle integrated) cross section were fitted together with respective parameters of the fast source to reproduce the shape of the spectra and their angular dependence.

Values of the parameters obtained from the fits enabled us to derive interesting conclusions on the mechanism of the reactions responsible for the high energy part of the spectra: (i) The velocity of the fast emitting source is in most cases larger than that which can be obtained by the target nucleus after complete momentum transfer from the proton projectile, *i.e.* the emitting source must be significantly lighter than the target; (ii) The recoil of the emitting source, which can be estimated from the dependence of the temperature parameter on the mass of the ejectile, allows to state that the mass of the fast source is approximately equal to 20, (iii) The total (angle integrated) cross section parameters enables us to determine the contribution of the preequilibrium process to the reaction under consideration. It turned out that ^{4,6}He and ^{6,7,8}Li are mainly (more than ∼ 80%) emitted from the slow source, *i.e.* from the compound nucleus. On the contrary, the heavier ejectiles ^{7,9,10}Be, ^{10,11}B, and ^{3}He appear predominantly as result of preequillibrium processes.

2.6.2 JESSICA Experimental Results

With the JESSICA experiment new cold moderator materials have been investigated and new developed neutron scattering law data S(α,β,*T*) have been validated. α denotes the impulse transfer of the neutron and β the energy transfer of the neutron to the molecule at a given temperature *T*. For the first time methane hydrate was studied in a realistic target-moderator-reflector environment and it was demonstrated that this materials is feasible to be used in a real facility. The great advantage of JESSICA is the possibility to measure the number of incident protons in the short pulse and thus allowing the normalization of the spectra to absolute values. With these spectra particle transport codes and the applied new neutron scattering kernels — mandatory below a kinetic energy of 4 eV — could be validated. For the first time a methane-hydrate moderator was studied at JESSICA. It has been known from neutron scattering experiments that a methane molecule encaged in an ice cage formed by six water molecules shows the same molecular dynamics than normal methane. The idea of methane hydrate is to combine the molecular dynamics of ice and methane in one single material. In Fig. 25 the energy spectrum of methane-hydrate is compared with ice and methane at T=20 K. einheit

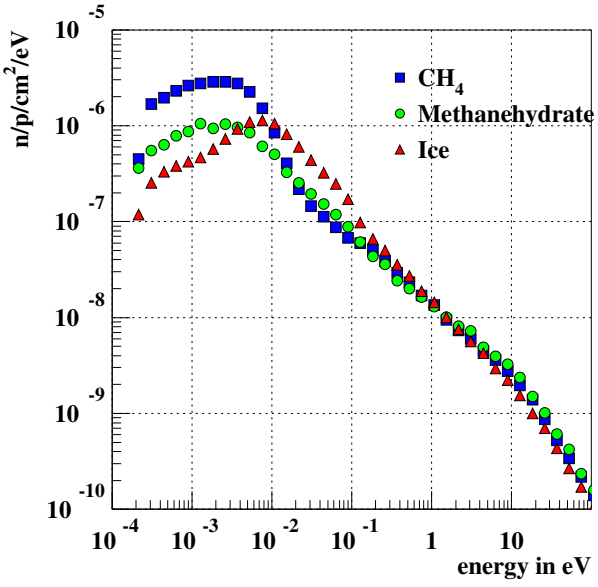

Fig. 25: Comparison of the energy spectra of methane, ice, and methane-hydrate at T=20 K.

It was found that due to lower hydrogen density in methane-hydrate compared to the hydrogen density in methane and ice, the intensity of the neutron flux is reduced. In a further analysis it could be shown, that the

ice cage is less effective for the moderation of neutrons than normal ice. Although the neutron spectra of ice are known from former experiments, up to now it was not possible to calculate the neutron spectra with Monte-Carlo transport codes due to a lack of data. In the framework of the JESSICA experiments this lack was closed and MCNPX simulations applying the newly developed neutron scattering law data $S(\alpha,\beta,T)$ for ice in the temperature range from 20 K to 273 K were compared with the obtained experimental data. Not only the energy spectra show a nice agreement between the simulated and measured data, but also the wavelength dependent time of flight spectra agree.

3 Physics at External Facilities

3.1 ATRAP Experiment at CERN

The ATRAP experiment at the CERN antiproton decelerator AD aims for a test of the CPT invariance by a comparison of hydrogen (H^0) - to antihydrogen ($\bar{H}^0$) atom spectroscopy. The $\bar{H}^0$ production is routinely operated at ATRAP in a nested Penning trap configuration. Detailed studies concerning shape parameters of the antiproton ($\bar{p}$) and positron (e^+) clouds, N-state distribution of the produced Rydberg $\bar{H}^0$ and $\bar{H}^0$ velocity have been performed to improve the production efficiency of useful $\bar{H}^0$ atoms. For high precision measurements of atomic transitions cold $\bar{H}^0$ in the ground state is required which has to be trapped due to the low number of available $\bar{H}^0$ atoms compared to the cold H^0 beam used for H^0 spectroscopy. Trapping of neutral $\bar{H}^0$ atoms works via the force on the magnetic moment in a magnetic field gradient.
The ATRAP experiment is divided into two phases: ATRAP-I in operation since 2000 using the superconducting magnet of the former TRAP collaboration at LEAR with severe space limitations and ATRAP-II presently set-up at a new super-conducting magnet with a central bore as large as 0.5 m in diameter giving ample space for further installations as detectors, Ioffe-trap and laser access. Figure26 shows a photo of the installed magnet with the photomultipliers of the outer scintillator paddles around the magnet.

Fig. 26: ATRAP-II magnet and C. Storry during assembly.

ATRAP-I served successfully for trapping cold e^+'s and cold $\bar{p}$'s, overlapping of these two clouds, cooling $\bar{p}$'s with e^- and e^+, and finally combining $\bar{p}$'s and e^+ to form $\bar{H}^0$. For the first time ever ATRAP has measured the velocity of slow $\bar{H}^0$ produced in three-body recombinations. Comparing the data to a simple model calculation indicates an kinetic energy of the $\bar{H}$ atoms of ≈ 200 meV (2400 K in temperature units).
ATRAP succeeded in demonstrating a second, entirely new method for producing slow $\bar{H}^0$ atoms. This method is distinguished from the three body recombination specially since it is expected that the velocity of the $\bar{H}^0$ atoms is as cold as the $\bar{p}$ from which they form. Two lasers excite Cs atoms to high Rydberg states Cs^*. Two resonant charge exchange collisions:

$$Cs^* + e^+ \rightarrow Ps^* + Cs^+ \quad \text{and} \quad Ps^* + \bar{p} \rightarrow \bar{H}^{0*} + e^-$$

transfer the laser-selected Cs^* binding energy to an excited positronium - (Ps^*) and then to an excited $\bar{H}^{0*}$ atom. Very slow $\bar{H}^{0*}$ atoms are expected since a Ps^* transfers little kinetic energy to a $\bar{p}$ (which is at liquid He temperature) as $\bar{H}^{0*}$ forms. The experimental sequence displayed in Fig. 27 is as follows: Ground state Cs atoms from an oven are excited with two lasers of wave lengths of 510.7 nm and 852.2 nm to well defined Rydberg states. These atoms collide with trapped e^+'s to form Ps^* atoms. A small fraction of the Ps^* collides with trapped $\bar{p}$'s to produce $\bar{H}^{0*}$. Again, a small fraction of the $\bar{H}^{0*}$ enters the detection trap, is ionized by the electric field in this region and deposits $\bar{p}$'s in the trap to be counted afterwards.

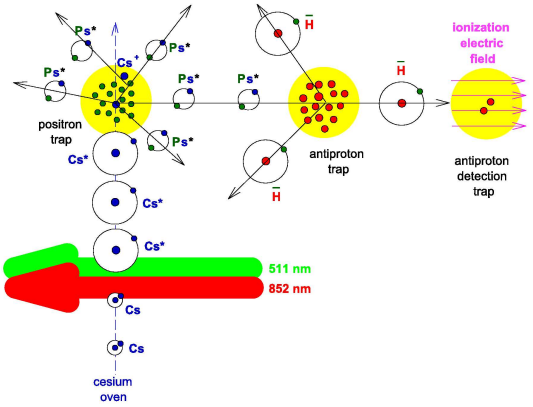

Fig. 27: Schematic of laser-controlled $\bar{H}^0$ production.

The $\bar{p}$ captured from ionized $\bar{H}^0$ are released when the well depth was reduced through zero. One count in Fig. 28 indicates a coincidence of signals from at least two scintillating fibers in different layers of the three layer fiber hodoscope, located just outside the trap vacuum enclosure. The most convincing evidence that these counts are from $\bar{H}^0$ atoms is that the potential wells are carefully arranged so that the only way to get a $\bar{p}$ in the detection trap is by ionizing an $\bar{H}^{0*}$ within it. Control experiments without positrons or with detuned laser wave lengths result in no counts in the relevant region. This proof-of-principle experiment demonstrates the first laser-controlled $\bar{H}^{0*}$ production using essentially background free detection of a few atoms.

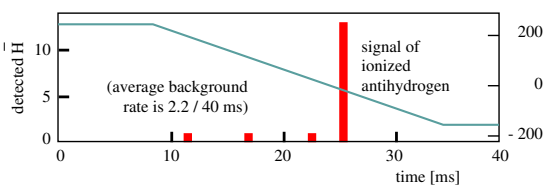

Fig. 28: $\bar{H}^0$ detection (peak) as the potential well containing the ionized $\bar{H}^{0*}$ is ramped down (right scale).

3.2 Pionic Hydrogen at PSI

The hadronic effects of the ground-state X-ray transitions in pionic hydrogen (πH) are directly related to the pion-nucleon (πN) isoscalar and isovector scattering lengths $\mathbf{a}^+$ and $\mathbf{a}^-$. Whereas $\mathbf{a}^+$ is connected to the πN sigma term being sensitive to the strangeness content of the nucleon, from $\mathbf{a}^-$ the πN coupling constant is extracted by dispersion relation methods. The pion-nucleon interaction measured in πH constitutes the (almost) free case being the anchor point for comparison to the in-medium case.
When analyzing the energies and widths of the πH X-ray lines the de-excitation processes in the atomic cascade must be disentangled unambiguously from the hadronic effects in order to achieve the envisaged accuracy of about 1% for the hadronic broadening. For that reason, the experiment has been continued measuring for the first time a muonic hydrogen (μH) transition with a crystal spectrometer (Fig. 29). Here, only the Doppler broadening caused by non-radiative de-excitations contributes to the line width after taking into account the crystal spectrometer response. For that, the spectrometer response had to be determined with unprecedented precision. This became possible by using helium-like X-ray transitions in sulphur, chlorine, and argon produced in an electron-cyclotron-resonance ion trap (ECRIT) setup for that purpose.

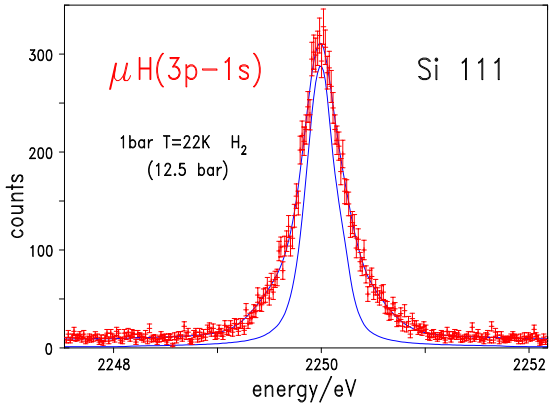

Fig. 29: μH(3p-1s) transition measured with the 111 reflection of a spherically curved Si crystal. The narrow line represents the resolution as determined from ECRIT measurements. Its asymmetry is due to the 2 hyperfine components.

First conclusions from the ECRIT and μH measurements are:

- the ECRIT having one of the largest mirror ratios realized in such devices and operating at 6.4 GHz only produces X-rays from highly ionized atoms at a rate of several 1000 per minute,
- Doppler broadening owing to de-excitation processes during the atomic cascade is clearly identified in the μH spectrum and will be used to improve cascade calculations to allow a better determination of the hadronic width in μH,
- for the first time, experimental evidence for a statistical population of the 1s hyperfine states in μH is given which is essential in experiments deducing the induced pseudovector coupling constant from muon capture, and
- no evidence was found for satellite X-ray transitions originating from molecular formation predicted to be at a level of about 10%.

The experimental program will be continued in 2005 with a high-statistics measurement of the πH(3p-1s) transition for the final determination of the strong-interaction parameters.

4 Theoretical Investigations

4.1 Challenges in Hadron Physics

Hadron physics investigates strongly interacting matter. While it is primarily concerned with the structure of baryons and mesons and their mutual interactions, it also has an impact on astrophysics and cosmology, where knowledge about matter under extreme conditions and about various reaction rates is required.

The basic theory of the strong interaction, Quantum Chromodynamics (QCD), is a nonabelian gauge theory with matter made of quarks and interactions being mediated by gluons. In the light quark sector, it possesses an additional chiral symmetry that determines to a large extent the interaction between the fundamental constituents of hadronic matter. For the heavy quarks, the dynamics is essentially nonrelativistic and largely constrained by heavy quark symmetry.

For processes involving large momentum transfers (the ultraviolet regime), QCD can be treated accurately in perturbation theory, in close analogy to Quantum Electrodynamics. This is due to an important property of QCD, asymptotic freedom, which implies a decrease of the coupling strength between quarks and gluons as the momentum transfer increases. In the infrared regime (energies up to a few GeV) — the so-called non-perturbative regime — the coupling becomes too strong to allow for a perturbative treatment of QCD. To make predictions for non-perturbative phenomena is a great challenge for hadron theory.

One of the most exciting aspects of non-perturbative hadron physics is known as confinement: Quarks and gluons, the fundamental particles of QCD, have never been observed in isolation. The only strongly interacting particles that can be counted in detectors are color-neutral composites of quarks and gluons, *i.e.* baryons and mesons. An explanation of confinement is a fundamental goal of hadron physics closely linked to an understanding of the spectrum of mesons, baryons as well as exotica. In the last years the issue of exotica has become again one of the truely hot topics in QCD. Another basic question concerns the origin of the spontaneous breaking of chiral symmetry, the ratio of the light quark masses and the values of the quark condensates.

4.2 Directions and Expertise in the Theory Group

The theory group focuses their activities on investigations that will improve our understanding of the strong interactions in the non-perturbative regime:

1. Reactions in few-hadron systems allow to study hadron dynamics in the non-perturbative regime of QCD in very fine detail. Experimental research projects are performed at electron and hadron facilities, where one investigates reactions at low to moderate momentum transfers. Such processes allow to investigate symmetries of QCD and their realization, such as chiral and isospin symmetry and thus give access to fundamental QCD parameters like the light quark mass ratios or the size of certain condensates. The basic tool employed is chiral perturbation theory and its extensions to few-baryon systems, which are studied experimentally to investigate the breaking of the isospin symmetry.The theory group has been very successfull in developing and employing these effective field theory (EFT) methods for processes involving one or a few nucleons, and is presently extending these studies to threshold meson production in nucleon-nucleon and deuteron-deuteron collisions. This is a long-term project that can only be undertaken within the Helmholtz infrastructure.

2. Properties of exotica. Another open problem addressed here is the question whether hadrons are limited to quark-antiquark and three-quark bound states or whether other, so-called exotic combinations of quarks, antiquarks and gluons, such as glueballs or pentaquarks, which are allowed from a theoretical point of view, are also realized in nature. Strangeness production and reactions with kaons gives access to nature of the $\Lambda(1405)$ or certain properties of the pentaquark $\Theta^+(1540)$. The theory group has particular expertise in coupled-channel dynamics and the analysis of final-state interactions. This led to important contributions concerning the question of the nature of the scalar mesons a_0 and f_0, the Roper resonance and the properties and of the charm-strange mesons D^*_{sJ}. Furthermore, the theory group has suggested a model-independent way to determine the parity of the pentaquark and worked out limits for the width of the Θ^+. Also, a large program exists to guide and interpret data obtained at COSY for the procduction of the scalar mesons and the $\Lambda(1405)$ in pd and dd collisions.

3. Nuclear structure attracts new theoretical investigations. The recent advances in EFT have generated a systematic approach to both two- and three-nucleon interactions which separates pion dynamics from short-range interactions. The isospin dependence of the nucleonic interactions is also predicted. This is of crucial importance for studies of the bulk properties of both stable and unstable nuclei. The theory group will apply its expertise in nuclear structure to develop EFT for nuclei. A first project dealing with doubly magic nuclei has started which will give access already to a large variety of interesting exotic nuclei. A second step will generalize EFT to deformed nuclei, where pairing effects are relevant. The study of collective excited states, such as the giant dipole resonances, provides complementary information

about the isospin structure of nuclei and related bulk properties. The structure of halo nuclei and pigmy resonances are currently investigated.

4. Deep inelastic scattering (DIS) and other hard processes probe hadrons and nuclei at large momentum transfer. In DIS off nuclei there emerges a new large scale, the so-called saturation scale Q_A, and simultaneous interaction with several nucleons of the nucleus becomes a dominant feature of hard processes. The standard pQCD factorization theorems break down and are to be supplanted by a new concept of nonlinear $k_\perp$-factorization. The focus of the current research is an extension of nonlinear $k_\perp$-factorization from DIS of leptons to proton-nucleus collisions at RHIC with an emphasis on jet production and the Landau-Pomeranchuk-Migdal effect. The potential of polarized Drell-Yan process at the HESR of the FAIR facility at GSI to the determination of the transversity structure function of the proton will be investigated.

4.3 Pentaquark Properties from Hadronic Reactions

In the last two years increasing evidence has accumulated for the existence of a narrow strangeness $S = +1$ exotic baryon — baptised the Θ^+. Its valence quark structure must consist of at least four quarks and one antiquark and therefore, if confirmed, this pentaquark would be the first state unambiguously not fitting into the naive quark model.

It is clear that only dedicated experiments can finally resolve the issue of the existence or non-existence of this exotic state. However, theory can supply important insights into and constraints on its properties which can then serve as useful guidelines for such experiments. In the last year we provided two well recognized contributions in this field, namely a detailed analysis of the width allowed for the pentaquark given that it was not yet observed in kaon scattering experiments, and a recommendation for the ideal observable to measure the parity of the Θ^+ (and narrow baryon resonances in general). The latter point becomes especially important in view of the recent observation that no model independent parity extraction is possible with photon induced reactions. We will now briefly comment on both aspects:

Bound on the width from data on K^+d

The known properties of the Θ^+ resonance, $m_\Theta \approx 1540$ MeV and strangeness $S = +1$, imply that it can couple to the kaon-nucleon (KN) system. For this system and the closely related kaon-deuteron system there are scattering data available in the relevant energy range. Those data do not show any clear evidence of the Θ^+ resonance. However, this absence of a resonance signal is also very useful because it provides rather strong constraints on the width of the Θ^+ resonance, a quantity that is important for understanding the nature of this state.

Recently our group has performed a model calculation of the reaction $K^+d \to K^0pp$. The calculation is done in the standard impulse approximation. However, and that is important, it takes into account "medium" effects such as the broadening of the resonance by the Fermi motion of the nucleons in the deuteron and the full final three-body kinematics.

In Fig. 30 we present results for the integrated $K^+d \to K^0pp$ cross section as a function of the kaon momentum in comparison to the available experimental information. Evidently there are data exactly in the region where the Θ^+ is supposed to be located (the largest and smallest resonance masses reported so far are indicated by bars in Fig. 30) and those provide rather restrictive constraints for the Θ^+ width. Fortunately, there are two independent measurements in the critical energy range. One can see from Fig. 30 that none of the model calculations with a Θ^+ width larger than 1 MeV is compatible with the data. Widths of 1 MeV or less can be certainly accommodated though we should say here that we did not explore the effect of such narrow widths in an actual model calculation.

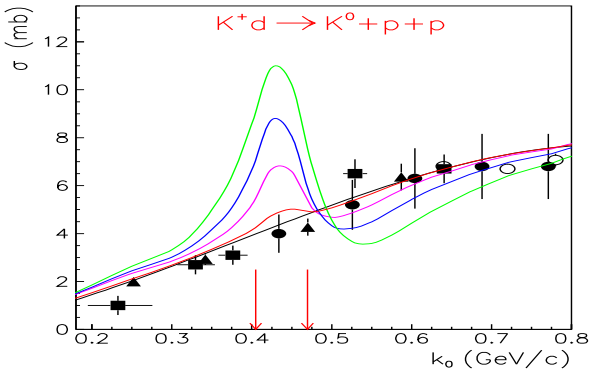

Fig. 30: Total $K^+d \to K^0pp$ cross section as a function of the kaon momentum. The curves show our full results for the original Jülich KN model without the Θ^+ resonance (black line) and the variants with a Θ^+ and with different widths (Γ_Θ=1 MeV - orange; 5 MeV - red; 10 MeV - blue; and 20 MeV - green). The vertical arrows indicate the range of kaon momenta corresponding to the smallest and the largest values found experimentally for the mass of the Θ^+ resonance.

If we disregard the two data points that lie within the Θ^+ region then there is a gap that allows to fit in such a resonance with a width of $\Gamma_\Theta \approx 5$ MeV without increasing the χ^2/data by more than 10%.

Parity determination

The parity of a hadron contains significant information on its substructure. Unfortunately, especially for spin–1/2 particles, the determination of the parity is a non–trivial problem especially when we talk about narrow states. For the case of the Θ^+ it was demonstrated recently that it is not possible to model independently extract its parity from photon-induced reactions.

To determine the parity of a narrow resonance model independently one has to exploit the link between spin and parity provided by the Pauli-Principle for NN systems: It is well known that a two-nucleon state acquires a phase $(-)^{L+S+T}$ under permutation of the two particles, where L, S, and T denote the angular momentum, the total spin and the total isospin of the two nucleon system. The required antisymmetry of the NN wavefunction thus implies that $L+S+T$ has to be odd. For example, for a proton–proton state $T=1$ and the parity is given by $(-)^L$ — thus each $S=1$ state has odd parity and each $S=0$ state has even parity. Therefore, preparing a pure spin state of a pp system means preparing a NN state of known parity. In case of a $T=0$ state, the assignment of spin and parity needs to be reversed.
This observation, first made by A.W. Thomas and collaborators, was exploited by us in a detailed investigation. Especially we identified the energy dependence of the spin triplet cross section (where we use the definition by Meyer for the polarization observables, where A_{xx} and A_{yy} both refer to perpendicular beam and target polarizations, however, rotated by 90 degrees and σ_0 denotes the unpolarized cross section)

$$ {}^3\sigma_\Sigma = \frac{1}{2}\sigma_0\,(2+A_{xx}+A_{yy}) $$

as the key observable to unambiguously identify the parity of a narrow resonance in a NN induced binary reaction. This is demonstrated in the last line of Fig. 31 for three representative models. Please observe that a measurement of ${}^3\sigma_\Sigma$ does not require the difficulty to handle the observable A_{zz} that needs longitudinal polarization. The only assumption necessary for deriving this result was that the energy dependence of a particular partial wave with angular momentum L is $(p')^L$ within the first 50 MeV above the production threshold. To illustrate this point we constructed various models for the Θ^+ production (to be concrete we show results for a spin 1/2 resonance only, however, all results hold for higher spin resonances as well). Obviously we can not prove model independence through models, but we can use models to illustrate the generality of a particular results. To meet that goal we tuned the parameters of the K^* exchange such that e.g. in the model that has both K and K^* exchange the s-wave is small in the model for positive parity pentaquarks.

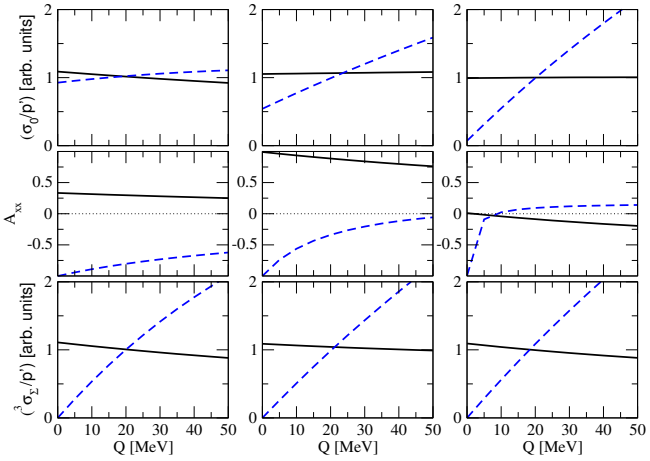

Fig. 31: Model results for σ_0, A_{xx} and the spin triplet cross section ${}^3\sigma_\Sigma$ for the reaction $pp \to \Theta^+\Sigma^+$. The first, second and third column shows the results for a model where the production mechanism is a pure K-exchange, a pure K^*-exchange and a mixture of both, respectively. Solid lines denote the results for a negative parity pentaquark and dashed lines for a positive parity pentaquark.

4.4 High Prescision Effective Field Theory for Few-nucleon Systems

The use of chiral Lagrangians to investigate in a systematic manner the problem of the interactions between two, three, a few nucleons was proposed by Weinberg about 15 years ago. Within this scheme, the few-nucleon potential is constructed based on power counting and used as an input to generate the bound and scattering states from the suitably regularized Lippmann-Schwinger eqaution. This appraoch offers many advantages: It is systematic and can be improved by going to higher orders, it allows to consistenly study two- and three-nucleon forces as well as the quark mass dependence of nuclear forces, (gauge) symmetries are treated properly and it can be extended to inelastic processes. Until recently, calculations were restricted to next-to-next-to-leading order (NNLO) in the chiral expansion. This led to promising results and was close to the acuracy achieved in phenomelogical or boson-exchange potentials. We have now studied the interactions between two nucleons at next-to-next-to-next-to-leading oder (N^{3}LO). At this order, the two-nucleon potential consists of one-, two- and three-pion exchanges and a set of contact interactions with zero, two and four derivatives, respectively. We have applied spectral function regularization to the multi-pion exchange contributions. Within this framework, we have shown that three-pion exchange can safely be neglected. The low-energy constants (LECs) related to the dimension two and three $\bar{N}N\pi\pi$ vertices are taken consistently from studies of pion-nucleon scattering in chiral perturbation theory, performed earlier at the IKP. In the isospin limit, there are 24 LECs related to four-nucleon interactions which feed into the S-, P- and D-waves and various mixing parameters. In addition, various isospin breaking mechanisms were considered. In the actual calculations, we have included the leading charge-independence and charge-symmetry breaking four-nucleon operators, the pion and nucleon mass differences in the one-pion-exchange, and the same electromagnetic corrections as done by the Nijmegen group. This is done because we fit to the Nijmegen partial waves. In the future, it would be important to also include mass differences in the two-pion-exchange, $\pi\gamma$-exchange

and the isospin breaking corrections to the pion-nucleon scattering amplitude. We therefore have phases for the *pp*, *np* and *nn* systems. To obtain the bound and scattering states, we use the Lippmann-Schwinger equation with the relativistic form of the kinetic energy. Such an approach can easily be extended to external probes or few-nucleon systems. The total of 26 four-nucleon LECs has been determined by a combined fit to some *np* and *pp* phase shifts from the Nijmegen analysis together with the *nn* scattering length value $a_{nn} = -18.9\,\mathrm{fm}$. The resulting LECs are of natural size. The description of the low phase shifts (S, P, D) is excellent, see Fig. 32 for the S-waves.

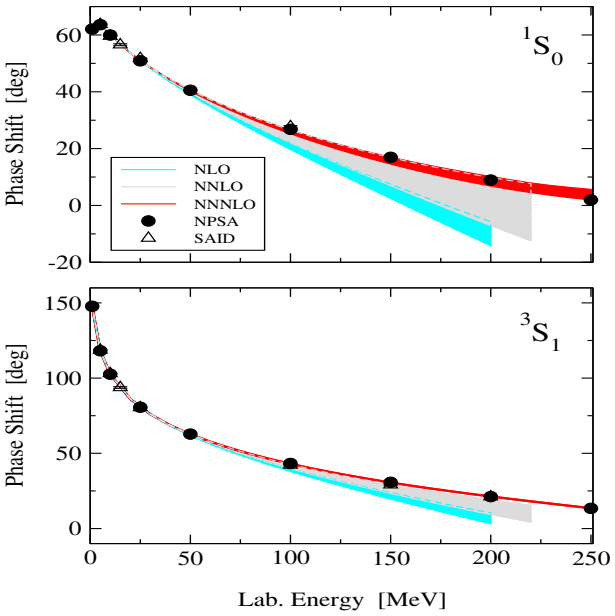

Fig. 32: The S-waves in *np* scattering. Shown are the theoretical results at NLO (blue band), NNLO (grey band) and N^{3}LO (red band) in comparison to the Nijmegen phase shift analysis (circles) and the SAID PSA (triangles).

In all cases, the N^{3}LO result is better than the NNLO one with a sizeably reduced theoretical uncertainty. This holds in particular for the problematic $^3P_0$ wave which was not well reproduced at NNLO. The peripheral waves (F, G, H, ...), that are free of parameters, are also well described with the expected theoretical uncertainty related to the cut-off variations. We stress that the description of the phases in general improves when going from LO to NLO to NNLO to N^{3}LO, as it is expected in a converging EFT. The resulting S-wave scattering lengths and range parameters in the *np* and *pp* systems are in good agreement with the ones obtained in the Nijmegen PWA. In addition, we can give theoretical uncertainties for all these quantities, which are mostly in the one percent range. The scattering observables (differential cross sections, analyzing powers) for the *np* system are well described, with a small theoretical uncertainty at the order considered here. The deuteron properties are further predictions. In particular, we have not included the binding energy in the fits, the deviation from the experimental value is in the range from 0.4 to 0.07%. The asymptotic *S*-wave normalization and the asymptotic D/S ratio are also well described: $A_S = 0.882 - 0.883\ [0.8846(9)]\,\mathrm{fm}^{-1/2}$ and $\eta_d = 0.0254 - 0.0255\ [0.0256(4)]$, respectively (the numbers in the brackets are the experimental values). The remaining discrepancies in the quadrupole moment and the rms matter radius are related to the short-ranged two-nucleon current not considered so far. We are presently extending these calculations to three-body forces at N^{3}LO and the inclusion of electroweak currents.

4.5 Four-body Physics

Effective theories allow for a systematic calculation of low-energy energy observables in a model-independent way. If the scattering length a of two particles is much larger than the typical low-energy scale ℓ of the system, one can use an effective theory with contact interactions only, to compute observables in an expansion in ℓ/a. The fact that no assumptions are made about the true nature of the underlying interaction, besides that the resulting potential is short-ranged and produces a large scattering length, allows for a systematic comparison of physical systems at different length scales. A particular feature of this theory is that in the three-body system a three-body force at leading order is needed to renormalize observables. As a consequence one three-body input as for example the three-body binding energy is needed to fix the value of the three-body force. Once the three-body force is fixed from this input, predictions can be made for other observables. Recently, we have applied this theory to the nonrelativistic four-body system and computed the binding energies of the ^{4}He tetramer, a bound state of four ^{4}He atoms, and the α-particle and obtained surprisingly good results taking into account the small number of parameters. We achieved this by generating the leading order potential of our theory and employing the Yakubovsky equations to solve for the wavefunction and the binding energies of the four-body system. To fix the value of the three-body coupling constant we used the Faddeev equations to compute the binding energies of the ^{4}He tetramer and triton and tuned the three-body force such that the desired binding energies were reproduced. Taking advantage of the features of our framework, one can now keep the observables in the two-body sector constant while changing the value of the three-body binding energies by tuning the three-body force accordingly. This leads to a linear correlation of the four-body binding energies and three-body binding energies, a phenomenon well-known in nuclear physics that is called the Tjon line. This linear correlation is shown for the α-particle in Fig. 33.
We also show some calculations using phenomenological potentials and a chiral EFT potential with explicit pions. The remaining deviation from the experimental value can be attributed to effective range corrections which have to be included at next-to-leading-order (NLO). A corresponding linear correlation also exists in the atomic ^{4}He

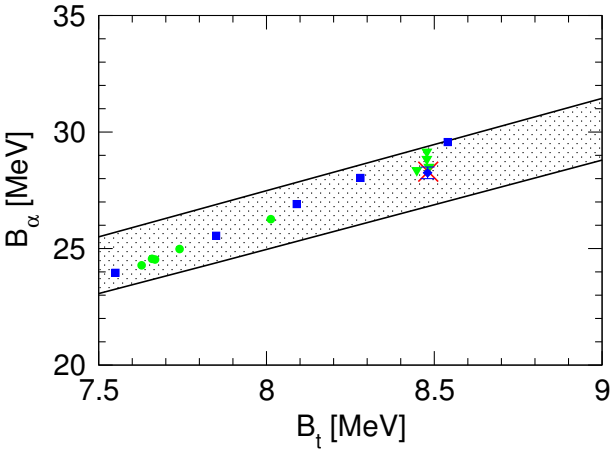

Fig. 33: The correlation between the binding energies of the triton and the α-particle (the Tjon-line). The lower (upper) line shows our leading order result using a_s and B_d (a_s and a_t) as two-body input. The grey dots and triangles show various calculations using phenomenological potentials without or including three-nucleon forces, respectively. The squares show the results of chiral EFT at NLO for different cutoffs while the diamond shows the N^{2}LO result. The cross shows the experimental point.

system between the ground states of the trimer and the tetramer but also between the excited states of these systems. Consequently, the Tjon line and the corresponding linear correlation in the atomic sector can be understood as a universal feature of four-body systems with large two-body scattering length.

4.6 Electromagnetic Structure of Halo Nuclei

Ordinary atomic nuclei are hard to break into pieces with electromagnetic radiation. A new sort of nuclei was discovered in recent years that responds much more readily to low-energy gamma rays. In such nuclei one nucleon or a few of them live comfortably far away from the densely packed core of protons and neutrons and form an extended halo. These halo nuclei with an excess of neutrons or protons as compared to normal nuclei are produced with the new radioactive beam facilities all over the world, like at GSI (Darmstadt/Germany), RIKEN (Japan) or MSU (East Lansing/USA). In the present paper it has become possible to understand this peculiar soft response to electromagnetic radiation. The key observation is that the ratio of the radius of the core to the extension of the nuclear halo is a very small number. Making use of a method introduced by Bethe in 1949 for low energy nuclear scattering, a calculational scheme was set up which expands this response in powers of this small ratio. All the details of the notoriously complicated nuclear motion are encoded in a few effective quantitites, namely binding energy and a strength constant that characterizes the interaction of the neutron with the core. In Fig. 34 the electromagnetic strength distribution of a beryllium isotope with 4 protons and 7 neutrons is shown which consists of a core and a single halo neutron. The electromagnetic response of ordinary nuclei shows up only at around 20 MeV, well outside the figure.

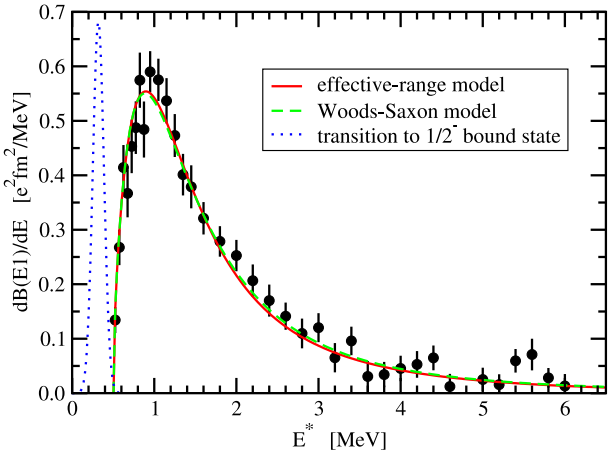

Fig. 34: Reduced transition probability as a function of the excitation energy E^* compared to experimental data

One can see that our theory can very well explain the experimental data obtained recently at GSI (Darmstadt). This characteristic low energy peak due to the halo nature is a universal phenomenon seen in other (up to now mainly light) nuclei as well. With the advent of new powerful rare isotope facilities like FAIR (GSI/Darmstadt) or RIA (USA) one hopes to discover neutron-halo nuclei also in heavy systems. They are not only of interest to nuclear structure physics but also to astrophysics: in the astrophysical r-process, heavy elements that are essential to our very existence are formed by neutron capture, which is directly determined by the electromagnetic response studied here.

4.7 Transversity in Drell-Yan Processes at HESR Energies

Transversity $h_1^q(x,Q^2)$ is the last leading-twist missing information on the quark spin structure of the nucleon. The reason why h_1^q, despite its fundamental importance, has never been measured is that it is a chiral-odd function, and consequently it decouples from inclusive Deep Inelastic Scattering (DIS). The double spin asymmetry $A_{TT}^{p\bar{p}}$ in polarized Drell-Yan antiproton-proton collisions at the HESR storage ring of the future FAIR facility at GSI is uniqely placed to measure the transversity distribution $h_1^q(x,Q^2=M^2_{e^+e^-})$ for valence quarks in the proton. The predicted asymmetry is large, of the order of 30%, as shown in Fig. 35, and is entirely dominated by the u-quark contribution, with no flavour admixture and no quark-antiquark entanglement.
A point is made that the measurements of $A_{TT}^{p\bar{p}}$ can be extended to and below the J/Ψ mass region which sub-

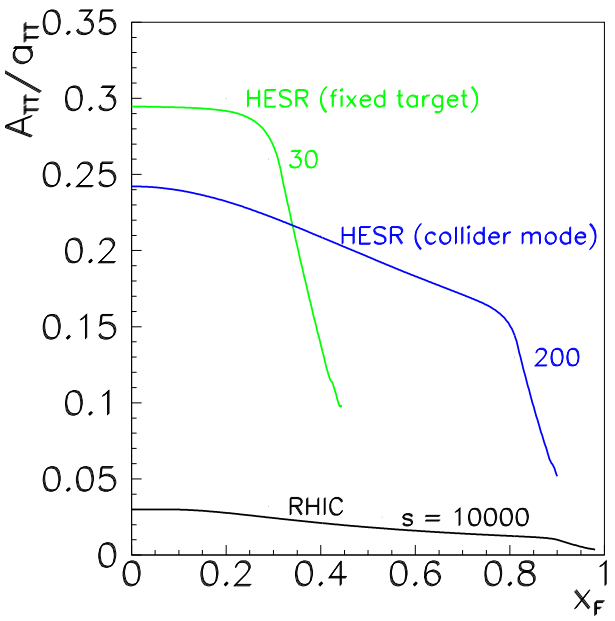

Fig. 35: The $p\bar{p}$ Drell-Yan double transverse spin asymmetry $\tilde{A}_{TT}^{p\bar{p}}(M^2, x_F)$ as a function of x_F, for $M_{e^+e^-} = 4$ GeV/c^2 (green curve: fixed-target option of PAX at HESR, $s = 35$ GeV^2; blue curve: asymmetric-collider option of PAX at CSR-HESR, $s = 300$ GeV^2; the RHIC-like $\bar{p}p$ collider at $s = 10^4$ GeV^2).

stantially enhances the counting rate. A much broader kinematical range of x, Q^2 comparable to that studied in DIS experiments by the HERMES Collaboration, becomes accessible with the asymmetric CSR+HERMES collider option at FAIR. In contrast, at RHIC energies the expected asymmetry is at the several per cent level (still smaller for proton-proton collisions at RHIC because of the suppression of transverse spin from valence to sea quarks) and its interpretation is not simple because it involves the theoretically poorly understood transversity distribution of sea quarks. The large predicted transversity signal makes the polarized Drell-Yan production at HESR the flagship experiment of the polarization program at FAIR.

5 COSY Operation and Developments

As always, high reliability of the accelerator complex had been a prime focus. Obviously, the effort connected with this responsibility continues to rise as time goes by, since certain components begin to reach a critical age. In spite of this the accelerator crew succeeded in keeping the overall reliability above 90% in the current year. Another central task is the development of new operational modes to stay abreast with the ever-changing demands of the experimental collaborations. A formidable achievement in this context was for instance the new peak energy of 2.88 GeV, which was decisive for the feasibility of a new experiment. This value significantly surpasses the original design value of 2.5 GeV and was possible due to a new elaborated operational mode. Equally remarkable has been the advanced spin manipulation of circulating polarized ion beams inside COSY reaching spin-flip efficiencies of 99.9%. As in the previous years we have shared our expertise in the Framework of EU projects like HIPPI and CARE. Inside and outside institutions have benefited from irradiations performed with the cyclotron. The FAIR-project of the GSI and specifically the antiproton ring HESR has been playing an increasingly important role as it will set the mid- and long-term perspective in the field of hadron physics. Because of this the IKP did allocate significant resources for this project. As the HESR resembles in many ways COSY, it seemed natural to take on a leading role in the HESR consortium that bundles resources and expertise of the GSI, the TSL (Sweden) and the IKP. This consortium succeeded in 2004 in finalizing the "Technical Report on the HESR", which describes design, construction, commissioning, and important R&D work for this groundbreaking facility.

5.1 Operation

In 2004 COSY delivered a total of 6836 h of beam time, 5468 h of which were used for experiments by the users. Like in the years before, different particle species were accelerated. Polarized ions continued to play an important role and even exceeded their unpolarized counterpart in usage by nearly a factor of two in case of deuterons. The distribution between unpolarized and polarized protons and deuterons is depicted in the upper pie chart of Fig. 36.

The PAC allocated in 2004 beam time for 19 different experimental requests. Serving external as well as internal experiments to almost the same amount, one third of the scheduled time was used for maintenance, setting up the beam, or performing accelerator physics experiments, see Fig. 36.

To weed out weak or improve unreliable components a careful, long-term statistical survey had been conducted for each year, which breaks down the causes according to failure categories. This instrument has turned out to be

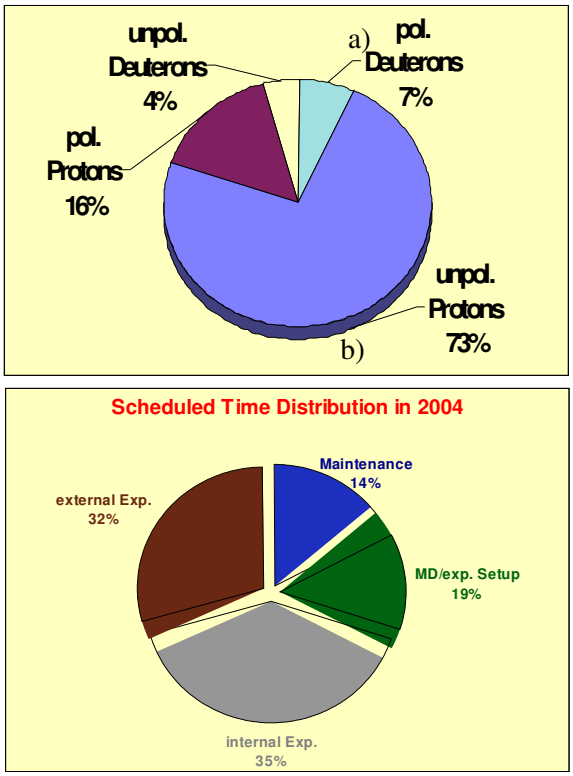

Fig. 36: Upper: Particle beams delivered in 2004. Lower: Beams for experimental groups were equally shared between external and internal target stations. The remaining time was split between machine development and maintenance.

a very effective tool to improve and maintain reliability. In the current year an overall reliability of over 90% had been achieved. This high number could have been even surpassed if the availability of the pre-accelerator, the more than 40-year old cyclotron, could have been raised substantially beyond 95%. Averaging over all years since 1993 an overall reliability of 92.6% was achieved for the accelerator complex.

5.2 Electron-beam Neutralization

The electron cooler of the HESR of the FAIR project is a core component for achieving the projected beam quality. It presents a formidable challenge as it carries the energy of the cooling electrons into the megavolt region. Possible detrimental effects have to be studied beforehand to avoid unnecessary delays in its completion. The stability of antiproton beams inside the HESR ring is of crucial importance. For instance neutralizing ions inside the cooling electron beams could jeopardize its function. It has been shown that even a few percent neutralization can appreciably lower the stability threshold. To research this phenomenon cooling experiments at COSY with 45 MeV protons attempted to free the electron beam from field distorting ions by exciting resonant ion oscillations with a transverse sinusoidal electric field (a so called shaker).

The influence of the neutralization on the proton beam stability at COSY is well illustrated in Fig. 37. Without shaker operation or using non-resonant shaker frequencies a coherent instability leads to a fast particle losses after 25 s (Fig. 37a). Clearing the electron beam from one of the ion species, here N^2_+, by applying a shaker frequency of 114 kHz, the instability develops much later (65 s). In addition, the ion loss rate is about 3 times smaller as seen in Fig. 37b.

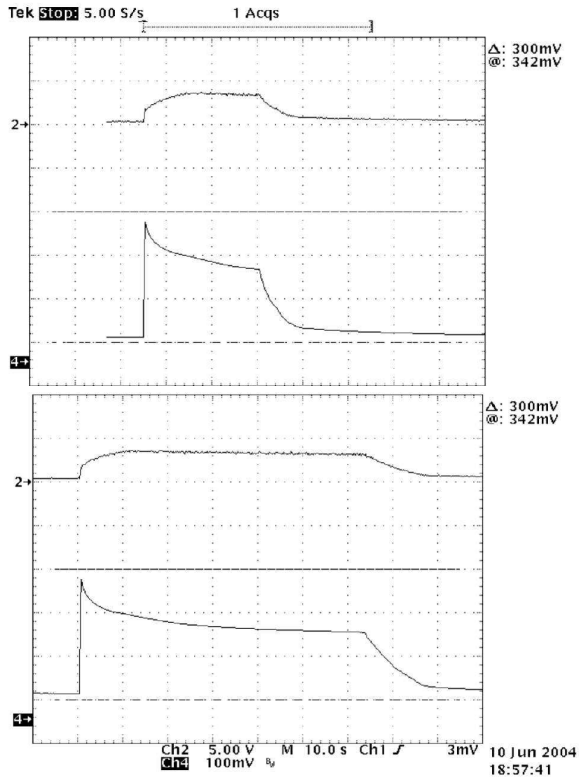

Fig. 37: Proton beam current (lower curves) and H^0 count rate (upper curves) versus time: a) Shaker is off or non-resonant excitation, One division corresponds to 1 mA beam current. b) Excitation with the resonant frequency of 114 kHz.. One division corresponds to 1 mA beam current.

5.3 Extraction of Cooled Beams

TOF experiments require ion beams with the highest possible brilliance at the target position. To suppress stray projectiles, counters in front of the target veto any data connected with beam halo. For the April run of TOF, a 3.065 GeV/c proton beam was prepared and extracted via the slow extraction system. Prior to acceleration the beam's phase space was reduced via electron cooling. The set-up of the ultra slow extraction was markedly eased by the reduced beam size. Additionally, the energy spread of the beam was smaller compared to the uncooled case. The increased quality of the extracted beam was such that the signal to background ratio was improved by a factor of 20. This enabled the experiment to run with higher beam currents as the rate of the veto counter had previously been the limiting factor.

5.4 Raising the Energy Limit

The maximum energy of an accelerator is a key feature that determines the range of experiments that can be performed. This holds especially for threshold experiments whose feasibility hinges exactly on this figure. Understandingly, there has always been a strong demand from the experimenters to raise the energy of COSY, in particular as the old energy limit was just below some interesting physics thresholds. By developing new operational modes COSY succeeded in reaching now an energy of 2.88 GeV. This value dramatically surpasses the original design value of 2.5 GeV and was crucial *e.g.* for experiments on a_0/f_0- and ϕ-meson production carried out at ANKE. The maximum energy for extracted beam is at present somewhat lower, because it is limited by the capability of the power converter used for the magnetic extraction septum.

5.5 Spin-Flip of Circulating Ion Beams

Another important topic of accelerator research is the spin manipulation of circulating polarized ion beams by using special manipulators, so called "rf-dipoles". Specifically for this investigation an international collaboration "Spin at COSY" has been established. All experiments were carried out in a close collaboration with the Michigan State University. Besides the high scientific relevance for accelerator physics these results have great implications for conducting polarized experiments inside accelerators. The reversal of the spin direction of the circulating beam will allow them to decrease drastically systematic errors. In 2004 experiments were continued with a new a ferrite-loaded rf-dipole, which allowed to reach much higher fields. The rf-dipole was exited with a sweeping frequency. Using this spin manipulator it was possible to reverse the spin direction of a 2.1 GeV/c polarized proton beam with an efficiency of 99.9%. As clearly visible in Fig. 38, the polarization was still above 60% even after undergoing 50 spin-flips.

5.6 Transverse Beam Feedback System

The intensity of electron-cooled beams is limited due to coherent oscillations that are fanned when a certain number of circulating particles is exceeded. A vertical feedback system that had been installed in the previous year had proven to be very effective in dampen those oscillations. To improve this system further a damping loop for the horizontal plane was added in 2004. The whole system has been integrated meanwhile into the standard control system of COSY. This enables the machine to deliver now routinely high-intensity cooled beams to experiments.

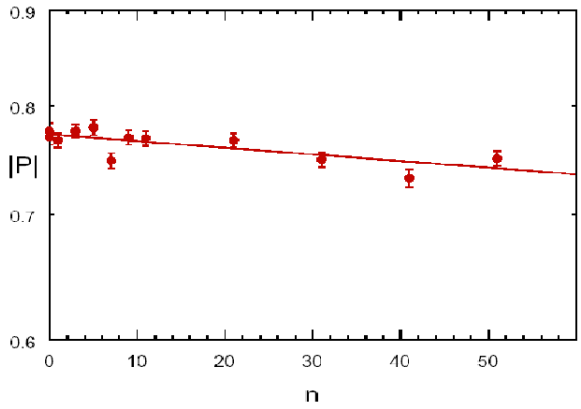

Fig. 38: Proton polarization at 2.1 GeV/c plotted versus the number of spin-flips.

5.7 Preparations for WASA at COSY

The preparatory work for inserting the WASA detector inside the COSY ring was continued and intensified in 2004. The space created by removing the now obsolete old accelerating cavity visibly changed the appearance in the COSY tunnel.

Work was also invested in rearranging any impeding water cooling pipes and electric cabling for quadrupoles and other components. To gain extra space for the much-needed supplementary forward detector alternatives have been considered for steerer magnets presently used to correct the beam direction. Extra windings on existing quadrupoles have been investigated and could take over their functionality. This method has been successfully used at other locations in the past. Additionally, quite a few other activities took place, which were immediately concerned with the transfer of the WASA detector to Jülich. The status of preparations is in line with the scheduled transfer of the WASA detector in summer 2005.

The physics potential of WASA will be enhanced by the higher energies and the higher beam intensities available at COSY. Studies have been conducted to evaluate the luminosities for the planned experiments and to raise the available beam intensities. For instance the number of unpolarized protons at maximum momentum has been increased to $1.5 \cdot 10^{11}$ particles in the framework of the intensity upgrade program. This figure was achieved in the single injection mode.

Experiments always aim to get an optimal average luminosity. Constraints due to target technology and/or required energy resolution are limiting boundary conditions. To lengthen the beam life-time, internal targets have to be either very thin or the heating effect of thicker targets has to be compensated by a powerful beam cooling system. The peak luminosity's dependence on the target thickness and number of circulating or extracted particles is shown in Fig. 39 and varies in the range of $10^{26} - 10^{32}\,\mathrm{cm}^{-2}\mathrm{s}^{-1}$. The luminosity is calculated for a typical range of circulating particles (10^9 to 10^{11}) in COSY with a revolution frequency of 1 MHz. For external experiments an extraction time of 100 s is assumed. A shortened extraction time would raise the luminosity for the extracted beams.

To optimize data taking efficiency it is necessary to balance target thickness and beam life times. Typical beam life times in dependence of target type are listed in Table 1. The efficiency of the applied cooling technique does greatly influence the useful data taking time.

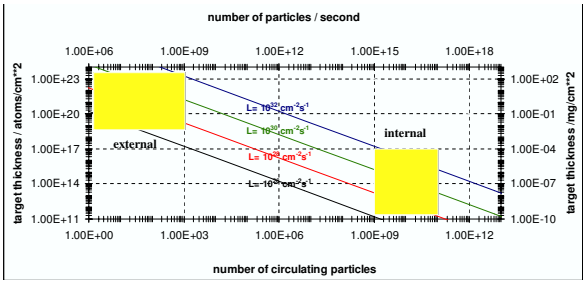

Fig. 39: Peak luminosity for internal and external experiments for different effective target thickness at COSY. Useful Areas are marked in yellow.

Table 1: Beam life time for circulating COSY beams.

Type of internal target	Time
Solid targets	ms to s
Pellet targets	≈minutes
Cluster targets	$<$ 1h
Cluster targets with stochastic cooling	several hours
Atomic beam targets	10 to 100h
Atomic beam storage cells	1 to 10 h
Without target	10 to 100 h

5.8 Improving Beam Diagnostics

A newly developed non-destructive beam profile monitor underwent its first successful test in the extraction beam line to JESSICA. A short beam burst with a length of approximately 200 ns was extracted using a fast kicker system that allows to extracts the circulating beam within one revolution. The measurement technique is based on the excitation of residual gas atoms by the passing ion beam. These atoms emit light when returning to their ground state. The emitted photons are observed with a set of sensitive photomultipliertubes and allow determining beam position and extend simultaneously. In Fig. 40 the beam profile is shown using an eight-channel system. The peak generated by light from atoms that have been excited by the beam clearly stands out from the background. This first test demonstrates that this non-intercepting method for monitoring beams is a viable option especially for high intensity beams. It can be expected that future refinements will greatly improve the performance seen in this first test.

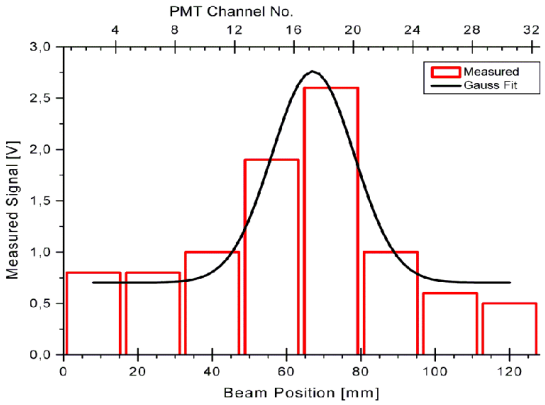

Fig. 40: Gauss fit of beam profile measured by looking at the light from the residual gas.

5.9 HESR activities

The accelerator division has initiated a task group to advance the HESR of the FAIR-project at the GSI. The consortium formed for this purpose bundles the resources and expertise of the FZ-Jülich, the GSI (Darmstadt) and the TSL (Uppsala) and other expert groups. The similarities between COSY and the HESR eased the task of taking on a leading role in this project. An outstanding feature of the new facility is the combination of phase space cooled beams with internal targets and a detector system (PANDA) that nearly covers the full solid angle. To break new ground in physics, demanding beam parameters have to be met. Foreseen are two operational modes. A high luminosity mode with beam intensities up to a few times 10^{11}, and a high-resolution mode with a momentum spread down to 10^{-5}. The latter mode will require a powerful electron cooling system, which makes the leap from present systems into the megavolt regime and constitutes a technological challenge in itself. One important milestone on the road map to the HESR was the timely completion of the Technical Report. More details concerning this are found in the “FAIR” section of this brochure.
Short articles found in the accompanying CD-ROM present additional information on the various topics and activities.

6 Preparations for FAIR

6.1 Evolving from COSY to the HESR

6.1.1 Introduction

The high energy storage ring for anti-protons (HESR) will be a groundbreaking facility for the future antiproton physics in the 10 GeV region. It is part of the antiproton branch of the FAIR project. Antiprotons will be generated in a production target, collected, accumulated, pre-cooled, and accelerated or decelerated to the desired energy in subsequent rings before they are injected and stored in HESR (cf. Fig. 41). One of the physics goals of the HESR is the understanding of the nature of the quark confinement. A powerful detector dubbed PANDA, which is an integral part of the HESR will be the tool to get new important insights *e.g.* by the investigation of bound states of $c\bar{c}$-mesons. This kind of physics represents a natural progression of the present science program of the IKP to a new realm.

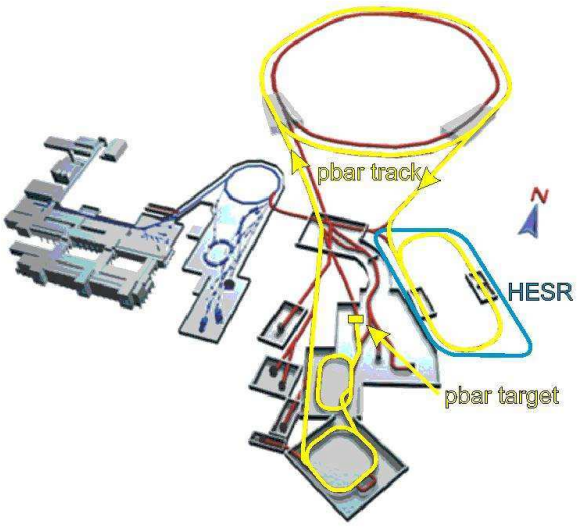

Fig. 41: The antiproton part of the FAIR facility is highlighted in yellow. After production at 3 GeV, antiprotons are accumulated, cooled down, and accelerated in the SIS100 (top) to the desired energy. The HESR is the final link in this chain. There the beam properties are refined and data is taken with PANDA.

By the striking similarities between COSY and the HESR the IKP felt compelled to take a leading role in the consortium that bundles the resources and expertise of the GSI, the TSL (Sweden), the FZJ, and other related groups involved in this project.

6.1.2 Lattice Considerations

Moving towards the first milestone the original Conceptual Design Report (CDR) had to be transformed into a Technical Report that would lay the groundwork for identifying essential R&D effort and be the basis for engineering the various components.
The envisioned physics program made it necessary to realize beam parameters inside the HESR that will require reaching new standards in accelerators design. In a high-resolution mode a momentum resolution of 10^{-5} has to be reached, in the high luminosity mode still 10^{-4} is required. Table 2 summarizes some essential parameters.

Table 2: Requirements implicated by the envisioned physics program

Ion species	Antiprotons
Production rate	$2{\cdot}10^7$/s ($1.2 \cdot 10^{10}$ per 10 min)
Energy variation	in SIS100
Momentum range Kin. energy range	1.5 – 15 GeV/c 831 MeV – 14.1 GeV
Number of particles	10^{10} up to few times 10^{11}
Target thickness	10^{15} – 10^{16} cm^{-2}
Transverse emittance	0.1 – 0.001 mm mrad
Betatron amplitude at interaction point	< 1 m
High luminosity mode	$2{\cdot}10^{32}$ cm^{-2}s^{-1} av. luminosity, rms momentum spread $\sim 10^{-4}$
High resolution mode	10^{31} cm^{-2}s^{-1} av. luminosity, rms momentum spread $\sim 10^{-5}$

Like COSY the HESR is a particle ring containing electron cooling and stochastic cooling. While COSY allows high-resolution experiments with polarized and unpolarized protons in the strange quark region the HESR enables to make experiments with antiprotons in the charmed quark region (momenta between 1.5 GeV/c and 15 GeV/c). The higher energy of the HESR results in a circumference of 574 m, which is much larger than that of COSY despite the use of superconducting magnets. As the HESR will be solely a storage ring energy variations have to be performed in the SIS100, which serves as injector. Therefore, the injection devices have to cover the whole momentum range.
Undoubtedly, the greatest challenge is the requirement to combine high luminosity with high phase space density of the antiproton beam. To be able to cool up to the highest momentum, the high voltage of the electron cooler has to go up to 8 MV. This significantly exceeds the presently achieved operating voltage of the Fermi Lab electron cooler of about 4.3 MV. To achieve short cooling times the specific strengths of both cooling methods, stochastic and electron, have to be combined. Electron cooling is most effective when operating in the mode of magnetized cooling but requires a pre-cooled beam. This can be provided via stochastic cooling, which is most efficient in the initial cooling process. Simulations have revealed shortcomings of the present models used to describe the cooling process. Because of this, additional R&D work will be required to verify quantitatively the cooling strength and the optimal combination and inte-

gration of these systems into the HESR.
One of the most far reaching and crucial decisions was finalizing the lattice of the ring. Extensive studies of different lattice structures have been carried out to make sure that no promising possibility was overlooked. Even designs using normal conducting magnets have been studied to verify that superconducting magnets were indeed superior. Numerous simulations confirmed that it is essential to have a lattice with a negative momentum compaction factor. The layout that finally evolved for the HESR is shown in Fig. 42. This lattice uses superconducting magnets in the arc sections and allows different magnet settings, which can be adjusted according to the required beam momentum. In Fig. 43 examples of the corresponding Twiss functions are plotted.

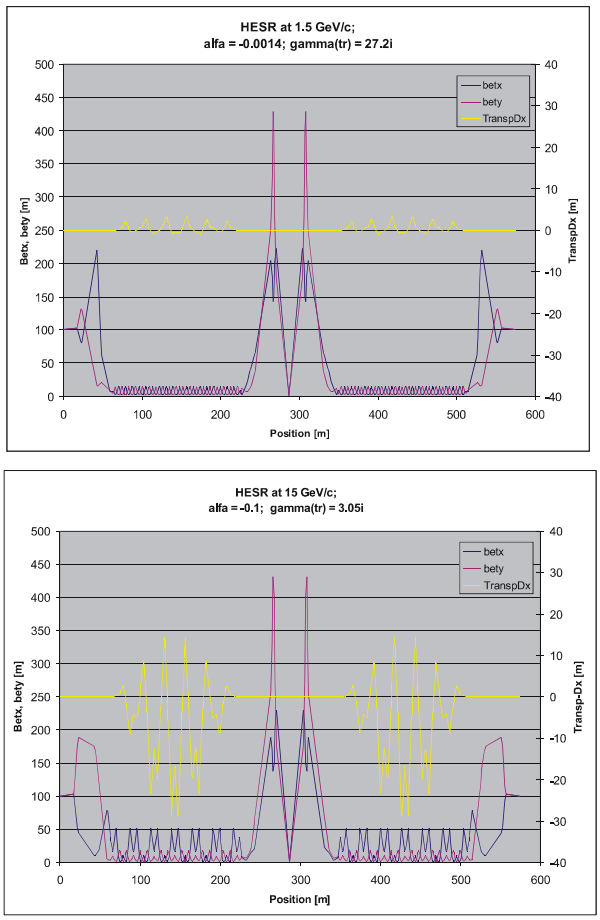

Fig. 43: β-functions and dispersion function for a low energy (upper) and a high energy (lower) HESR lattice. The target is located at 287 m. The HESR will operate with an imaginary gamma-transition value over the entire momentum range.

6.1.3 R&D Program

Presently efforts on the one hand are focused on a more detailed investigation of machine properties, which are dominated by collective effects. On the other hand several technical issues are studied already in more depth. These topics are included in the current R&D priority program, which has been developed and is substantially supported by the European Union (FP6 Design Study DIRAC Secondary Beams; the HESR consortium will receive 1.3 M€ support for a total effort of 3.7 M€.
As detailed in a contribution contained in the accompanying CD-ROM the R&D program covers high-energy electron cooling, pick-up development for stochastic cooling, suitable injection schemes, and rf-cavity investigation. Each topic is broken down in subtasks, which receive suitable priorities.
All design efforts concerning the electron cooler are led by the Svedberg Laboratory (Uppsala University). Two different approaches have been investigated to meet the performance requirements of the electron cooler. In accord with the most visible difference, the orientation of the accelerating column, they are named the horizontal respectively the vertical cooling system. A main technical difference is the generation of the high voltage of 8 MV. The acceleration column for the electron beam of up to 1 A will be operated in a high pressure insulating gas, usually SF_6.
As there is a lack of experimental data on magnetized electron cooling and its associated technology, an experimental program at COSY has been proposed to study in depth the behavior with the aid of a 2 MV electron cooler. This would constitute an indispensable intermediate step to secure the technological and experimental know-how for the successful construction of the 8 MV electron cooler of the HESR.

6.1.4 Magnet Investigations

The research started with an intense exploration to find a suitable superconducting dipole magnet that had a proven record. The D0 magnet of RHIC turned out to be a good candidate. If one could keep magnet length below ca. 1.8 m a straight magnet design would provide the necessary field quality. Tradeoffs in this approach are the large influence of fringe fields and a more demanding cryo system. Opting for a much larger length would require using curved superconducting dipole magnets with a radius of about 14 m. There is no proven design available at present. A 2D-calculation of the B-field is shown in Fig. 44. Putting such a setup inside the planned HESR tunnel is shown in Fig. 45.
The layout of the HESR has also to be optimized with respect to cryogenic losses and a small circumference. Both issues are closely intertwined with the cryostat layout. The study shows that building the arc section as one cold system inside a segmented cryostat should be possible. Moreover, the minimum distance between two adjacent superconducting magnets is reduced to be only 1 m, following the experience of CERN and BNL. The associated cryogenic scheme is sketched in Fig. 46.
Figure 47 depicts the CAD design of a combined superconducting quadrupole-dipole section. The required number of elements would be joined to form a complete 180°arc.

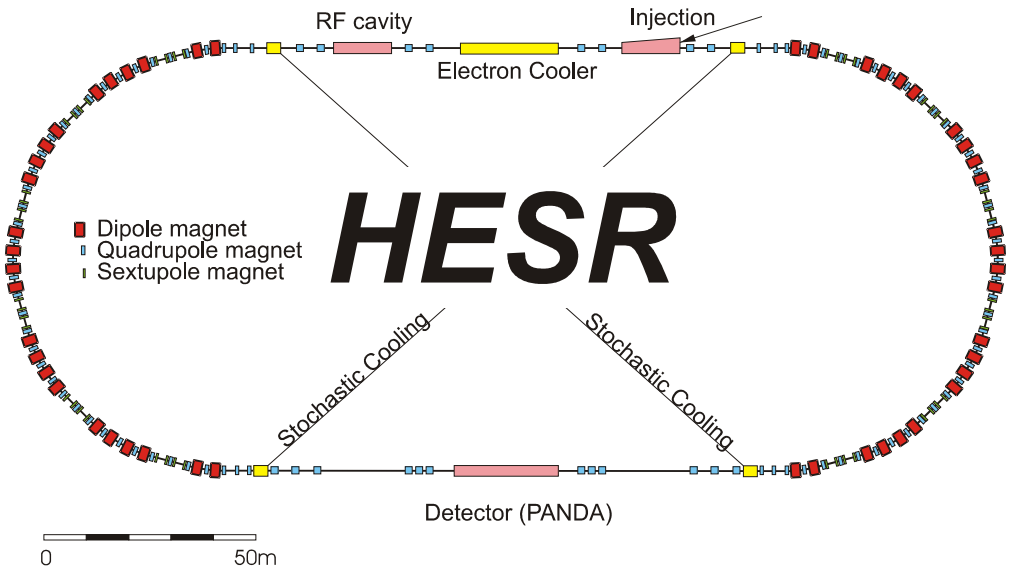

Fig. 42: Layout of the HESR.

6.1.5 Stochastic Cooling System

A stochastic cooling system has been proposed to be used above 6 GeV/c. Acceptable cooling times below 300 s with an RF power below 2 kW are reachable for realistic system parameters (mechanical and electromagnetic properties of pickups and kickers, ion optical functions of the HESR). As an example of the many calculations the dependence of the transverse overlap frequencies on the relevant parameters is shown in Fig. 48.

6.1.6 Experimental Facility

The PANDA setup as defined by the PANDA collaboration has been integrated inside the HESR. The arrangement shown in Fig. 49 was chosen because the target will then be located in a dispersion free region. Whether the magnets D1 and D2 will be combined into one stronger magnet is not decided yet. The compensating solenoid would be placed upstream.

6.1.7 Outlook

The successful completion of the Technical Report has been a first and important milestone on the road towards the HESR. It confirmed that there are no insurmountable obstacles on the way to its realization. But the investigations also clarified that significant R&D work lies ahead as many of the systems needed for operation have no precedent.
This concerns especially the electron cooling system where present computer programs have not matured enough. To fill this gap a prototype with 2 MV would be the ideal testing ground and COSY the ideal machine to get realistic data in that important field. The internal targets of COSY and specifically the future pellet target would give reliable information on target-heating/beam-cooling interaction and pave the way for an optimal design for the HESR.

6.2 The PANDA Experiment

A major component of the approved Facility for Antiproton and Ion Research (FAIR) at the GSI in Darmstadt is the High Energy Storage Ring (HESR) with the PANDA (Proton ANtiproton Detector Array) experiment. HESR will provide a unsurpassed high intensity, phase space cooled antiproton beam with momenta up to 15 GeV/c which allows the detailed study both of the structure of hadrons in the charmonium mass range and the spectroscopy of double hyper nuclei. To serve this wide physics program the general purpose PANDA detector is planned.
Figure 50 shows a schematic overview of the PANDA detector. It is divided into two main parts, the central spectrometer directly around the target station and the forward spectrometer to measure particles emitted at small polar angles in this fixed target kinematics. The overall length of the detector is 12 m.
The innermost subdetector of the central spectrometer is a micro vertex detector for precise tracking information. It is surrounded by the central tracker built either of straw tubes (STT) or a time projection chamber (TPC) in the barrel part, and a set of mini drift chambers (MDC) in the forward direction. For particle identification two ring imaging Cherenkov counters are foreseen. They are surrounded by a compact electromagnetic calorimeter made out of $PbWO_4$ crystals. This system is situated in a 2 T solenoidal magnetic field. The return yoke of the magnet is covered with muon detectors.
The forward spectrometer consist of a 2 T·m dipole magnet with a set of multiwire drift chambers (MuDC) for tracking, a RICH detector for particle identification, electromagnetic and hadronic calorimeters for charged and

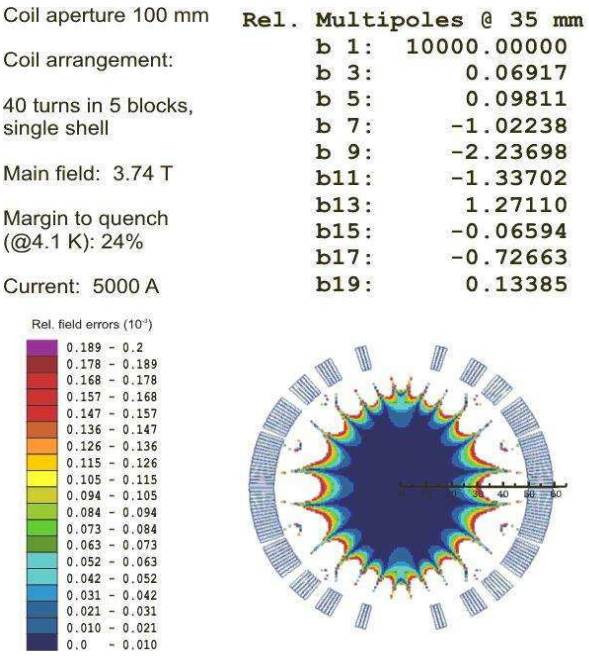

Fig. 44: Coil arrangement and calculated 2D-field quality for the superconducting HESR dipole magnets designed as a shortened version of the original RHIC-D0 magnet.

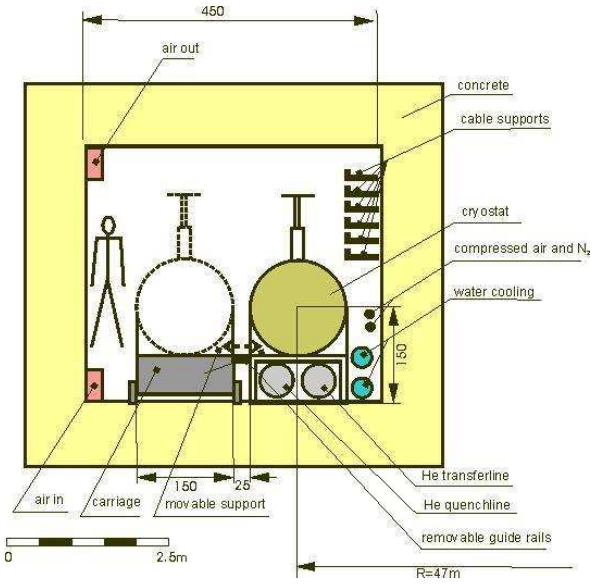

Fig. 45: Cross section of the tunnel with cryostat segment in operating position. The transport position is indicated.

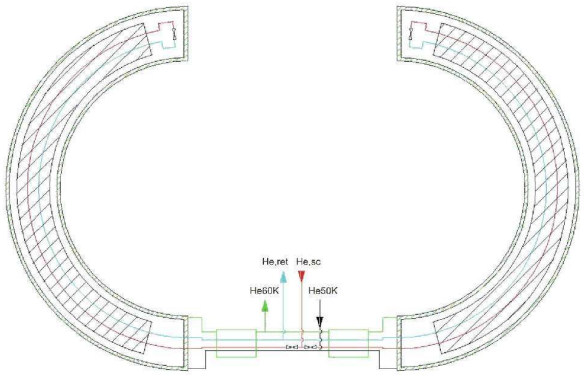

Fig. 46: Flow scheme for the cryogenic system of the HESR, optimized for lowest cryogenic losses.

neutral particles and a layer of myon counters at the end of the calorimeter.
The activities of the IKP for the PANDA detector are focused in three parts:

- the micro vertex detector
- the straw tube tracker
- the simulation of the tracking detectors

6.2.1 Micro Vertex Detector

The Micro Vertex Detector (MVD) plays a major role in the PANDA experiment to identify open charm and strangeness by detecting secondary decays of particles displaced from the primary interaction point. These decay lengths range from several 10 μm for charmed mesons and baryons up to several cm for strange hadrons. To efficiently track the ionizing particles in the solenoidal magnetic field of the detector five sensitive layers are foreseen. Due to the high occupancy and the radiation dose close to the interaction point at least the innermost layers have to be pixel detectors. For the outer layers strip detectors could be used which have the advantages that they are thinner and have fewer readout channels.
Several different technologies could be used for the basic detector component of the MVD. The first question is whether to use monolithic pixel detectors where the sensor and the first amplification stage are on one substrate or hybrid pixel module where the sensor and the electronics are on separate substrates. Monolithic pixel detectors offer the advantage of a high spatial resolution below 10 μm, low power consumption and a low material budget, but their time resolution and radiation hardness are currently not sufficient for the PANDA experiment. Therefore the PANDA collaboration concentrates on the development of a hybrid pixel detector. The first option here is to modify one of the pixel detector concepts developed in the last years by the ATLAS or the CMS collaboration which are close enough to the requirements of the PANDA experiment to be used. The second option is a complete new design of a least the front-end-electronics which would lead to an optimum matching between electronics and requirements but is very time and manpower consuming thus it is not the baseline solution for the PANDA MVD.
Therefore the main task of the IKP in the next year is the evaluation of the ATLAS and CMS front-end electronics in terms of the strict requirements of the PANDA detector

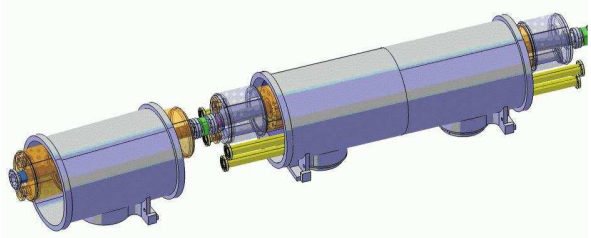

Fig. 47: A detailed study for minimizing the inter magnet distance. The long cryostat segment contains superconducting dipole magnet, the shorter cryostat segment houses the superconducting quadrupole magnet. The beam pipe for antiprotons is shown in dark blue. The yellow pipes transport the He.

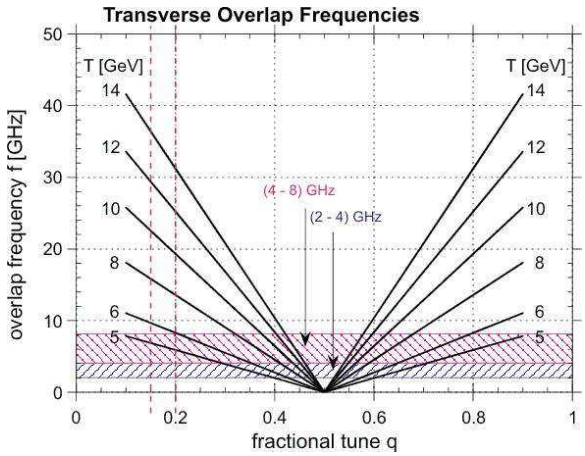

Fig. 48: Dependence of transverse overlap frequencies for stochastic cooling at final energy and fractional tune for different bandwidths. The expected working point of 0.16 is indicated. A higher bandwidth shortens the cooling time. Above 6 GeV a 4–8 GHz system can be used.

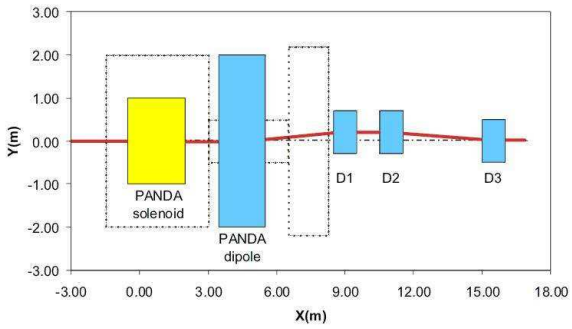

Fig. 49: Details of the PANDA insertion with extra space left for experimental equipment. Solenoid (yellow) and analyzing dipole (big blue one) belong to the experiment. A compensation solenoid can be placed upstream, further dipole magnets for the orbit chicane (small blue ones) are also shown.

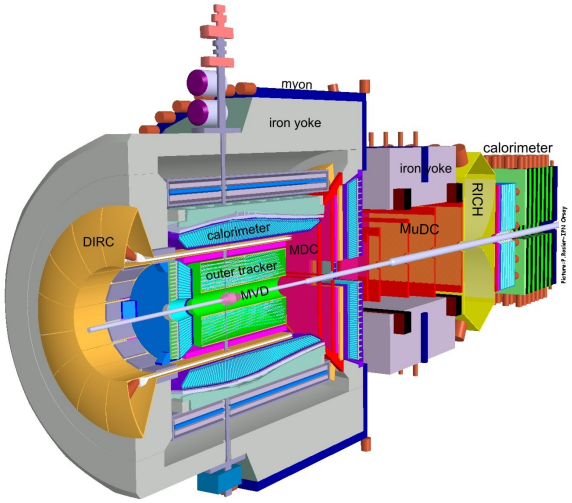

Fig. 50: Schematic view of the general purpose PANDA detector.

and a design of a full micro vertex detector based on one of these solutions.

For a first start of a realistic design of the MVD a module with eight to sixteen ATLAS front-end chips were take which have 25,000 to 50,000 pixel cells with a size of 50 x 400 μm^2. Figure 51 shows a schematic view of the MVD design without the five forward disks. The three innermost barrel layers consist of 70 of the described modules with radii of 1 cm, 2 cm and 4 cm around the beam axis. The barrel part of the MVD is accomplished by two additional layers of strip detectors to get at least four to five track points per charged particle flying through the MVD. In the forward direction two disks out of pixel detectors and three disks out of strip detectors measure the particles with low transverse momentum. The pixel part is already equipped with a liquid cooling system and a lightweight carbon support structure which can be opened to two half-shells for mounting. The cooling and support structure for the strip part of the detector is still missing in this design.

6.2.2 Straw Tube Tracker

The main tracking element of the Panda spectrometer is the Central Tracker (CT). It will occupy a region inside the superconducting solenoid starting at a radial distance of 15 cm from the beam line, up to 42 cm. Along the beam (z) this region extends from 40 cm upstream to 110 cm downstream of the target.

Two different detector technologies are under investigation for the CT: as the baseline option a straw tube tracker (STT) and as an alternative a time projection chamber (TPC) with a GEM readout structure.

With the experience gained by the TOF experiment at COSY the IKP is one of the main contributors to the first option, the straw tube tracker. It will consist of 11 double-layers of 150 cm long straw tubes which are able to han-

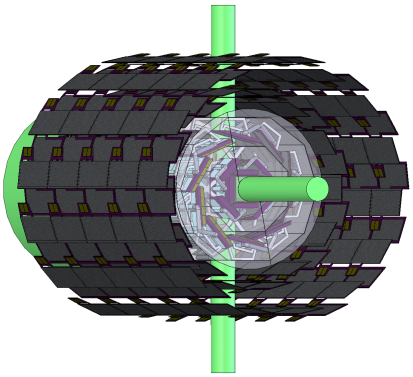

Fig. 51: Schematic view of the micro vertex detector (without the forward disk section)

dle the high rate of 10^7 events per second with a multiplicity of 4–6 charged particles per event with a spatial resolution of 150 μm in both x and y directions. In the baseline design of the straw tube tracker it is foreseen to achieve the required z-resolution of several mm by tilting the different layers by 2° to 3° towards each other like it is done in the WASA experiment. Unfortunately, there are several serious drawbacks to this scheme. First of all, the geometry of skewed layers is rather complicated which leads to geometrical inefficiencies at the end of the tubes. Secondly, the tracker needs a massive side support. Thirdly, the reconstruction of the z-coordinate is complicated posing a difficulty for the online triggering.
An alternative option is the use of charge division and/or time difference techniques. These methods use preamplifiers at both ends of the straws which allows to calculate the z-coordinate of the track by the amplitude ratio between the two signals. This gives a fast track information which is very important for the online triggering, allowing a homogeneous detector layout without any holes in the acceptance and can be self supporting without the need of a massive side support.
A first prototype of a straw tube with double sided readout is under construction in Jülich (figure 52) and first studies about the achievable z-resolution are on its way.

6.2.3 Simulation

The main purpose of Monte Carlo simulations of the detector is to demonstrate if the proposed detector setup can fulfill the physics cases the detector is planed for. Comparisons between some detector configurations should give a rough indication for an ideal detector design. Therefore several benchmark channels were selected which cover the most relevant physics topics.
One of the main topics is the precise charmonium spectroscopy where the tracking detectors play an essential role in the detection of an open charm production. Thus the two physics channels

$$p\overline{p} \rightarrow \psi(3770) \rightarrow D\overline{D}$$

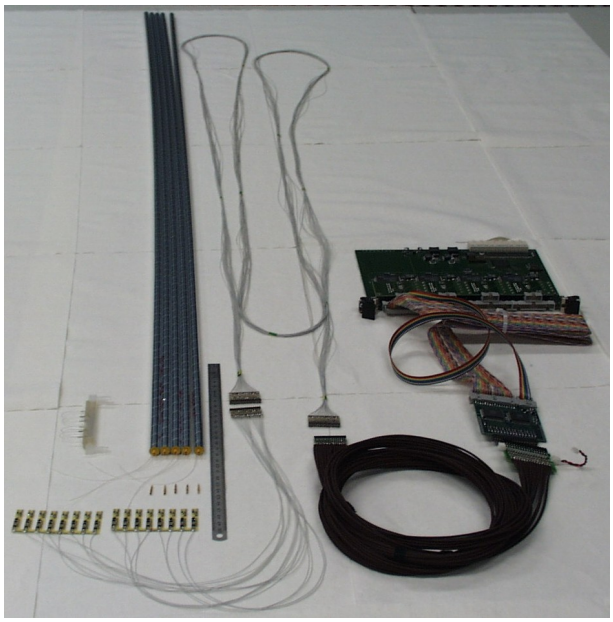

Fig. 52: A photograph of the first 1.5 m straw tube prototype with double sided readout

$$p\overline{p} \rightarrow \psi(4040) \rightarrow D^{*-}D^{*+}$$

were selected as benchmark channels for the tracking detectors.

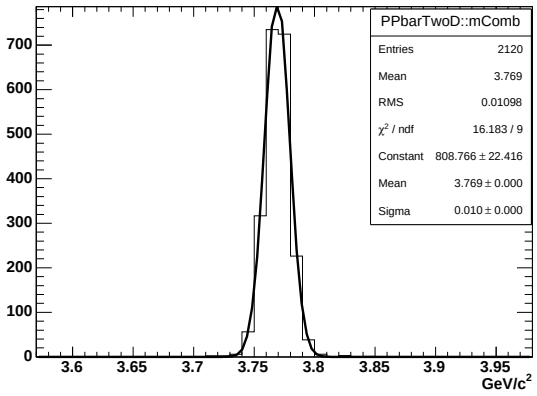

Fig. 53: Invariant mass distribution for simulated $D\overline{D}$ candidate events from the decay of the $\Psi(3770)$.

For the first channel the decay of the $D^{\pm} \rightarrow K^{\mp}\pi^{\pm}\pi^{\pm}$ was chosen for further analysis, because it can be reconstructed using only the tracking and PID information. The D meson has a relatively long lifetime of $c\tau = 311.8\,\mu$m therefore the detection of a displaced decay vertex by the MVD is the most selective condition in this analysis.
As a result of this analysis the invariant mass distribution of the $\Psi(3770)$ was reconstructed from 50 000 simulated events without background (figure 53). A Gaussian fit to the distribution gives the mass resolution of the STT plus the MVD with the excellent value of 10 MeV/c^2. The achievable signal to background ratio is calculated to be

on the order of three.
In the second channel the $D^{*\pm}$ decays by 67.7% into a D^0 and a $\pi^{\pm}$. These pions have very low transverse momentum, thus their registration is based only on the forward part of the MVD. In addition the D^0 only has a lifetime of $c\tau = 123\,\mu$m which imposes specially high demands on the secondary vertex detection ability of the MVD.

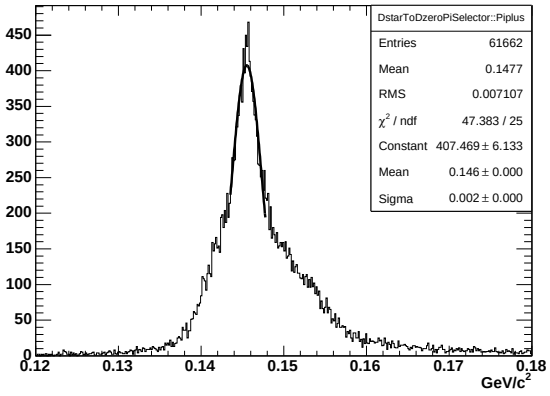

Fig. 54: The difference between the invariant masses of D^{*+} and D^0 mesons. This difference is proportional to the momentum resolution of the MVD for the slow pions from D^* decays.

Figure 54 shows the invariant mass difference between the reconstructed D^{*+} and D^0 meson candidates which shows the ability of the MVD to reconstruct the slow pions with a high accuracy. Together with the straw tube tracker an invariant mass resolution of 19 MeV/c^2 can be achieved for the fully reconstructed $\Psi(4040)$.

6.2.4 PANDA-Meeting in Jülich

The last PANDA collaboration meeting in 2004 took place in Jülich (November, 29 – December, 1). With more than 150 participants, it was the biggest PANDA collaboration meeting to date. The collaboration meeting was dominated by the preparations for the Technical Progress Report which was submitted in January 2005. With about 400 pages, the report will be the guideline for the development of the PANDA detector within the next few years.

6.3 QCD Physics with Polarized Antiprotons at GSI

The possibility to test the nucleon structure via double spin asymmetries in polarized proton-antiproton reactions at the HESR ring of FAIR at GSI has been suggested by the PAX collaboration last year. Since then, there has been much progress, both in understanding the physics potential of such an experiment and in studying the feasibility of efficiently producing polarized antiprotons (http://lanl.arXiv.org/abs/hep-ex/0412063). The physics program of such a facility would extend to a new domain the exceptionally fruitful studies of the nucleon structure performed in unpolarized and polarized deep inelastic scattering (DIS), which have been at the center of high energy physics during the past four decades. It suffices to mention the unique possibility of a direct measurement of the transversity distribution function h_1, one of the last missing fundamental pieces in the QCD description of the nucleon. In the available kinematic domain of the proposed experiment, which covers the valence region, the Drell-Yan double transverse spin asymmetry was recently predicted to be as large as 30%. Other novel tests of QCD at such a facility include the polarized elastic hard scattering of antiprotons on protons and the measurement of the phases of the time-like form factors of the proton. A viable practical scheme which allows us to reach a polarization of the stored antiprotons at HESR-FAIR of $\simeq 30\%$ has been worked out and is accepted for publication in Phys. Rev. Lett. The basic approach to polarizing and storing antiprotons at HESR-FAIR is based on solid QED calculations of the spin transfer from electrons to antiprotons, which is being routinely used at Jefferson Laboratory for the electromagnetic form factor separation, and which has been tested and confirmed experimentally in the FILTEX experiment at TSR-Heidelberg.
The PAX collaboration proposes an approach that is composed of two phases. During these the major milestones of the project can be tested and optimized before the final goal is approached: A **Polarized Antiproton-Proton Asymmetric Collider**, in which polarized protons with momenta of about 3.5 GeV/c collide with polarized antiprotons with momenta up to 15 GeV/c. These circulate in the HESR, which has already been approved and will serve the PANDA experiment. The overall machine setup at the HESR is schematically depicted in Fig. 55:

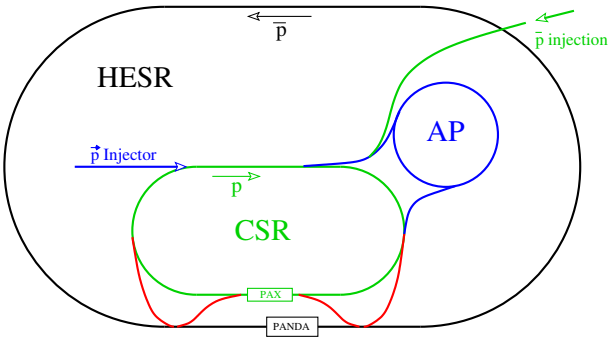

Fig. 55: The proposed accelerator set-up at the HESR (black), with the equipment used by the PAX collaboration in Phase I: CSR (green), AP, beam transfer lines and polarized proton injector (all blue). In Phase II, by adding two transfer lines (red), an asymmetric collider is set up. It should be noted that, in this phase, also fixed target operation at PAX is possible.

1. An Antiproton Polarizer (AP) built inside the HESR area with the crucial goal of polarizing antiprotons at kinetic energies around ≈ 50 MeV ($p \approx 300$ MeV/c), to be accelerated and injected into the other rings.

2. A second Cooler Synchrotron Ring (CSR, COSY-like) in which protons or antiprotons can be stored with a momentum up to 3.5 GeV/c. This ring shall have a straight section, where a PAX detector could be installed, running parallel to the experimental straight section of HESR.

3. By deflection of the HESR beam into the straight section of the CSR, both the collider or the fixed-target mode become feasible.

It is worthwhile to stress that, through the employment of the CSR, effectively a second interaction point is formed with minimum interference with PANDA. The proposed solution opens up the possibility to run two different experiments at the same time. The physics program should be pursued in two different phases.

Phase I A beam of unpolarized or polarized antiprotons with momentum up to 3.5 GeV/c in the CSR ring, colliding on a polarized hydrogen target in the PAX detector. This phase is independent of the HESR performance. This first phase, at moderately high energy, will allow for the first time the measurement of the time-like proton form factors in single and double polarized $\bar{p}p$ interactions in a wide kinematical range, from close to threshold up to $Q^2 = 8.5$ GeV^2. It would enable to determine several double spin asymmetries in elastic $\vec{p}^{\uparrow}p^{\uparrow}$ scattering. By detecting back scattered antiprotons one can also explore hard scattering regions of large t: In proton-proton scattering the same region of t requires twice the energy. There are no competing facilities at which these topical issues can be addressed.

Phase II This phase will allow the first ever direct measurement of the quark transversity distribution h_1, by measuring the double transverse spin asymmetry A_{TT} in Drell-Yan processes $p^{\uparrow}\vec{p}^{\uparrow} \to e^+e^-X$ as a function of Bjorken x and Q^2 (= M^2)

$$A_{TT} \equiv \frac{d\sigma^{\uparrow\uparrow} - d\sigma^{\uparrow\downarrow}}{d\sigma^{\uparrow\uparrow} + d\sigma^{\uparrow\downarrow}} = \hat{a}_{TT} \frac{\sum_q e_q^2 h_1^q(x_1, M^2) h_1^{\bar{q}}(x_2, M^2)}{\sum_q e_q^2 q(x_1, M^2) \bar{q}(x_2, M^2)},$$

where $q = u, \bar{u}, d, \bar{d} \ldots$, M is the invariant mass of the lepton pair and $\hat{a}_{TT}$, of the order of one, is the calculable double-spin asymmetry of the QED elementary process $q\bar{q} \to e^+e^-$. Two possible scenarios might be foreseen to perform the measurement:
(a) **Asymmetric Collider:** A beam of polarized antiprotons from 1.5 GeV/c up to 15 GeV/c circulating in the HESR, colliding on a beam of polarized protons with momenta up to 3.5 GeV/c circulating in the CSR. This scenario however requires to demonstrate that a suitable luminosity is reachable. Deflection of the HESR beam to the PAX detector in the CSR is necessary (see Fig. 55).
By proper variation of the energy of the two colliding beams, this setup would allow a measurement of the transversity distribution h_1 in the valence region of $x > 0.05$, with corresponding $Q^2 = 4 \ldots 100$ GeV^2. A_{TT} is predicted to be larger than 20% over the full kinematic range, up to the highest reachable center-of-mass energy of $\sqrt{s} \sim \sqrt{200}$. The cross section is large as well: With a luminosity of $5 \cdot 10^{30}$ cm^{-2}s^{-1} about 2000 events per day can be expected. A first estimate indicates that in the collider mode luminosities in excess of 10^{30} cm^{-2}s^{-1} could be reached. (We are presently evaluating the influence of intra-beam scattering, which seems to be one of the limiting factors.) For the transversity distribution h_1, such an experiment can be considered as the analogue of polarized DIS for the determination of the helicity structure function g_1, *i.e.* of the helicity distribution $\Delta q(x, Q^2)$; the kinematical coverage (x, Q^2) will be similar to that of the HERMES experiment.
(b) **High luminosity fixed target experiment:** If the required luminosity in the collider mode is not achievable, a fixed target experiment can be conducted. A beam of 22 GeV/c (15 GeV/c) polarized antiprotons circulating in the HESR is used to collide with a polarized internal hydrogen target. Also this scenario requires the deflection of the HESR beam to the PAX detector in the CSR (see Fig. 55).
A theoretical discussion of the significance of the measurement of A_{TT} for a 22 GeV/c (15 GeV/c) beam impinging on a fixed target is given in http://lanl.arXiv.org/abs/hep-ex/0412063. The theoretical work on the K-factors for the transversity determination is in progress. This measurement will explore the valence region of $x > 0.2$, with corresponding $Q^2 = 4 \ldots 16$ GeV^2. In this region A_{TT} is predicted to be large (of the order of 30%, or more) and the expected number of events can be of the order of 2000 per day.
To summarize, we note that the storage of polarized antiprotons at HESR will open unique possibilities to test QCD in hitherto unexplored domains. This will provide another cornerstone to the antiproton program at FAIR.

7 Technical Developments

7.1 Targets

7.1.1 Polarized Internal Target for ANKE

The polarized hydrogen and deuterium atomic beam source (ABS), which will feed the storage-cell gas target of the spectrometer ANKE, and the Lamb-shift polarimeter (LSP), and which will be used to measure the nuclear target polarization, are ready for installation at the new target chamber of ANKE. A computer-controlled positioning device will allow us to install target cells and to center them onto the COSY-beam axis. Prior to the transfer, an essential improvement of the LSP has been made by the installation of a non-evaporable getter (NEG) pump around the ionization volume of the ionizer, leading to an appreciable reduction of the background in the ion beam. All infrastructure components, developed together with Zentralabteilung Allgemeine Technologie of FZJ, and the slow control system of ABS and LSP, developed with Zentralinstitut für Elektronik of FZJ, are available. ABS and LSP have been transferred to the "LKW-Schleuse", a separate area within the COSY hall outside the accelerator tunnel. Figure 56 shows the assembly there.

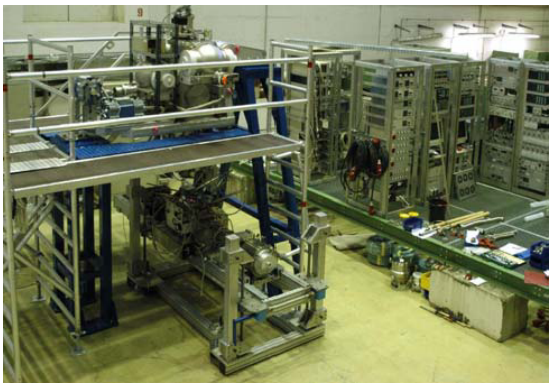

Fig. 56: The experimental setup in the "LKW-Schleuse" of the COSY hall: The ABS (vertical) in its horizontal support bridge, the LSP (horizontal) in the lower support system, and the ISTC chamber underneath the ABS. On the right-hand side the movable platform (green) with the supply units for ABS and LSP is shown.

The vertical ABS is mounted in the new horizontal frame, which is carried by two support posts. The LSP is horizontally mounted in a support, which allows one to change the height. In the lower position, with the ionizer mounted vertically and followed by a 90° deflector, the direct beam from the ABS can be studied, whereas in the higher position, with the ionizer mounted horizontally, investigations of gas samples extracted from test cells fed by the ABS become possible. All the supply units are assembled on a moveable platform. Thus, a few crane movements only are needed to transfer the ABS in its support bridge, LSP, and supply units to and from the ANKE target place. Between the beam-times, where ABS and LSP are used at ANKE, these instruments are employed in the "LKW-Schleuse" combined with an additional device, developed at the St. Petersburg Nuclear Physics Institute (PNPI) in Gatchina in the framework of an International-Science-and-Technology-Center (ISTC) project. This worldwide unique combination of ABS, the PNPI chamber with exchangeable test cells in a strong magnetic field produced by a superconducting magnet, and the LSP for polarization analysis, will allow hitherto inaccessible studies of the recombination process of polarized hydrogen or deuterium atoms on various wall materials as function of the wall temperature and of the nuclear polarization maintained in the recombined molecules.

7.1.2 The Frozen Pellet Target

The assembly of the Moscow-Jülich pellet target — which will allow for experiments at internal target stations with highest luminosities up to few 10^{32} $cm^{-2}s^{-1}$ — has been finalized. It is located in a dedicated test stand in the COSY accelerator hall. During 15 test runs in 2001 – 2004 reliable production of pellets from H_2 and N_2 has been demonstrated over periods of several days. Other target materials like D_2, N_2, Ar and Xe can also be used.

In a pellet target a continuous flow of droplets is generated by injecting a liquefied gas through a thin vibrating nozzle into a triple-point chamber (TPC), where temperatures and pressures close to TP conditions for the particular target material are maintained (*e.g.* about 14 K / 100 mbar for H_2 or 83 K / 800 mbar for Ar). The diameter of the droplets and, finally, of the frozen pellets can be adjusted by changing the nozzle diameter and/or the jet velocity.

During the test runs, nozzles of different materials have been used. All of them have been produced and tested at the Institute for Theoretical and Experimental Physics in Moscow. The first nozzle type with diameters 20 – 50 μm is made of stainless steel. The second, shown in Fig. 57, with diameters 10 – 40 μm comprises capillaries from quartz glass which are glued into brass housings. With both nozzle types stable droplet production has been achieved, the pellet sizes are slightly larger than the nozzle diameters, *e.g.* 15 – 50 μm for the glass/brass type. The jet velocities are roughly two times smaller when using steel nozzles.

When the droplets pass through a sluice (length $\sim$5 cm, inner diameter $\sim$0.6 mm) into the accelerator vacuum they are further cooled by surface evaporation, thus producing the frozen pellets. Figure 58 shows a video-camera image (obtained with stroboscope illumination) of nitrogen pellets just behind this sluice. The diameter of the pellets is $\sim$30 μm, the nozzle for droplet production has a diameter of $\sim$17 μm. Systematic tests showed that the size and frequency stability of the pellets is not worse than 10%. For 2005 it is planned to prepare the target

Fig. 57: Nozzles from quartz glass and brass for droplet production.

for installation at COSY in order to perform systematic investigations of beam-target interactions.

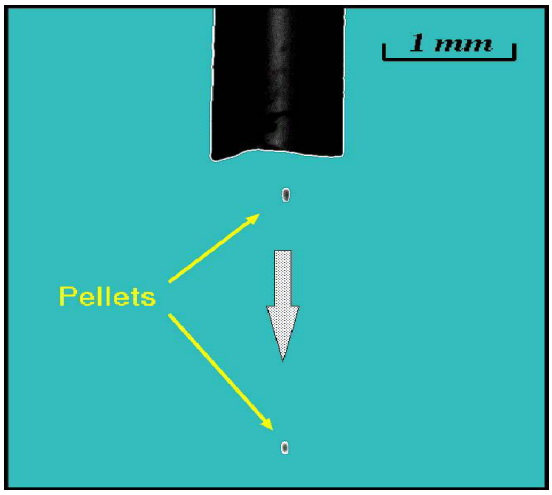

Fig. 58: Photo of Nitrogen pellets with ø∼30 μm leaving the sluice behind the triple-point chamber (TPC) into high vacuum.

7.1.3 Polarized Target for COSY-TOF

In the near future, it is planned to measure the spin correlation coefficient A_{xx} at COSY to determine the parity of the Θ^+ from the reaction $\vec{p}\vec{p} \to \Sigma^+\Theta^+$ near the production threshold. The measurement of A_{xx} requires transverse polarized protons in the initial state provided by a polarized beam and a polarized target, respectively. There can be significant technical problems in the use of a polarized target for the proposed experiment. To detect the charged particles of the nominal process exiting the target with a reasonable efficiency, the first detector components must be placed as close as possible to the interaction vertex, which limits the outer diameter of the target refrigerator. In order to achieve the necessary statistical precision, one must have a reasonably thick target with a high polarization. The target material should also be resistant to localized beam heating and radiation damage to avoid depolarizing the sample unevenly, particularly in the region of the beam.
To obtain a reasonable count rates in the case of a limited beam intensity, a wide opening angle with the ability to place detector components as close as possible to the target material is needed. This can be achieved with the concept of the frozen spin target. A reliable technique has been demonstrated by the Bonn-Bochum Polarized Target group with the PS185 experiment where the spin-transfer parameter D_{nn} in hyperon production ($\bar{p}p \uparrow\!\!\rightarrow \Lambda\bar{\Lambda}$) was measured at the antiproton accelerator LEAR (CERN) in 1996. A maximum proton polarization of about $\pm$70% has been reached in a polarizing field of 2.5 T, typical relaxation times of $\tau \sim 100$ h led to an average polarization magnitude over the entire data taking period of about 62%.
Both experiments, the planned parity measurement of the Θ^+ at COSY and the D_{nn}-measurement at PS185/3, are comparable in various demands and it is proposed to combine the existing frozen spin target used at the PS185/3 experiment with a new TOF-start counter setup. However, with respect to the special boundary conditions of the experimental area at COSY and the TOF-detector as well as the experimental requirements of the scattering observable, the target has to be partially modified and adapted to the detector setup.
The mechanical structure containing the main target components like the dilution refrigerator and the superconducting polarization magnet, placed in front of the TOF-detector arrangement has to be renewed. The second main modification on the target system concerns the target material itself. To get a reasonable luminosity and a high acceptance for the reconstruction of the nominal process, the beam intensity has to be maximized and the beam spot on the production target to be minimized. We aim at an intensity of 10^7 protons/s at a beam spot of about 1 mm^2. The preparation of the material and measurements of the polarization behavior will be done at the Bochum polarized target laboratory. In the meantime, the complete target setup is being installed and tested at Bonn University. As soon as all components including the target material are running with the expected parameters (high polarization and long relaxation times) the system will be moved to the IKP and installed at the TOF experimental area at COSY. A schematic view of the new setup is shown in Fig. 59.

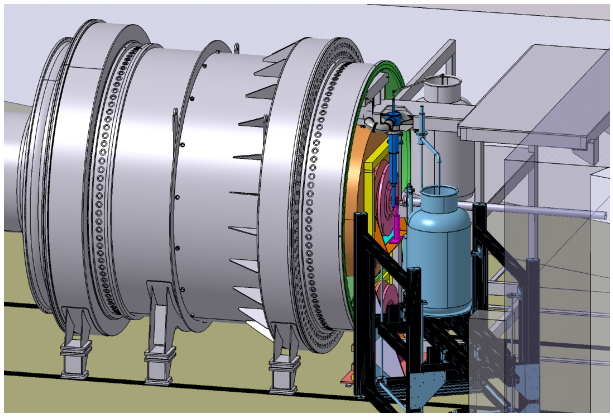

Fig. 59: The new COSY-TOF setup which will include the polarized target.

7.2 Achievements of the Laboratory for Semiconductor Detectors

7.2.1 Introduction

Semiconductor detectors play an indispensable role in physics due to their outstanding characteristics. This includes small size, and high energy- and spatial resolution. Their biggest drawback is that it is hard to find dependable suppliers especially in constraining situations that demand specific stopping capability, high granularity, and very good energy resolution.

As in many cases the feasibility of experiments hinges on the availability of an appropriate detector the only way out is to have a detector laboratory that is capable to manufacture custom made detectors. The IKP has been for a long time in the favorable situation to draw on the expertise and excellence of its detector laboratory that has been accumulating for decades the know-how that enables them to provide tailor made solutions to otherwise unsolvable problems. This ability has won them worldwide recognition and quite a few world-class laboratories (*e.g.* GSI, Lawrence Livermore National Laboratory (LLNL), Naval Research Laboratory) have asked for help to obtain custom made detectors with attached electronic modules for preprocessing the signals.

7.2.2 ANKE and Si(Li) detectors

For the ANKE vertex group three additional Si(Li) detectors were built. The detectors with an active area of 64 mm $\times$ 64 mm possess a thickness of 5.1 mm. Position resolution is given through an electrode structure of 96 strips on the front- and, arranged orthogonally, 96 strips on the backside. Support was given in mounting, gluing and bonding.

The development of 10 mm thick detectors has been initiated. One of the 10 mm thick Si(Li) orthogonal-strip detectors is now being used as the scatter detector of the Compact Si+Ge Compton Camera at LLNL, is shown in Fig. 60. Energy resolutions [FWHM] between 1.5 and 2.0 keV have been achieved at LN_2-temperature when operating all channels. By combining two-dimensionally segmented semiconductor detectors such as Si, Ge or CdZnTe with pulse-shape processing one can obtain three-dimensional position information of interactions to an accuracy of about 0.5 mm in all three dimensions at 122 keV with a "pixel" size of 2 mm $\times$ 2 mm.

7.2.3 GEM and Ge-detectors

The unique Germanium Wall, a highly granular germanium telescope having a 1.8 mm thick "Quirl" with 200 spirals on the front and 200 spirals on the back and three 17 mm thick segmented germanium disks has been successfully regenerated by removing any detrimental radiation damage before using it in two runs in 2004.

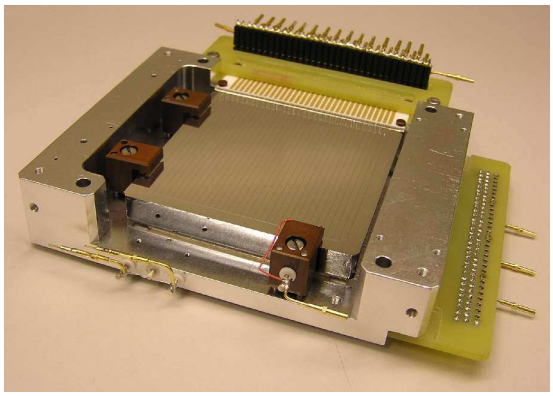

Fig. 60: The Si(Li) detector (9.7 mm thick) mounted in the LLNL holder.

Two-dimensional Ge-strip detectors with their inherent advantages concerning spectroscopy and imaging capabilities as well as polarization sensitivity are central for precision X-ray spectroscopy of highly charged heavy ions at GSI-Darmstadt. To manufacture them a newly developed method for producing position sensitive structures on germanium detectors having amorphous Ge contacts (a-Ge contacts) has been utilized. Detectors were successfully used at GSI for the spectroscopy of atomic transitions in the hard X-ray regime above 15 keV and for polarization studies. For the first prototype a germanium diode (70 mm $\times$ 41 mm, 11 mm thick) with 128 strips of boron implanted p+-contacts on the junction side and a blocking a-Ge contact of 48 strips on the other side was prepared. The detector is mounted in a cryostat, which allows any orientation of the detector with respect to a photon source even if the dewar is full. A view of the detector holder and the connection to the preamplifiers placed outside the vacuum system is shown in Fig. 61.

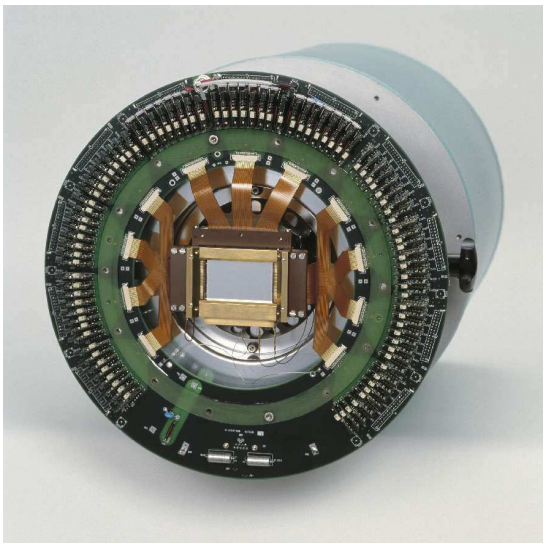

Fig. 61: View of the Ge-detector and one half of the preamplifiers with open cryostat cap.

7.2.4 Outlook

Efforts are underway to raise the thickness of Si(Li) detectors. A 20 mm thick diode with a diameter of 102 mm is in the process of being drifted. Meanwhile more than half of the thickness has already been Li-compensated. Driftable material with diameters of 5 to 6 inches seems to become available soon and would open new applications for this kind of detectors.

A Councils

A.1 Scientific Council

Prof. J.P. Blaizot	CEA Saclay, FR	
Prof. P. Braun-Munzinger	GSI Darmstadt, DE	Chairperson
Prof. D.F. Geesaman	Argonne National LAboratory	
Prof. H. Halling	ZEL, FZ-Jülich, DE	
Prof. M. Harakeh	KVI Groningen, NL (Chairman PAC)	
Prof. D. von Harrach	Universität Mainz, DE	
Prof. E. Hilger	Universität Bonn, DE	
Prof. Y. Nagai	RCNP, JP	
Prof. A.W. Thomas	Thomas Jefferson National Lab, U.S.A.	
Dr. D. Trines	DESY Hamburg, DE	

A.2 Program Advisory Committee

Prof. H. Freiesleben	TU Dresden, DE	
Prof. B. Friman	GSI Darmstadt, DE	
Prof. M. Garçon	CEA Saclay, FR	
Prof. M.N. Harakeh	KVI Groningen, NL	Chairperson
Prof. T. Johansson	Uppsala Universitet, SE	
Prof. R. Landua	CERN, CH	
Prof. V. Metag	Universität Gießen, DE	
Prof. W. Meyer	Universität Bochum, DE	
Prof. W.T.H. van Oers	University of Manitoba, CA	
Prof. E. Oset	Universitat de Valencia, ES	
Prof. E. Radermacher	CERN, CH	
Prof. C. Schaerf	INFN Roma II, IT	

B Personnel

Scientific Staff

Msc. M.-M. Abdel-Bary (E1)

Dr. Abdel Samad (E1)

DP S. An (GG)

Prof. Dr. G. Baur (TH) (a.o. Prof. Univ. Basel)

Dr. U. Bechstedt (GG)

DP A. Bogdanov (GG) until Jul., 2004

DP V. Bollini (E1) (until Feb. 5, 2004)

Dr. K. Bongardt (GG)

DI N. Bongers (GG)

DI W. Borgs (E2)

DI W. Bräutigam (GG)

DI R. Brings (GG)

DP A. Bubak (E1) (until Feb. 19, 2004)

Dr. M. Büscher (E2)

DP D. Chiladze (E2)

R. Czyzykiewicz (E1)

Dr. habil. J. Dietrich (GG) (PD Univ. Dortmund)

Dr. A. Djalois (E1)

DP A. Dzyuba (E2)

Dr. R Eichhorn (GG)

Dr. R. Engels (E2)

DI F.-J. Etzkorn (GG)

Dr. K. Fan (GG)

Dr. P. Fedorets (E2) (since Sep., 2004)

Dr. O. Felden (Rs)

Prof. Dr. D. Filges (E1) (apl. Prof. Univ. Wuppertal) (until Jan 31, 2004)

DP M. Frink (TH) (until Oct. 31, 2004)

Dr. W. Gast (E1)

Dr. R. Gebel (GG)

Dr. habil. A. Gillitzer (E1) (PD Univ. Bonn)

Dr. habil. F.Goldenbaum (E1) (PD Univ. Wuppertal)

Dr. habil.D. Gotta (E2) (PD Univ. Köln)

Dr. F. Grümmer (TH)

Dr. D. Grzonka (E1)

Dr. habil. J. Haidenbauer (TH) (PD Univ. Graz)

Dr. C. Hanart (TH)

Dr. M. Hartmann (E2)

Dr. V. Hejny (E2)

DI K. Henn (GG)

DP V. Kamerdjiev (GG)

DP I. Keshelashvili (E2)

Prof Dr. K. Kilian (E1) (until Jul. 31, 2004)

DP D. Kirillov (GG) (since Oct. 19, 2004)

Dr. V. Kleber (E2)

Dr. St. Kliczewski (E1)

Prof. Dr. S. Krewald (TH) (apl. Prof. Univ. Bonn)

DI K. Kruck (GG)

Dr. P. Kulessa (E2)

Dr. A. Lehrach (GG)

DP V. Lenski (TH) (since Mar. 8, 2004)

DI B. Lensing (E1) (until Aug. 6, 2004)

DP V. Leontyev (E2)

DP M. Lesiak (E1) (since Sep. 1, 2004)

DP E. Lieder (E1) (until Oct. 31, 2004)

Dr. B. Lorentz (GG)

Prof. Dr. H. Machner (Prof. Univ. Duisburg-Essen)

Dr. Y. Maeda (E2)

Prof. Dr. R. Maier (GG) (Prof. Univ. Bonn)

DI J. Majewski (E2) (Jun. 1 to Dec. 31, 2004)

Dr. S. Martin (GG)

Prof. Dr. U.-G. Meißner (TH) (Prof. Univ. Bonn)

DI I. Mohos (GG)

Dr. H.-P. Morsch (E1)

Dr. P. Moskal (E1)

DP A. Mussgiller (E2)

Dr. M. Nekipelov (E2)

Prof. Dr. N. N. Nikolaev (TH)

Dr. K. Nünighoff (E1)

Prof. Dr. W. Oelert (E1) (apl. Prof. Univ Bochum)

Dr. H. Ohm (E2)

DI N. Paul (E1)

DP F. Pavlov (TH)

DP B. Piskor-Ignatowicz (E1) (since Mar., 1, 2004)

L. Platter (TH)

Dr. H. Polinder (TH) (since Jun., 14, 2004)

Dr. D. Prasuhn (GG)

DP D. Protic (Dt)

Dr. habil. F. Rathmann (E2) (PD Univ. Erlangen)

DI A. Richert (GG)

Prof. Dr. J. Ritman (E2) (Prof. Univ. Bochum) (since Sep., 17, 2004)

Dr. E. Roderburg (E1)

Dr. P. v. Rossen (GG)

DP T. Rozek (E1)

DI J. Sarkadi (Ec)

DP F. Sassen (TH)

Dr. H. Schaal (E1)

Dr. S. Schadmand (E1) (since Sep. 1, 2004)

Dr. W. Schäfer (TH) (until Dec. 31, 2004)

Dr. R. Schleichert (E2)

Dr. A. Schnase (GG)

DP S. Schneider (TH) (until Apr. 30, 2004)

DI H. Schneider (GG)

DI G. Schug (GG)

Dr. Th. Sefzick (Ec)

DI E. Senichera (GG) (since Apr. 1, 2004)

Dr. Y. Senichev (GG)

Dr. A. Sibirtsev (TH) (until Oct. 31, 2004)

DI M. Simon (GG)

DP A. Sokolov (E1) (since Aug. 1, 2004)

DI R. Stassen (GG)

Dr. H.-J. Stein (E2)

G. Sterzenbach (E1)

Dr. H. Stockhorst (GG)

Prof. Dr. H. Ströher (E2) (Prof. Univ. Köln)

Prof. Dr. J. Tang (GG) (until Mar. 12, 2004)

Dr. R. Tölle (GG)

DP A. Ucar (E1)

DP Y. Valdau (E2)

DI T. Vashegi (GG)

DP N. Vasiukhin (GG)

DP P. Vlasov (E1) (since Sep. 3, 2004)

Dr. K.-H. Watzlawik (E2)

J. Wimmer (E1)

DP P. Winter (E1)

Dr. P. Wintz (E1)

Dr. A. Wirzba (TH) (since Aug. 16, 2004)

DI J.-D. Witt (GG)

Dr. M. Wolke (E1)

DP A. Wronska (E2) (until Aug. 30, 2004)

Dr. E. Zaplatin (GG)

DP D. Z. Zhang (E1) (since Oct. 10, 2004)

B.1 Technical and Administrative Staff

C. Berchem (Ec)

P. Birx (GG)

H.-G. Böge (GG) (until Nov. 30, 2004)

M. Böhnke (GG)

J. Borsch (GG)

J. But (Ws)

M. Comuth (Ad)

W. Derissen (Cd)

N. Dolfus (Ec)

G. D'Orsaneo (E2)

R. Dosdall (E1) (since Sep., 2004)

B. Dahmen (GG)

C. Deliege (GG)

R. Enge (GG)

J. Engel (GG) (until Dec. 31, 2004)

B. Erkes (GG)

W. Ernst (Ec)

K. Esser (Ad)

H.-P. Faber (GG)

G. Fiori (Dt)

H.-W. Firmenich (Ws)

N. Gad (GG)

D. Gehsing (GG)

J. Göbbels (Rs)

H. Hadamek (Ws)

R, Hecker (GG)

E. Heßler (Cd)

M. Holona (Ws)

H.-M. Jäger (E1)

H. J. Jansen (Ws)

R. Jansen (Ad) (until Jul., 2004)

M. Karnadi (E2)

A. Kieven (GG)

K. Krafft (Rs)

Ch. Krahe (Ws)

M. Kremer (Ws)

Th. Krings (Dt)

G. Krol (GG)

M. Küven (Ws)

K.-G. Langenberg (GG)

G. Lürken (Ec)

H. Metz (Dt)

S. Müller (Ad)

R. Nellen (Ec)

H. Pütz (GG)

G. Roes (Ad)

N. Rotert (GG)

D. Ruhrig (GG)

T. Sagefka (GG)

F. Scheiba (GG)

H. Schiffer (Ec)

J. Schmitz (GG)

F. Schultheiß (Ws)

K. Schwill (Dt)

H. Singer (GG)

D. Spölgen (E2)

J. Strehl (Ws)

V.N. Tika (E1) (until Apr. 30, 2004)

J. Uehlemann (E1)

P. Wieder 9E2)

H. Zens (GG)

Ad = Administraion
Cd = Construction
Dt = Detectors
E1 = IKP-1
E2 = IKP-2
Ec = Electronics
GG = Accelerator Division
Rs = Radiation Safety
TH = Theory
Ws = Workshop

C Publications 2004

1. Experiment

1. **Determination of the $\bar{K}^0 d$ scattering length from the reaction $pp \to d\bar{K}^0 K^+$**
   A. Sibirtsev, M. Büscher, V.Yu. Grishina, C. Hanhart, L.A. Kondratyuk, S. Krewald, U.-G. Meißner
   Phys. Lett. B **601** *(2004) 132*

2. **$a_0^+(980)$ resonance production in the reaction $pp \to d\pi^+\eta$ close to the $K\bar{K}$ threshold**
   P. Fedorets, M. Büscher, V.P. Chernyshev, S. Dymov, V.Yu. Grishina, C. Hanhart, M. Hartmann, V. Hejny, V. Kleber, H.R. Koch, L.A. Kondratyuk, V. Koptev, A.E. Kudryavtsev, P. Kulessa, S. Merzliakov, S. Mikirtychiants, M. Nekipelov, H. Ohm, R. Schleichert, H. Ströher, V.E. Tarasov, K.-H. Watzlawik, I. Zychor
   sub. to Phys. Atom. Nucl. [Yad. Fiz.] [arXiv:nucl-ex/0501027]

3. **Near-threshold production of ω mesons in the $pn \to d\omega$ reaction**
   S. Barsov, I. Lehmann, R. Schleichert, C. Wilkin, M. Büscher, S. Dymov, Ye. Golubeva, M. Hartmann, V. Hejny, A. Kacharava, I. Keshelashvili, A. Khoukaz, V. Komarov, L. Kondratyuk, N. Lang, G. Macharashvili, T. Mersmann, S. Merzliakov, A. Mussgiller, M. Nioradze, A. Petrus, H. Ströher, Y. Uzikov, B. Zalikhanov
   Eur. Phys. J. A **21** *(2004) 507*

4. **Inclusive K^+-meson production in proton-nucleus interactions**
   M. Büscher, V. Koptev, M. Nekipelov, Z. Rudy, R. Schleichert, H. Ströher, Yu. Valdau, S. Barsov, M. Hartmann, V. Hejny, V. Kleber, N. Lang, I. Lehmann, N. Lang, S. Mikirtychiants, H. Ohm
   Eur. Phys. J. A **22** *(2004) 301*

5. **Measurement of the analyzing power in $\vec{p}d \to (pp)n$ with a fast forward $^1S_0$-diproton**
   S. Yaschenko, S. Dymov, V. Komarov, G. Macharashvili, F. Rathmann, S. Barsov, M. Hartmann, R. Gebel, A. Kacharava, A. Khoukaz, P. Kulessa, A. Kulikov, V. Kurbatov, N. Lang, I. Lehmann, B. Lorentz, T. Mersmann, S. Merzliakov, S. Mikirtytchiants, A. Mussgiller, M. Nioradze, H. Ohm, D. Prasuhn, R. Schleichert, H. Seyfarth, E. Steffens, H.J. Stein, H. Ströher, Yu. Uzikov, B. Zalikhanov, N. Zhuravlev
   Phys. Rev. Lett., in print [arXiv:nucl-ex/0407018]

6. **Spectator detection for the measurement of proton-neutron interactions at ANKE**
   I. Lehmann,S. Barsov, R. Schleichert, C. Wilkin, M. Drochner, M. Hartmann, V. Hejny, S. Merzliakov, S. Mikirtychiants, A. Mussgiller, D. Protic, H. Ströher, S. Trusov, P. Wüstner
   Nucl. Instr. Meth. A **530** *(2004) 275*

7. **Experimental study of $pp\eta$ dynamics in the $pp \to pp\eta$ reaction**
   P. Moskal, H.H. Adam, A. Budzanowski, R. Czyżykiewicz, D. Grzonka, M. Janusz, L. Jarczyk, B. Kamys, A. Khoukaz, K. Kilian, P. Kowina, K. Nakayama, W. Oelert, C. Piskor-Ignatowicz, J. Przerwa, T. Rozek, R. Santo, G. Schepers, T. Sefzick, M. Siemaszko, J. Smyrski, S. Steltenkamp, A. Tächner, P. Winter, M. Wolke, P. Wüstner, W. Zipper
   Phys. Rev. C **69** *(2004) 025203*

8. **Total and differential cross sections for the $pp \to pp\eta'$ reaction near threshold**
   A. Khoukaz, I. Geck, C. Quentmeier, H.H. Adam, A. Budzanowski, R. Czyżykiewicz, D. Grzonka, L. Jarczyk, K. Kilian, P. Kowina, N. Lang, T. Lister, P. Moskal, W. Oelert, C. Piskor-Ignatowicz, T. Rozek, R. Santo, G. Schepers, T. Sefzick, S. Sewerin, M. Siemaszko, J. Smyrski, A. Strzałkowski, A. Täschner, P. Winter, M. Wolke, P. Wüstner, W. Zipper
   Eur. Phys. J. A **20** *(2004) 345*

9. **Energy dependence of the Λ/Σ° production cross section ratio in p-p interactions**
   P. Kowina, M. Wolke, H.H. Adam, A. Budzanowski, R. Czyżykiewicz, D. Grzonka, J. Haidenbauer, M. Janusz, L. Jarczyk, A. Khoukaz, K. Kilian, P. Moskal, W. Oelert, C. Quentmeier, C. Piskor-Ignatowicz, J. Przerwa, T. Rożek, R. Santo,G. Schepers, T. Sefzick, M. Siemaszko, J. Smyrski, S. Steltenkamp, A. Strzałkowski, P. Winter, P. Wüstner, W. Zipper
   Eur. Phys. J. A **22** *(2004) 293*

10. **Drift chamber with a c-shaped frame**
    J. Smyrski, Ch. Kolf, H.-H. Adam, A. Budzanowski, R. Czyzykiewicz, D. Grzonka, M. Janusz, L. Jarczyk, B. Kamys, A. Khoukaz, K. Kilian, W. Oelert, C. Piskor-Ignatowicz, J. Przerwa, T. Rozek, R. Santo, G. Schepers,T. Sefzick, M. Siemaszko, A. Taschner, P. Winter, M. Wolke, P. Wustner, W. Zipper
    Nucl. Instr. Meth. A, in print [arXiv:nucl-ex/0501023]

11. **A precision measurement of pp elastic scattering cross-sections at intermediate energies**
Albers,D., Bauer,F., Bisplinghoff,J., Bollmann,R., Büßer,K., Busch,M., Daniel,R., Diehl,O., Dohrmann,F., Engelhardt,H. P., Ernst,J., Eversheim,P. D., Gasthuber,M., Gebel,R., Greiff,J., Groß,A., Groß-Hardt,R., Heider,S., Heine,A., Hinterberger,F., Hüskes,T., Igelbrink,M., Jeske,M., Langkau,R., Lindlein,J., Maier,R., Maschuw,R., Mosel,F., Prasuhn,D., Rohdjeß,H., Rosendaal,D., von Rossen,P., Scheid,N., Schirm,N., Schulz- Rojahn,M., Schwandt,F., Schwarz,V., Scobel,W., Thomas,S., Trelle,H.-J., Weise,E., Welinghausen,A., Woller,K., Ziegler,R.
Eur. Phys. J. A, 22 (2004), 125

12. **Evidence for a narrow resonance at 1530 MeV/c^2 in the $K^\circ p$ system of the reaction $pp \to \Sigma^+ K^\circ p$ from the COSY-TOF experiment**
M. Abdel-Bary, S. Abdel-Samad, K.Th. Brinkmann, H. Clement, E. Doroshkevich, M. Drochner, S. Dshemuchadse, A. Erhardt, W. Eyrich, D. Filges, A. Filippi, H. Freiesleben, M. Fritsch, J. Georgi, A. Gillitzer, D. Hesselbarth, R. Jakel, B. Jakob, L. Karsch, K. Kilian, H. Koch, J. Kress, E. Kuhlmann, S. Marcello, S. Marwinski, R. Meier, P. Michel, K. Moller, H. Mortel, H.P. Morsch, N. Paul, L. Pinna, C. Pizzolotto, M. Richter, E. Roderburg, P. Schonmeier, W. Schroeder, M. Schulte-Wissermann, T. Sefzick, F. Stinzing, G.Y. Sun, A. Teufel, A. Ucar, G.J. Wagner, M. Wagner, A. Wilms, P. Wintz, St. Wirth, P. Wüstner
Phys. Lett. B **595** *(2004) 127*

13. **PISA — an experiment for fragment spectroscopy at the internal beam of COSY: application of an axial ionization chamber**
R. Barna, V. Bollini, A. Bubak, A. Budzanowski, D. De Pasquale, D. Filges, S. Förtsch, F. Goldenbaum, A. Heczko, H. Hodde, A. Italiano, L. Jarczyk, B. Kamys, J. Kisiel, M. Kistryn, St. Kistryn, St. Kliczewski, P. Kulessa, H. Machner, A. Magiera, J. Majewski, W. Migdał, H. Ohm, N. Paul, B. Piskor-Ignatowicz, K. Pysz, Z. Rudy, H. Schaal, R. Siudak, E. Stephan, D. Steyn, R. Sworst, T. Thovhogi, M. Wojciechowski, W. Zipper
Nucl. Instrum. Meth. A **519** *(2004) 610*

14. **Parameterization of the total cross-section for (p,^{7}Be) reaction**
A.Bubak, B. Kamys, M.Kistryn, B.Piskor-Ignatowicz
Nucl. Instrum. Meth. B **226** *(2004) 507*

15. **Ice moderator experiments at very low temperatures**
K. Nuenighoff, Ch. Pohl, V. Bollini, A. Bubak, H. Conrad, D. Filges, H. Glueckler, F. Goldenbaum, G. Hansen, B. Lensing, R.-D. Neef, N. Paul, D. Prasuhn, K. Pysz, H. Schaal, H. Soltner, H. Stelzer, H. Tietze-Jaensch, W. Bernnat, J. Keinert, M. Mattes, W. Ninaus, S. Koulikov, A. Smirnov, M. Wohlmuther
Eur. Phys. J. A **22** *(2004) 519*

16. **First laser-controlled antihydrogen production**
C.H. Storry, A. Speck, D. Le Sage, N. Guise, G. Gabrielse, D. Grzonka, W. Oelert, G. Schepers, T. Sefzick, H. Pittner, M. Herrmann, J. Walz, T.W. Hänsch, D. Comeau, and E. A. Hessels
Phys. Rev. Lett. **93** *(2004) 263401*

17. **Observations of cold antihydrogen**
J.N. Tan, N.S. Bowden, G. Gabrielse, P. Oxley, A. Speck, C.H. Storry, M. Wessels, D. Grzonka, W. Oelert, G. Schepers, T. Sefzick, J. Walz, H. Pittner, T.W. Hänsch, E.A. Hessels
Nucl. Instr. Meth. B **214** *(2004) 22*

18. **Aperture method to determine the density and geometry of anti-particle plasmas,**
P. Oxley, N. S.Bowden, R. Parrott, A. Speck, C. Storry, J.N. Tan, M. Wessels, G. Gabrielse, D. Grzonka, W. Oelert, G. Schepers, T. Sefzick, J. Walz, H. Pittner, T.W. Hänsch, and E. A. Hessels
Phys. Lett. B **595** *(2004) 60*

19. **First measurement of the velocity of slow antihydrogen atoms,**
G. Gabrielse, A. Speck and C.H. Storry, D. Le Sage, N. Guise, D. Grzonka, W. Oelert, G. Schepers, T. Sefzick, H. Pittner, J. Walz, T.W. Hänsch, D. Comeau, E.A. Hessels
Phys. Rev. Lett. **93** *(2004) 073401*

20. **Precision spectroscopy of light exotic atoms**
D. Gotta
Prog. Part. and Nucl. Phys. **52** *(2004) 133-195*

21. **On the characterization of a Bragg spectrometer with X-rays from an ECR source**
D.F. Anagnostopoulos, S. Biri, D. Gotta, A. Gruber, P. Indelicato, B. Leoni, H. Fuhrmann, L.M. Simons, L. Stingelin, A. Wasser, J. Zmeskal
Nucl. Instr. Meth. A, to be published

22. **Studies of multi-nucleon transfer reactions in ^{90}Zr(^{18}O,X) and ^{90}Zr(^{16}O,X)**
V. Jha, B. J. Roy, A. Chatterjee, H. Machner
Eur. Phys. J. A **19** *(2004) 347*

23. **Exclusive η production in proton induced reactions**
F. Balestra, Y. Bedfer, R. Bertini, L.C. Bland, A. Brenschede, F. Brochard, M.P. Bussa, Seonho Choi, M.L. Colantoni, R. Dressler, M. Dzemidzic, J.-Cl. Faivre, A. Ferrero, L. Ferrero, J. Foryciarz, I. Frohlich, V. Frolov, R. Garfagnini, A. Grasso, S. Heinz, W.W. Jacobs, W. Kuhn, A. Maggiora, M. Maggiora, A. Manara, D. Panzieri, H.-W. Pfaff, G. Piragino, A. Popov, J. Ritman, P. Salabura, V. Tchalyshev, F. Tosello, S.E. Vigdor, G. Zosi (DISTO collaboration)
Phys. Rev. C. **69** *(2004) 064003*

24. **Production of ϕ mesons in Au+Au collisions at 11.7 A GeV/c**
B.B. Back, R.R. Betts, J. Chang, W.C. Chang, C.Y. Chi, Y.Y. Chu, J.B. Cumming, J.C. Dunlop, W. Eldredge, S.Y. Fung, R. Ganz, E. Garcia, A. Gillitzer, G. Heintzelman, W.F. Henning, D.J. Hofman, B. Holzman, J.H. Kang, E.J. Kim, S.Y. Kim, Y. Kwon, D. McLeod, A.C. Mignerey, M. Moulson, V. Nanal, C.A. Ogilvie, R. Pak, A. Ruangma, D.E. Russ, R.K. Seto, P.J. Stanskas, G.S.F. Stephans, H.Q. Wang, F.L.H. Wolfs, A.H. Wuosmaa, H. Xiang, G.H. Xu, H.B. Yao, C.M. Zou (BNL-E917 Collaboration)
Phys. Rev. C **69** *(2004) 054901*

25. **Precision spectroscopy of pionic 1s states of Sn nuclei and evidence for partial restoration of chiral symmetry in the nuclear medium**
K. Suzuki, M. Fujita, H. Geissel, H. Gilg, A. Gillitzer, R.S. Hayano, S. Hirenzaki, K. Itahashi, M. Iwasaki, P. Kienle, M. Matos, G. Münzenberg, T. Ohtsubo, M. Sato, M. Shindo, T. Suzuki, H. Weick, M. Winkler, T. Yamazaki, and T. Yoneyama
Phys. Rev. Lett. **92** *(2004) 072302*

26. **Axial observables in $\vec{d}\vec{p}$ breakup and the three-nucleon force**
H.O. Meyer, T.J. Whitaker, R.E. Pollock, B.v. Przewoski, T. Rinckel, J. Doskow, J. Kuros-Zolnierczuk, P. Thörngren-Engblom, P.V. Pancella, T. Wise, B. Lorentz, F. Rathmann
Phys. Rev. Lett. **93** *(2004) 112502*

27. **Analyzing powers and spin correlation coefficients for p+d elastic scattering at 135 and 200 MeV**
B.v. Przewoski, H.O. Meyer, J.T. Balewski, W.W. Daehnick, J. Doskow, W. Haeberli, R. Ibald, B. Lorentz, R.E. Pollock, P.V. Pancella, F. Rathmann, T. Rinckel, Swapan K. Saha, B. Schwartz, P. Thörngren-Engblom, A. Wellinghausen, T.J. Whitaker, T. Wise, H. Witala
Phys. Rev. C, accepted for publication

28. **Conceptual design and simulation of the PANDA detector**
J. Ritman
Nucl. Instrum. Meth. B **214** *(2004) 201*

29. **A method to polarize stored antiprotons to a high degree**
F. Rathmann, P. Lenisa, E. Steffens, M. Contalbrigo, P.F. Dalpiaz, A. Kacharava, A. Lehrach, B. Lorentz, R. Maier, D. Prasuhn, H. Ströher,
Phys. Rev. Lett. **94** *(2005) 014801*

2. Theory

30. **Accessing transversity via J/Ψ production in polarized $p\bar{p}$ interactions**
Anselmino, M.; Barone, V.; Drago, A.; Nikolaev, N. N.
Phys. Lett. B **594** *(2004) 97*

31. **Evidence that the a_0(980) and f_0(980) are not elementary particles**
Baru, V.; Haidenbauer, J.; Hanhart, C.; Kalashnikov, Yu.; Kudryavtsev, A.
Phys. Lett. B **586** *(2004) 53*

32. **The role of the nucleon recoil in low-energy meson nucleus reactions**
Baru, V.; Hanhart, C.; Kudryavtsev, A. E.; Meißner, U. G.
Phys. Lett. B **589** *(2004) 118*

33. **Flatte-like distributions and the a_0(980)/ f_0(980) mesons**
Baru, V.; Haidenbauer, J.; Hanhart, C.; Kudryavtsev, A.; Meißner, U. G.
Eur. Phys. J. A **23**, *(2005) 523*

34. **Theory of the Trojan-horse method**
Baur, G.; Typel, S.
Prog. Theor. Phys. Suppl. **154** *(2004) 333*

35. **Radiative neutron beta-decay in effective field theory**
Bernard, V.; Gardner, S.; Meißner, U.-G.; Zhang, C.
Phys. Lett. B **593** *(2004) 105*

36. **Cutoff schemes in chiral perturbation theory and the quark mass expansion of the nucleon mass**
Bernard, V.; Hemmert, T. R.; Meißner, U.-G.
Nucl. Phys. A **732** *(2004) 149*

37. **Infrared regularization for spin-1 fields**
Bruns, P. C.; Meißner, U.-G.
Eur. Phys. J. C, in print [arXiv:hep-ph/0411223]

38. **Improving the convergence of the chiral expansion for nuclear forces I: Peripheral phases**
Epelbaum, E.; Glöckle, W.; Meißner, U.-G.
Eur. Phys. J. A **19** *(2004) 125*

39. **Improving the convergence of the chiral expansion for nuclear forces II: Low phases and the deuteron**
Epelbaum, E.; Glöckle, W.; Meißner, U.-G.
Eur. Phys. J. A **19** *(2004) 401*

40. **The two-nucleon system at next-to-next-to-next-to-leading order**
Epelbaum, E.; Glöckle, W.; Meißner, U.-G.
Nucl. Phys. **A 747** *(2005) 362*

41. **Isospin dependence of the three-nucleon force**
Epelbaum, E.; Meißner, U.-G.; Palomar, J. E.
Phys. Rev. C **71** *(2005) 024001*

42. **Chiral extrapolations of baryon masses for unquenched three-flavor lattice simulations**
Frink, M.; Meißner, U.-G.
JHEP **07** *(2004) 028*

43. **Survey of charge symmetry breaking operators for $dd \to \alpha\pi^0$**
Gardestig, A.; Horowitz, C. J.; Nogga, A.; Fonseca, A. C.; Hanhart, C.; Miller, G. A.; Niskanen, J. A.; van Kolck, U.
Phys. Rev. C **69** *(2004) 044606*

44. **Radiative tritium β-decay and the neutrino mass**
Gardner, S.; Bernard, V.; Meißner, U.-G.
Phys. Lett. B **598** *(2004) 188*

45. **How to extract the ΛN scattering length from production reactions**
Gasparyan, A.; Haidenbauer, J.; Hanhart, C.; Speth, J.
Phys. Rev. C **69** *(2004) 034006*

46. **Near threshold production of a_0(980)-mesons in the reaction $pp \to dK^+\bar{K}^0$**
V.Yu. Grishina, L.A. Kondratyuk, M. Büscher, W. Cassing
Eur. Phys. J. A **21** *(2004) 507*

47. **On the pion cloud of the nucleon**
Hammer, H.-W.; Drechsel, D.; Meißner, U.-G.
Phys. Lett. B **586** *(2004) 291*

48. **Updated dispersion-theoretical analysis of the nucleon electromagnetic form factor**
Hammer, H.-W.; Meißner, U.-G.
Eur. Phys. J. A **20** *(2004) 469*

49. **How to measure the parity of the Θ^+ in $\vec{p}\vec{p}$ collisions**
C. Hanhart, M. Büscher, W. Eyrich, K. Kilian, U.-G. Meißner, F. Rathmann, A. Sibirtsev, and H. Ströher
Phys. Lett. B **590** *(2004) 39*

50. **Meson production in nucleon-nucleon collisions close to the threshold**
Hanhart, C.
Phys/ Rep. **397** *(2004) 155*

51. **On the determination of the parity of the Θ^+**
Hanhart, C.; Haidenbauer, J.; Nakayama, K.; Meissner, U. G.
Phys. Lett. B **606**, *67 (2005)*

52. **Comment on "Photoproduction of η mesic ^{3}He"**
Hanhart, C.
Phys. Rev. Lett. **94** *(2005) 049101*

53. **A cluster version of the GGT sum rule**
Hencken, K.; Baur, G.; Trautmann, D.
Nucl. Phys. A **733** *(2004) 200*

54. **Production of QED pairs at small impact parameter in relativistic heavy ion collisions**
Hencken, K.; Trautmann, D.; Baur, G.
Phys. Rev. C **69** *(2004) 054902*

55. **Parity nonconserving observables in thermal neutron capture on a proton**
Hyun, C.H.; Lee, S.J.; Haidenbauer, J.; Hong, S.W.
Eur. Phys. J. A, in print [arXiv:nucl-th/0411102]

56. **Improved analysis of coherent neutral pion electroproduction on deuterium in chiral perturbation theory**
Krebs, H.; Bernard, V.; Meißner, U.-G.
Eur. Phys. J. A **22** *(2004) 503*

57. **Orthonormalization procedure for chiral effective nuclear field theory**
Krebs, H.; Bernard, V.; Meißner, U.-G. *Ann. Phys.* **316** *(2005) 160*

58. **Lifetime of kaonium**
Krewald, S.; Lemmer, R. H.; Sassen, F. P.
Phys. Rev. D **69** *(2004) 016003*

59. **Spectrum and decays of kaonic hydrogen**
Meißner, U.-G.; Raha, U.; Rusetsky, A.
Eur. Phys. J. C **35** *(2004) 349*

60. **Evolution of high-mass diffraction from the light quark valence component of the Pomeron**
Nikolaev, N. N.; Schäfer, W.; Zakharov, B. G.; Zoller, V. R.
JETP Lett. **80** *(2004) 6, 371*

61. **Four-boson system with short-range interactions**
Platter, L.; Hammer, H.-W.; Meißner, U.-G.
Phys. Rev. A **70** *(2004) 052101*

62. **Universal properties of the four-boson system in two dimensions**
Platter, L.; Hammer, H.-W.; Meißner, U.-G.
Few-Body Systems **35** *(2004) 169*

63. **On the correlation between the binding energies of the triton and the alpha-particle**
Platter, L.; Hammer, H.-W.; Meißner, U.-G.
Phys. Lett. **B 607** *(2005) 254*

64. **The η-^{3}He scattering length revisited**
Sibirtsev, A.; Haidenbauer, J.; Hanhart, C.; Niskanen, J.
Eur. Phys. J. A **22** *(2004) 495*

65. **New results on the limit for the width of the exotic Θ^+ resonance**
Sibirtsev, A.; Haidenbauer, J.; Krewald, S.; Meißner, U.-G.
Phys. Lett. B **599** *(2004) 230*

66. **Bounds on the bound η-^{3}He system**
Sibirtsev, A.; Haidenbauer, J.; Niskanen, J.; Meißner, U.-G.
Phys. Rev. C **70** *(2004) 047001*

67. **Systematic analysis of charmonium photoproduction**
Sibirtsev, A.; Krewald, S.; Thomas, A. W.
Jour. Phys. G **30** *(2004) 1427*

68. **Analysis of Θ^+ production in K^+Xe collisions**
Sibirtsev, A.; Haidenbauer, J.; Krewald, S.; Meißner, U.-G.
Eur. Phys. J. **A 23** *(2005) 491*

69. **Near threshold enhancement of the $p\bar{p}$ mass spectrum in J/Ψ decay**
Sibirtsev, A.; Haidenbauer, J.; Krewald, S.; Meißner; U.-G., Thomas, A.W.;
Phys. Rev. D, in print [arXiv:hep-ph/0411386]

70. **Extended theory of finite Fermi systems: collective vibrations in closed shell nuclei**
Speth, J.; Kamerdzhiev, S.; Spethand, J.; Tertychny, G.
Phys. Rep. **393** *(2004) 1*

71. **Effective-range approach and scaling laws for electromagnetic strength in neutron-halo nuclei**
Typel, S.; Baur, G.
Phys. Rev. Lett. **93** *(2004) 142502*

72. **Nucleon-nucleon potential in finite nuclei**
Yakhshiev, U. T.; Meißner, U.-G.; Wirzba, A.; Rakhimov,A. M.; Musakhanov, M. M.
Phys. Rev. C, in print [arXiv:nucl-th/0409002]

3. Accelerator

73. **Achieving 99.9% proton spin-flip efficiency at higher energy with a small rf-dipole**
Leonova,M. A., Krisch,A. D., Morozov,V. S., Raymond,R. S., Wong,V. K., Gebel,R., Lehrach,A., Lorentz,B., Maier,R., Prasuhn,D., Schnase,A., Stockhorst,H., Eversheim,D. P., Hinterberger,F., Ulbrich,K.
Phys. Rev. Lett. **93** *(2004) 224801*

74. **Ion sources and low energy beam transport for the new superconducting injector linac for COSY/Jülich**
Gebel,R., Felden,O., von Rossen,P.
Rev. of Sci. Instr. **75** *(2004) 5, 1860*

75. **Instability phenomena of electron-cooled ion beams at COSY**
Kamerdzhiev,V., Dietrich,J., Maier,R., Meshkov,I., Mohos,I., Prasuhn,D., Sidorin,A., Stein,H. J., Stockhorst,H.
Nucl. Instr. and Meth. A **532** *(2004) 1/2, 285*

76. **Stripping injection at synchrotrons with electron cooling**
Meshkov,I. N., Sidorin,A. O., Stein,J., Dietrich,J., Kamerdzhiev,V.
Phys. of Part. and Nucl. **120** *(2004) 3, 4*

77. **Spin manipulation of 1.94 gev/c polarized protons stored in the COSY Cooler Synchrotron**
Morozov,V. S., Krisch,A. D., Leonova,M. A., Raymond,R. S., Wong,V. K., Yonehara,K., Bechstedt,U., Gebel,R., Lehrach,A., Lorentz,B., Maier,R., Prasuhn,D., Schnase,A., Stockhorst,H., Eversheim,D. P., Hinterberger,F., Rohdjeß,H., Ulbrich,K.
Phys. Rev., Accelerators and Beams **7** *(2004) 024002*

78. **Spin-flipping polarized deuterons at COSY**
Yonehara,J. C., Krisch,A. D., Morozov,V., Raymond,R. S., Wong,V. K., Bechstedt,U., Gebel,R., Lehrach,A., Lorentz,B., Maier,R., Prasuhn,D., Schnase,A., Stockhorst,H., Eversheim,D. P., Hinterberger,F., Rohdjess,H., Ulbrich,K., Scobel,W.
Inters. of Part. and Nucl. Phys. 8th Conf. 0-7354-0169-1. - 763 - 766

79. **Separatrix formalism applied to linacs accelerating particles with different charge to mass ratio**
Bogdanov,A., Maier,R., Senichev,Y
Proc. EPAC, Lucerne, CH, (2004) 92-9083-231-2. - 1252 - 1254

80. **Delta-T procedure for superconducting linear accelerator**
Bogdanov,A., Maier,R., Senichev,Y.
Proc. EPAC, Lucerne, CH, (2004) 92-9083-231-2. - 1249

81. **Beam position monitor development for the iThemba LABS cyclotron beamlines**
Dietrich,J., Mohos,I., Botha,A. H., Conradie,J. L., Delsink,J. L. G., Rohwer,P. F
Proc. EPAC, Lucerne, CH, (2004) 92-9083-231-2. - 2589 - 2591

82. **Luminosity considerations for internal and external experiments at COSY**
Lehrach,A., Bechstedt,U., Dietrich,J., Eichhorn,R., Gebel,R., Lorentz,B., Maier,R., Prasuhn,D., Schneider,H., Stassen,R., Stockhorst,H., Tölle,R.
Proc. EPAC, Lucerne, CH, (2004) 92-9083-231-2. - 1255 - 1257

83. **Status of the Cooler Synchrotron COSY-Jülich**
Lorentz,B., Bechstedt,U., Dietrich,J., Eichhorn,R., Gebel,R., Lehrach,A., Maier,R., Prasuhn,D., Schnase,A., Schneider,H., Stassen,R., Stockhorst,H., Tölle,R.
Proc. EPAC, Lucerne, CH, (2004) 92-9083-231-2. - 1246 - 1248

84. **High field gradient cavity for J-PARC 3 GeV RCS**
Ohmori,C., Anami,S., Ezura,E., Hara,K., Hashimoto,Y., Takagi,A., Toda,M., Yoshii,M., Nomura,M., Schnase,A., Tamura,F., Yamamoto,M.
Proc. EPAC, Lucerne, CH, (2004) 92-9083-231-2. - 123 - 125

85. **Methods and instrumentation for measurement of low ion beam currents at the cryring**
Paal,A., Källberg,A., Simonsson,A., Dietrich,J., Mohos,I.
Proc. EPAC, Lucerne, CH, (2004) 92-9083-231-2. - 2748 - 2749

86. **Lattice design study for HESR**
Senichev,Y., An,S., Bongardt,K., Eichhorn,R., Lehrach,A., Maier,R., Martin,S., Prasuhn,D., Stockhorst,H., Tölle,R.
Proc. EPAC, Lucerne, CH, (2004) 92-9083-231-2. - 653 - 655

87. **First results of pulsed superconducting half-wave resonators**
Stassen,R., Eichhorn,R., Esser,F. M., Laatsch,B., Maier,R., Schug,G., Tölle,R.
Proc. EPAC, Lucerne, CH, (2004) 92-9083-231-2. - 1258 - 1260

88. **Space charge problem in low energy super-conducting accelerators**
Vasyukhin,N. E., Maier,R., Senichev,Y.
Proc. EPAC, Lucerne, CH, (2004) 92-9083-231-2. - 1999 - 2001

89. **Dual harmonic acceleration with broadband ma Cavities in J-PARC RCS**
Yamamoto,M., Anami,S., Ezura,E., Hara,K., Hashimoto,Y., Ohmori,C., Takagi,A., Yoshii,M., Nomura,M., Schnase,A., Tamura,F.
Proc. EPAC, Lucerne, CH, (2004) 92-9083-231-2. - 1318 - 1320

90. **Triple-spoke cavities in FZJ**
Zaplatin,E., Braeutigam,W., Maier,R., Pap,M., Skrobucha,M., Stassen,R., Tölle,R.
Proc. EPAC, Lucerne, CH, (2004) 92-9083-231-2. - 1261 - 1263

4. Others

91. **Detection characteristics of Ge detectorsl with microstructured amorphous Ge contacts**
Protic,D., Krings,T.
IEEE Trans. on Nuc. Sci., 51 (2004), 1129 - 1133

92. **Time scales involved in emergent market coherence**
Kwapien, J.; Drozdz, S.; Speth, J.
Physica A **337** *(2004) 231 - 242*

93. **Zur Dämpfung der Globalisierung**
Otto W.B. Schult
Die Neue Ordnung **58** *(2004) 264 - 279*

D Beam Time at COSY 2004

Date	Experiment	Duration	Reaction
16.01.04–09.02.04	ANKE	3 weeks	$pp \to pp\phi$
13.02.–08.03.	ANKE	3 weeks	$pn \to da_0/f_0$
08.03.–16.03.	ANKE	1 week	$pA \to \Theta^+ X$
09.03.–29.03.	ENSTAR	1 week	*detector tests*
02.04.–19.04.	TOF	2 weeks	$\vec{p}p \to pp\omega$
23.04.–03.05.	SPIN@COSY	1 week	*spin manipulation*
21.05.–07.06.	PISA	2 weeks	pA→spallation
25.06.–19.07.	HIRES	3 weeks	$pp \to pK^+\Lambda$
19.07.–04.08.	JESSICA	2 weeks	pA→spallation
06.08.–30.08.	COSY-11	3 weeks	$pn \to pn\eta'$
03.09.–13.09.	JESSICA	1 week	pA→spallation
17.09.–27.09.	TRIC	1 week	$\vec{p}p \to pp$
15.10.–29.11.	TOF	6 weeks	$pp \to pK^0\Sigma^+$
03.12.–13.12.	GEM	1 week	$\vec{d}d \to {}^4He\eta$
13.12.–20.12.	SPIN@COSY	1 week	*spin manipulation*
Total ’04		31 weeks	

E Contents of the attached CD

1. This report as pdf file

2. Detailed reports for the Annual Report 2004

- ϕ-meson production in pp collisions close to threshold
- ϕ-meson production in pn collisions
- Investigation of the $a_0(980)/f_0(980)$ resonances in pp and pn interactions with ANKE
- The reaction $pp \to d\pi^+\eta$ at ANKE
- $K^-\alpha$ scattering length, the problem of K^--helium bound states and the reaction $dd \to \alpha K^+K^-$
- Evidence of an excited hyperon state in $pp \to pK^+Y^{0*}$
- Deuteron polarimetry at ANKE
- Cell tests at ANKE
- A new GEANT4 based simulation framework for ANKE
- Drift chamber with a C-shaped frame
- A method to disentangle single meson and multi-pion production rates in the missing mass spectra of the quasi-free $pn \to pnX$ reactions
- Bremsstrahlung radiation in the Deuteron-Proton Collision
- Two-proton correlation function for the $pp \to pp\eta$ reaction
- The analysis status of the $\vec{p}p \to pp\eta$ reaction at $Q = 10$ MeV
- Status of the analysis of the $pn \to pn\eta$ reaction
- Determination of the COSY beam polarization by means of the COSY-11 setup
- Development of the COSY-11 simulation program for the study of the $dp \to dp\eta$ reaction
- Investigation of the $pd \to {}^3He\eta'$ production at COSY-11
- Energy and momentum resolution of the COSY-11 neutron detector
- Excitation function of the $pp \to ppK^+K^-$ reaction near threshold
- Study of the reaction $np \to pp\pi^-$ for excess energies < 100 MeV above threshold
- Simulation of the detection efficiency of $pK^\circ\Sigma^+$ with a polarized target at COSY-TOF
- Detection of the η signal in the missing mass spectrum of $pp \to ppX$
- The analysis framework TOFROOT for online and offline analysis
- Resolution and efficiency of the straw tube tracker for COSY-TOF
- The $p-n$-reaction studies via FSI
- Evaporation of composite particles from the spallation of Au by energetic protons
- Preequilibrium mechanism of the spallation of Au by energetic protons
- Isoptope Identification with Hybrid BCD-Si Telescope
- Detailed studies on a cryogenic methane-hydrate moderator
- Discrepancies between simulation and experiment due to total reflected neutrons

- Comparison of the wavelength dependent time-of-flight spectra of Methane, Methan-Hydrate and Ice at $T = 20$ K
- Simulations for production of mesons via quasi-free proton-neutron scattering at the WASA 4π-detector
- Investigation of the η'-proton interaction at the COSY-11 and WASA-at-COSY facilities
- Detection possibilities of the quasi-free $pn \to pn\eta'$ reaction at the WASA detector
- Simulation of the reaction $pp \to d\pi^+\eta$ for WASA
- Usability of permanent magnets as Ioffe trap at ATRAP
- Charged particle cloud in a combined Penning/Ioffe trap
- High resolution spectroscopy of the $K\beta$ transition in muonic hydrogen
- The resolution function of a Bragg spectrometer at pionic hydrogen energies
- Study of the breathing mode of the nucleon in high energy proton-proton scattering
- Hyperon-Nucleon Interaction in Chiral Effective Field Theory
- Accuracy test of FSI approaches for extracting scattering lengths
- New results on the limit for the with of the exotic $\Theta^+(1540)$ resonance
- Analysis of $\Theta^+(1540)$ production in K^+-Xe collisions
- Some aspects of Θ parity determination in the reaction $\gamma N \to \Theta^+\bar{K} \to NK\bar{K}$
- Consistent analysis of the reactions $\gamma p \to p\eta'$ and $pp \to pp\eta'$
- Bounds on bound η^3He system
- Flatté-like distributions and the $a_0(980)/f_0(980)$ mesons
- Spectrum and decays of kaonic hydrogen
- Partial-wave analysis for $\vec{p}\vec{p} \to pp\pi^\circ$
- ω Production in pp Collisions
- Infrared regularization for spin-1 fields
- Orthonormalization procedure for chiral effective nuclear field theory
- Baryon masses in cut-off regularized chiral perturbation theory and application to lattice results
- Chiral extrapolations of baryon masses for unquenched three-flavor lattice simulations
- High precision calculation of the two-nucleon system in chiral effective field theory
- Isospin dependence of the three-nucleon force
- Universal Properties of the Four-Nucleon System
- Universal Properties of the Four-Boson System with Short-Range Interactions
- The Four-Boson System with Short-Range Interactions in two Dimensions
- Nucleon-Nucleon Potential in Finite Nuclei
- Ultraperipheral Collisions at Relativistic Heavy Ion Collisiders and Production of QED Pairs at RHIC
- Recent Developments in Electromagnetic Dissociation with Fast Heavy Ions
- Effective-Range Approach and Scaling Laws for Electromagnetic Strength in Neutron Halo Nuclei
- The Trojan-Horse Method: Investigation of the Threshold Region
- Near threshold enhancement of the $p\bar{p}$ mass spectrum in J/Ψ decay

- Radiative tritium β-decay and the neutrino mass
- Radiative neutron β-decay in effective field theory
- SPIN COSY: Spin manipulation of vector and tensor polarized beams stored in COSY
- Characteristic features of electron cooling at COSY
- Influence of electron beam neutralization on the stability of electron-cooled ion beams
- Stable longitudinal collective modes in an intense electron cooled proton beam
- Magnets alignment and new installations
- Synchronisation of function generators at COSY
- Overheating protection and monitoring system for the electromagnetic extraction septum
- Radiation protection
- Pulsed operation of the superconducting HWRs
- Warm measurements of the superconducting half-wave resonators
- Cold measurements of the superconducting half-wave resonators
- Study of strangeness-2 baryonic states at FLAIR
- The design of the micro-vertex detector for the PANDA experiment
- R&D work (2005–2008) for the high-energy storage ring
- Polarized Beams in the High-Energy Storage Ring
- Perturbation of the HESR lattice due to the Electron Cooling Insertion
- Studies of the Effect of Longitudinal Impedances on the HESR
-
- First polarization measurement of hydrogen atoms effusing from a storage cell into the Lamb-shift polarimeter and the removal of the components of the polarized target to COSY
- Observation of hydrogen and nitrogen pellets at the ANKE pellet target
- Polarized target for the COSY-TOF detector
- Gold fingers cryogenic target for external COSY experiments
- Residual gas analysis in the TOF high vacuum tank
- Studies for an external cryotarget for WASA at COSY
- Laboratory for semiconductor detectors
- Two-dimensional microstrip germanium detector for X-ray spectroscopy of highly-charged heavy ions
- Large-volume Si(Li) orthogonal-strip detectors for Compton-effect-based instruments
-
- Electronics laboratory

3. Chronicle of the IKP (prepared by Otto W.B. Schult